Control of ligand-receptor interaction by tuning the molecular environment

Valentina Lo Schiavo

AIX-MARSEILLE UNIVERSITÉ
FACULTÉ DE SCIENCES DE LUMINY

Control of ligand-receptor interaction by tuning the molecular environment

Doctoral Thesis

Valentina Lo Schiavo

Member of jury:
Dr. Olivier Thoumine, reviewer
Dr. Frédéric Pincet, reviewer
Dr. He Hai-Tao, examiner
Prof. Philippe Dumas, examiner
Prof. Pierre Bongrand, advisor
Dr. Laurent Limozin, co-advisor

Abstract.

Cell adhesion is a fundamental biological process mediated by specific molecular bonds formed by ligands and receptors attached to surfaces. Formation and rupture of these bonds depend on kinetic, mechanical and structural factors. The goal of this work was to observe how the ICAM-1 (Inter-Cellular Adhesion Molecule 1) – anti ICAM-1 interaction can be modified by modification in i) the multivalency of the molecules involved in the bond ii) the topography of the surface and iii) on the mobility of the ligands. The main technique used for this purpose was the *laminar flow chamber*, complemented by single-particle tracking in fluorescence.

The study on multivalency effects, using monomeric and dimeric ICAM-1, was performed in the absence or the presence of mechanical force, revealing the higher stability of divalent bonds. Also, a force- and time- strengthening dependence was found and described with a two-parameter function, showing, for divalent bonds, an intermediate behaviour between parallel and successive rupture of monovalent bonds. The adhesion frequency of monovalent and divalent bonds exhibit different values accounted for by the difference in length of these molecules.

Adhesion experiments were performed varying the topography of the substrate at the nanoscale for the investigated molecules. A comparison of bond kinetics on these surfaces did not show differences either in attachment or in rupture.

In the flow, the contact time between molecules is controlled by convection of microspheres. Recent results show that there is a minimal time required to form the bond (Robert et al. 2011). To test this prediction, ligands were anchored to supported lipid bilayer (SLB) to investigate how the diffusion can modify the adhesion. Experimentally, the adhesion frequencies of the bonds showed similar behaviour for fixed and fluid SLB. However, 2D numerical simulation predicted an effect on bond formation even at low ligand diffusion. The diffusion seemed to play a role in bond dissociation, strongly limiting the dissociation on the fluid bilayer. This effect can be explained by the possible presence of multiple bonds due to ligand accumulation at the contact area.

Laminar flow chamber and single-particle tracking allowed us to better understand the mechanisms of adhesion and the behaviour of interacting ICAM-1

molecules at single molecule level, when the molecular environment was modified. Similar work can be performed on other adhesion molecules in order to gain a wider knowledge of the adhesion mechanisms, or on TCR – pMHC bonds which are extremely important in immune response.

Resumé.

L'adhésion cellulaire est un processus biologique fondamental contrôlé par des liaisons moléculaires spécifiques entre ligands et récepteurs attachés à des surfaces. La formation et la rupture de ces liens dépendent de facteurs cinétiques, mécaniques et structurels. Le but de ce travail était d'observer comment l'interaction ICAM-1 (Inter-Cellular Adhesion Molecule 1) - anti ICAM-1 pouvait être modifiée en jouant i) sur la multivalence de molécules impliquées dans la liaison ii) sur la topographie de surface et iii) sur la mobilité des ligands. A cette fin, on a principalement utilisé une chambre à flux laminaire, complété par une détection de molécule unique par fluorescence.

L'étude sur les effets de multivalence, utilisant des monomères et dimères d'ICAM-1, a été réalisée en absence ou en présence d'une force mécanique, montrant la plus grande stabilité des liaisons divalentes. En outre, un renforcement avec la force et le temps a été trouvé et décrit avec une fonction à deux paramètres, montrant, pour les liaisons divalentes, un comportement intermédiaire entre rupture parallèles et successives des liaisons monovalentes. La fréquence d'adhésion des liaisons monovalentes et divalentes présente différentes valeurs causées par la différence de longueur de ces molécules.

Les expériences d'adhésion ont été effectuées en variant la topographie du substrat à l'échelle nanométrique pour les molécules étudiées. Une comparaison des cinétiques de liaisons sur ces surfaces ne montrent pas de différences soit dans la formation ou dans la rupture.

Dans l'écoulement, le temps de contact entre les molécules est contrôlé par la convection de microsphères. Des résultats récents montrent qu'un temps minimum est requis pour former la liaison (Robert et al. 2011). Pour tester cette prédiction, les ligands sont ancrés à une bicouche lipidique (SLB) pour étudier comment la diffusion peut modifier l'adhésion. Expérimentalement, les fréquences d'adhésion des liaisons ont

montré un comportement similaire pour les SLB fixes et fluides. Toutefois, une simulation numérique 2D prédit un effet sur la formation de la liaison, même lorsque la diffusion des ligands est faible. Il semblerait que la diffusion joue un rôle dans la dissociation de la liaison, limitant fortement la dissociation de la bicouche fluide. Cet effet peut être expliqué par la présence éventuelle de liaisons multiples dues à l'accumulation des ligands sur la surface de contact.

La chambre à flux laminaire et le suivi de particule individuelle a permis de mieux comprendre les mécanismes d'adhésion et le comportement de l'interaction des molécules d'ICAM-1 au niveau de molécule individuelle, lorsque l'environnement moléculaire a été modifiée. Des travaux similaires peuvent être effectuées sur d'autres molécules d'adhésion afin d'atteindre une connaissance beaucoup plus large des mécanismes d'adhésion, ou sur les liaisons entre TCR et pMHC qui sont extrêmement importantes dans la réponse immunitaire.

Acknowledgements

First of all, I offer my most sincere gratitude to my supervisors, Prof. Pierre Bongrand and Dr. Laurent Limozin who have supported me throughout my thesis with their immense knowledge and professionalism. This thesis would not have been possible without their patience and their passion.

I would like to show my gratitude to Dr. Philippe Robert who showed me the secrets of flow chamber. His brilliant ideas were important during scientific discussions and his jokes were well appreciated too. I am sure he will be so funny even with the little Alice!

I would like to thank Dr. Kheya Sengupta who introduced me to the Langmuir-Blodgett-Schaefer world and read the manuscript correcting all the mistakes due to my 'Italian English'. Many thanks to Dr. Zohar Mishal who kindly performed AFM measurements on my samples and strongly encouraged me during the hardest moments. I will remember him when I will win the Nobel Prize and I will be called “Martyr of Science”.

I owe my deepest gratitude to Dr. Pierre-Henri Puech who has made available his support both at scientific and personal levels. His suggestions and technical computer skills made my thesis work easier, while his kindness and availability were precious in a country whose language was totally unknown to me. I wait for a new painting for the day of the defence!

I am also indebted to many of my colleagues for their support, overall Dr. Roxane Fabre, my “sister”. I cherish our free time together and hope that we will be able to stay in touch despite the large distances between us. “See you later alligator, in a while crocodile!”.

I thank my parents for supporting me throughout all my studies at University, from Messina to Marseilles, via Rome. I know it was not easy for them letting their daughter follows her dreams far from them, but they have never hampered me (well, my dad tried it a bit, but without results!).

Many thanks to my Italian friends, Pippo, Ciccio, Piero and Crispilla who have always been with me, in spite of the distances between us. I am grateful to Sergy (Sergio & Angy, just married!)...too many things to say...just thanks for existing! (Is my personal b&b moving from Rome to San Francisco?).

Finally, I would like to thank Luca...

Table of contents

Introduction

Chapter 1

Cellular adhesion

1.1 Main functions

Cell adhesion is the process by which a cell binds to a surface. The surface can be a membrane of another cell or the extracellular matrix (ECM) or some an inanimate surface. This process has been studied extensively in embryonic cells of higher organisms, where species and tissue specificity of adhesion has been shown (Benoit et al., 2000). Adhesion is a common feature in the life of most organisms. To accomplish adhesion, special protein called cell adhesion molecules (ligands and receptors) serve as linkes that hold the cell to a surface. These proteins can generally be found on the surface of a cell's membrane. There are several different kinds of cell adhesion proteins, and most work towards the general purpose of binding a cell to a surface. These proteins generally have three principle parts:

1. The intercellular domain that is able to interact with and bind to a cell's cytoskeleton which is a protein polimeric structure within the cell's cytoplasm that maintains cellular structure and shape.
2. The transmembrane domain that is able to interact with and bind to the cell's plasma membrane.

3. The extracellular domain that binds with molecules outside of the cell, such as other cell adhesion proteins or the extracellular matrix.

The extracellular matrix (ECM) is commonly involved in cell adhesion because it provides structure and organization to large groups of cells and must be physically connected to them to do so. It regulates and directs chemical communication between cells, in order to avoid that cells receive too many unnecessary stimuli.

Interactions between two cell surfaces may be quite specific, involving certain types of cell-surface protein molecules, or in general, involving production of the ECM that surrounds the cell (Springer, 1994). Most phases of cell development and function are highly dependent on adhesive interactions: cellular recognition, generation and maintaining of form or pattern, migration, regulation and differentiation (Hynes, 2002).

Different kinds of cells in an organism must be bound together for a variety of different purposes. Cell adhesion processes differ by organism type. It is a common process in eukaryotic organisms and is used for many purposes such as binding some specialized cells to blood cells. Adhesion also occurs in prokaryotes such as bacteria when they bind to a host before infecting it. Even viruses use cell adhesion. Indeed, they bind to the cells they overrun. Prokaryotic microorganisms, differently from eukaryotes, adhere to surfaces forming biofilms. When their adhesion is addressed to the cells of higher plants and animals it causes diseases (Arciola et al., 2005).

1.2 Cellular adhesion and diseases

Adhesive interactions are involved in many different pathologies including cardiovascular diseases. In that case, they regulate thrombus formation, making possible the infiltration of leukocyte, the migration and proliferation of some muscle cells. This processes lead to an inability of the deposition of fibrotic tissue (Hillis & Flapan, 1998). Cell adhesion also plays a critical role in many other disease processes: atherosclerosis, acute coronary syndromes, reperfusion injury and allograft vasculopathy (Jang et al., 1994). Atherosclerosis is an important cardiovascular disease (it is probably the first

cause of death in "rich" countries), where monocyte/endothelium adhesion may be an important early event. In neurology, neural cell adhesion proteins play important roles in neural development and are involved in various neurological diseases (Uyemura et al., 1994). In the brain, connection between cell surface adhesion proteins and neurotransmitter receptors with the cytoskeleton proteins are important in neuronal cell migration, synapse formation and synapse plasticity. Dysfunction of cell adhesion molecules may contribute to several psychiatric disorders, and development of brain pathology such as multiple sclerosis and Alzheimer disease (Cotman et al., 1998). Finally, in oncology, it is known that cancer progression is a process in which some adhesion molecules play a pivotal role in the development of recurrent, invasive, and distant metastasis. Evidence indicates that alterations in the adhesion properties of neoplastic cells are fundamentally involved in the development and progression of cancer. Loss of intercellular adhesion allows malignant cells to escape from their site of origin, degrade the ECM, and finally, invade and metastasize.

In addition to this, adhesion molecules regulate or strongly contribute to many physiological functions including signal transduction, cell growth, differentiation, site-specific gene expression, morphogenesis, immunologic function, cell motility, wound healing, and inflammation (Okegawa et al., 2002; Harington & Syrigos, 2000)

Novel therapy development requires the knowledge of cells' adhesive properties. Indeed, cell adhesion to artificial substrates is of fundamental importance in a number of therapeutic and diagnostic techniques such as new bone formation and osseointegration in orthopedic and dental implants, cell recruitment on tissue scaffolds, the operation of biosensors and cell based sensors, and the differentiation of stem cells (Decuzzi & Ferrari, 2010).

Chapter 2

Physical approach

2.1 From biology to biophysics

Although biology and physics are different sciences, nowadays they are becoming much closer. Physicists are increasing their interest in the properties of biological matter, since many processes involving the kinetics of molecular motors, the folding of biomolecules or the viscoelastic properties of the cell are important subjects to study from a physical point of view. On the other hand, biologists are interested in the physical techniques and methods.

Single-molecule techniques have been largely developed by physicists, providing a lot of quantitative information about molecular processes that have to be analysed using statistical methods. These methods attract the attention of molecular biologists and biochemists because they offer complementary tools to investigate problems of their interest. “This gives rise to an unprecedented excitement between physicists and biologists, who are joining efforts and expertise to accomplish common scientific goals” (Ritort, 2006).

Cell adhesion is a process which involves couplings between biochemistry, structural mechanics and surface physics. Therefore, it represents a perfect example of the relationship among physical mechanisms and biological effects. In the last years, the

structure and the biomechanics of the cell was better investigated and understood through important advances in experimental techniques, theoretical models and computational methods. In order to have a more detailed insight of the molecular mechanisms involved in cell adhesion and regulation of cell dynamics, as well as for technological applications, quantitative analysis and modelling of these systems is indispensible. (Orsello et al., 2001).

2.2 Cellular model vs acellular model

There are two approaches used to better understand the mechanisms which underpin cell adhesion:

1. the first one involves the study of cellular models. This approach is closer to the real system. However, it results in complex data since there are a lot of parameters which come into play. Properties related to the interaction between proteins which mediate cell adhesion were often studied with a cellular model. Indeed, the influence of contact time in this kind of interactions (Rinker et al., 2001), or the molecular orientation and length (Huang et al., 2004), or the role of cell-surface topography (Williams et al., 2001; Wu et al., 2007), or the influence of lateral ligand mobility and receptor clustering on cell attachment (Thid et al., 2007) were investigated in presence of cells.
2. The second approach implies the use of an acellular model which reproduces the system under study, simplifying it by focusing just on the properties and components involved in the investigated process. However, in this situation, certain characteristics and properties of cells, such as the presence of microvilli or the cellular motors, which may be important for adhesion, are difficult to take into account. This kind of modelling was used for the present work, where the molecules under study where attached on surfaces such as glass slides or on microspheres.

2.3 Models for ligand and receptor

The study of ligand-receptor interaction was carried out using two pairs of antigen-antibody as models: the main and more studied one here was the ICAM-1 – anti ICAM-1 couple and the second one was represented by pMHC – anti HLA.

ICAM-1. ICAM-1 (Inter-Cellular Adhesion Molecule 1) also known as CD54 (Cluster of Differentiation 54) is a molecule of the immunoglobulin superfamily proteins which include antibodies and T-cell receptors. ICAM-1 is a protein of 115 kDa and is 28 nm long; it is composed of 5 immunoglobulin domains in which the binding sites for integrin LFA-1 are present. It possesses an amino-terminus extracellular domain, a single transmembrane domain, and a carboxy-terminus cytoplasmic domain. The dominant secondary structure of the protein is the beta-sheet, leading researchers to hypothesize the presence of dimerization domains within ICAM-1. Indeed, it plays the role of ligand for the LFA-1 (Fig. 2.1) and MAC-1 integrins, receptors found on leukocytes and macrophages respectively. When leukocytes are activated, they bind to endothelial cells via ICAM-1/LFA-1 and then transmigrate into tissues in processes such as extravasation and the inflammatory response. Because of these binding characteristics, ICAM-1 has classically been assigned to the function of intercellular adhesion. Different cells, including endothelial cells, express ICAM-1. In response to different pro-inflammatory mediators, such as tumour necrosis factor alpha (TNFα) and interleukin-1 (IL-1), the expression of ICAM-1 can reach a value 40 times higher than the normal level (Dustin et al., 1986).

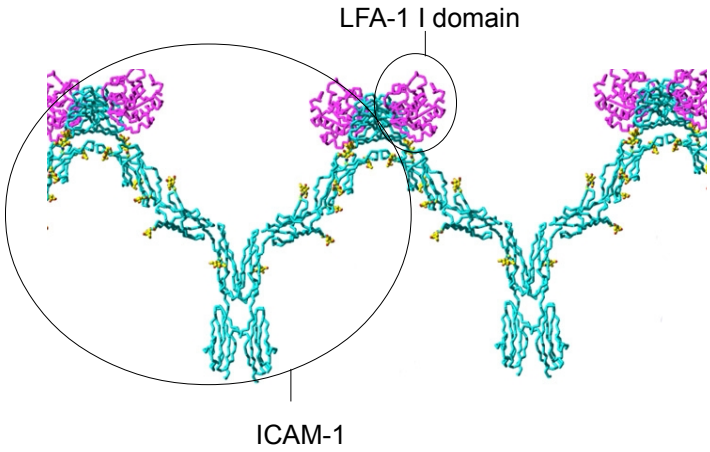

Figure 2.1 In this drawing, ICAM-1 D1–D5 molecules and D4–D4 dimers come together through D1–D1 contacts (D=domain). The W-shaped tetramers can further propagate into a band-like one-dimensional cluster on the antigen-presenting cell surface. The LFA-1 I domain (magenta) binds to ICAM-1 D1 at the opposite face of D1–D1 dimerization. The glycans on ICAM-1 are in yellow (Carson, 1997)

pMHC. The major histocompatibility molecules (MHC), also referred to as HLA molecules in humans, play a vital role in the immune system and autoimmunity. Indeed, their function consists of alerting the immune system if foreign material is present inside a cell. MHC molecules, which are anchored on the cell membrane, display small pieces of their structure or "antigens" to T cells. The antigens may be "self" (coming from a protein of the organism itself), or foreign ("nonself"), originating from bacteria, viruses, etc. T cell surface receptors (TCR) are able to recognise the 8 nm long MHC-peptide (presented on the cell surface) through binding interactions, giving rise to the activation of the immune cell that leads to the development of an immune response against the presented antigen. The design of the pMHC-TCR interaction is such that T cells ignore the self-peptides while reacting appropriately to the foreign peptides.

There are two general classes of MHC molecules (Fig. 2.2): class I, which are found on all nucleated cells and present peptides to cytotoxic T cells, and class II that are found on certain immune cells, namely macrophages, B cells and dendritic cells. However, MHC class I and MHC class II differ significantly in the method of peptide presentation. Both types of molecules present antigenic peptides to T lymphocytes, which are responsible for the specific immune response leading to the destruction of the

pathogen producing those antigens. However, class I and II molecules correspond to two different pathways of antigen processing, and are associated with two different systems of immune defence.

MHC is not an adhesion molecule, but works with ICAM-1 in inflammatory response. The main role of MHC is in allowing the presentation of pMHC to T lymphocytes.

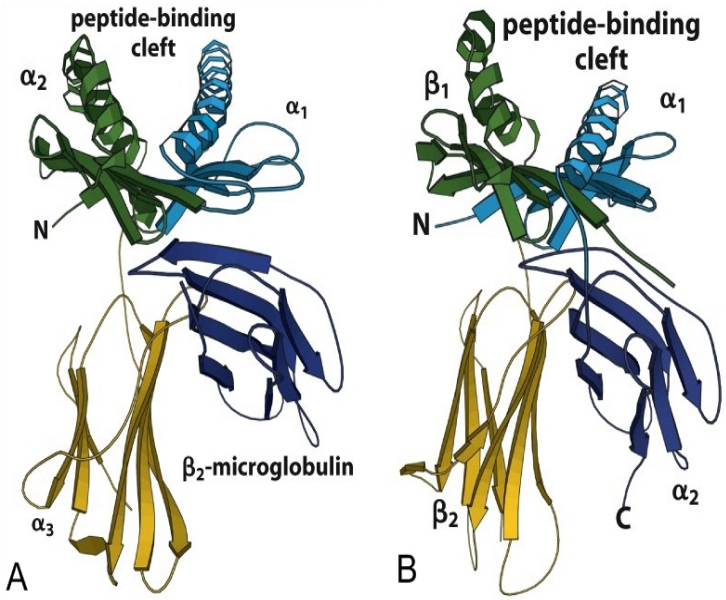

Fig. 2.2 Schematic representation of the MHC I and II extracellular domains coming from crystallographic results. **A**: MHC class I. The molecule is composed of three globular domains: α_1, α_2, α_3. La microglobulin β_2 is not covalently bound to the α chains. The two α helices form the peptide binding site. **B**: MHC class II. The molecule is composed of two transmembranes molecules α et β formed by two globular domains: α_1, α_2 , et β_1 et β_2. Again, the two α helices form the peptide binding site (Murphy et al., 2008)

Antibody. An antibody is a 150 kDa-protein. All antibodies belong to the immunoglobulin family of proteins produced in plasma cells. There are 5 classes of immunoglobulins (abbreviated as Ig). IgG are Y-shaped. The two arms of the "Y" have antigen binging sites, and the other end recognizes other structures. The length of an antibody is ~16 nm. It is involved in immune response, its role is to identify and neutralize bacteria, viruses, or other pathogens. The "Y" shape of antibodies is composed of basic structural units forming four chains: two large heavy chains (~55kDa) and two smaller light chains (~25kDa). In each tip of the "Y" of an antibody there is a region, also known as hypervariable region, which is able to recognize

specifically a particular part, named epitope, of the foreign target (antigen). In this way, the two molecules can bind each other with a very high precision (Fig. 2.3). Although the general structure of all antibodies is similar, thanks to the extreme variability of the hypervariable region, many antigen binding sites can be recognized. Antibodies are used extensively as diagnostic and research reagents. Nowadays, their importance in therapeutic tool to treat disease is recognized. Indeed, antibodies are employed for analysis, purification, and mediation of physiological responses (Lipman et al., 2005).

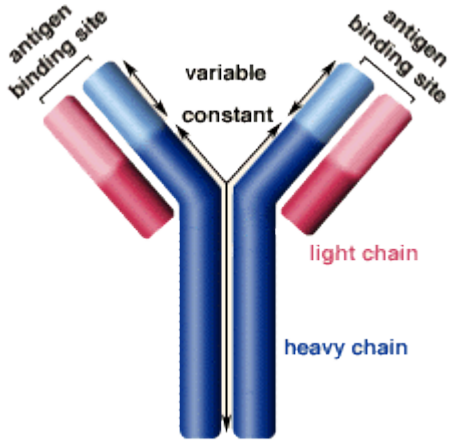

Figure 2.3 Antibody structure. In blue the two heavy chains, while the light one are in pink. The hypervariable region is in light blue and pink, at the tip of the "Y", showing the antigen binding site.

The role of antibodies in the immune response are:

1. binding to an epitope on an antigen with the arms (monovalent antibody fragment (Fab[1]) domain) of the Y. Each Fab[1] domain has a binding site, making the antibody at least bivalent.
2. The tail of the Y (Fc domain) gives to the antibody the biological functions of killer cell activation and activation of the phagocytosis (Lipman et al., 2005).

When the immune response to an antigen is stimulated, multiple non-identical B cells are activated against the specific epitope on that antigen. This leads to a production of a large number of antibodies (polyclonal antibodies) with different specificities and epitope affinities. Polyclonal antibodies are largely used for biological research, such as immunoprecipitation, enzyme linked immunosorbent assays (ELISA), diagnosis of disease, etc.

In contrast, monoclonal antibodies are synthesized by a single population of

identical B cells belonging to the same clone.

In 1975 Kohler and Milstein developed a technology to generate monoclonal antibodies of a desired specificity, by fusing immortal heteromyleoma cells with B-cells, The resulting cell, called a hybridoma is an immortal cell able to produce monoclonal antibody. Monoclonal antibodies can be produced to bind almost any substance, becoming then an important tool in biochemistry, molecular biology and medicine.

The anti ICAM-1 and anti HLA that were used in this study are monoclonal antibodies reacting with ICAM-1 molecules and histocompatibility antigen respectively. The first binds the domain 1 of ICAM-1, meaning the integrin binding site, while the pMHC binding site for anti HLA depends on the type of anti HLA: the mouse anti HLA A2 recognise the α_2 helix and the turn of one of the underlying β strands, while the rat anti HLA ABC binds the α_1 domain of pMHC.

Chapter 3

Single molecule studies

As already stated, cell adhesion is a fundamental biological process that is mediated by specific interactions between adhesion receptors and their ligands on cell surfaces or in ECM. In this chapter I will enter more in detail into this interactions explaining their importance, their advantages and the kinetics of bonds.

3.1 Role and importance of proteins interaction in cell adhesion

Cell adhesion molecules mediate adhesive interactions by forming specific bonds between proteins. In addition, they often link directly to protein complexes which mediate interactions with the cytoskeleton and signal transduction pathways. Consequently, these cell adhesion and signalling complexes also help to obtain extracellular and signal transduction information within cells (Yamada, 2003).

In cell-to-cell adhesion, an adhesion receptor binds to a target protein which can be a "counter-receptor" or a complex carbohydrate on a protein anchored to the plasma membrane. In cell-to-matrix interactions, a plasma membrane adhesion protein such as an integrin, can bind to an ECM protein that is itself considered to be an adhesive protein. Consequently, adhesion molecules or receptors can be grouped in two main

groups: i) the first one is anchored on plasma membrane frequently as a transmembrane protein; this type of molecule consists of a hydrophobic transmembrane domain, a cytoplasmic domain or tail and an extracellular domain containing domains or sites for interactions; ii) the second class of adhesion molecules consists of proteins that are classified as cell surface or ECM proteins (fibronectins, laminins, etc.) and contain domains or sites involved in cellular adhesion.

It has become clear that cell adhesion molecules also play a critical role in cellular signalling. In this case, these proteins cluster together or bind other proteins in order to enhance their enzymatic function on the substrates which are going into contact. In the immune system, an example of these type of bonds is the interaction between T lymphocytes and the antigen-presenting cell.

The mechanical function of adhesion proteins often implies the application of forces on the bond. For example, in case of leukocytes adhesion to endothelium, there is a reinforcement of the interaction between selectins when a force is applied (Marshall et al., 2003). This property seems to enhance the adhesion of leukocytes to the walls of blood vessels, where the strong force acting on the bond is due to the bloodstream (Hammer, 2005).

3.2 Advantages of single-molecule study

Single-molecule studies are central to biophysical research because they allow us to enter into the details of molecular processes. Indeed, with single-molecule studies it is possible to measure kinetics of biomolecular reactions or time-dependent processes being able to follow the movement, and spatially and temporally localise individual molecules. A problem with multivalent attachments is that the relationship between molecular properties and attachment and detachment kinetics are dependent on a number of environmental parameters that are not easy to control. Single molecule properties are "intrinsic".

There are several advantages of studying individual ligand–receptor pairs instead of ensembles of molecules:

- A lot of molecules have the tendency to aggregate when their concentration is sufficiently high. In the experimental conditions of single molecule studies the number of molecules involved in a process is not so high and/or cooperative and clustering effects are minimized. Consequently, one can easily know the number of molecules involved in reactions (Weisel et al., 2003).
- It is possible to reveal the structural and functional heterogeneity of seemingly identical molecules.
- Single molecule studies allow us to apply forces on single molecules and observe their response under the imposed constraint. Indeed, directly quantifying the magnitudes and working distances of forces in ligand–receptor interactions gives an insight into the relationship between molecular structure and the thermodynamics of bond dissociation (Bongrand, 1999).
- At any given time, a single molecule exists in a particular conformational state within a particular environment. Observing only population averages can hide important dynamic or mechanistic features of biological molecules. Watching individual events and distributions rather than observing average values may reveal rare but physiologically important functional fluctuations (Merkel, 2001; Hinterdorfer et al., 2001).

"Single-molecule analysis requires statistical data so that the observed behaviour of minor, unusual molecules is not overestimated. However, as single-molecule studies deal with small numbers of molecules, sampling noise is an inevitable problem of these analyses compared with conventional biochemical analyses" (Sako, 2003).

3.3 Affinity and kinetics parameters necessary to describe a bond

In order to well describe cellular adhesion processes, the knowledge of the average lifetimes as well as kinetic association and dissociation rates of ligand-receptor interactions that mediate this processes is required. To understand the mechanisms

governing the sensitivity, specificity, and regulation of cell adhesion, it is therefore necessary to be able to accurately characterize the kinetics of ligand-receptor interactions. However, it has been demonstrated (Seifert, 2000; Sulchek et al., 2006) that the kinetics and mechanics of multivalent attachment rupture depend on parameters such as receptor and surface topography, lateral mobility, length and flexibility of membrane anchors. Therefore, the study of ligand-receptor interaction is rather complex.

The interaction between ligand and receptor during adhesion processes can be characterized in terms of binding affinity. In general, high affinity ligand binding means that the binding sites are well occupied giving rise to the physiological response. In this situation, the concentration of ligand necessary to elicit a response is quite low. Conversely, low-affinity ligand binding implies the necessity of a high concentration of the ligand so that the binding sites are occupied and the physiological response to the ligand is achieved.

The affinity between a ligand and a receptor is commonly described in terms of the concentration of ligand at which half of the receptor binding sites are occupied, known as the dissociation constant (K_d). Ligand-receptor affinities are influenced by non-covalent intermolecular interactions between the two molecules such as those mediated by hydrogen bonds, electrostatic interaction, hydrophobic and Van der Waals forces. The formation of a ligand-receptor complex (LR) can be described by a two-state process:

$$L+R \underset{k_{off}}{\overset{k_{on}}{\rightleftharpoons}} LR \tag{3.1}$$

in which a complex LR is formed by the L and the R subunits. The kinetic constants k_{on} and k_{off} account for the forward and reverse rates according to the following equation:

$$d[LR]/dt = k_{on}\,[L][R] - k_{off}[LR] \tag{3.2}$$

where [R], [L] and [LR] represent molar concentrations of the receptor, ligand and complex, respectively, usually expressed in mole/litre. The forward and reverse rates allow us to classically describe the interactions between proteins at the non-equilibrium state: k_{on} describes the bond formation and k_{off} the bond rupture. The bond lifetime is

then dependent on the off-rate. The thermodynamic definition for the reaction (3.1) follows the relationship :

$$\Delta G^\circ = G_L^\circ + G_R^\circ - G_{LR}^\circ \quad (3.3)$$

where the quantity ΔG° is the standard Gibbs free energy of the reaction and G_L°, G_R° and G_{LR}° are the Gibbs free energies of reactants (L and R) and product (LR). Under pure thermodynamic reaction control, when the equilibrium has been reached, the ratio of product concentrations will equal the equilibrium constant K_{eq} and therefore be a function of the difference in Gibbs free energies:

$$ln([L]_{eq}[R]_{eq}/[LR]_{eq}) = ln\, K_{eq} = -\Delta G^\circ / R_g T \quad (3.4)$$

where "eq" means that we are dealing with equilibrium concentrations, R_g is the perfect gas constant and T is the absolute temperature. It is readily found that, whatever the initial conditions, the system will tend to an equilibrium state following the Guldberg-Waage law (Atkins & de Paula, 2002). When applied to reactions in solution, this is usually written as:

$$[L]_{eq}[R]_{eq}/[LR]_{eq} = k_{off}/k_{on} = K_d = 1/K_a \quad (3.5)$$

where K_a is called the affinity constant (in litre/mole) and K_d is the dissociation constant measured in mole/litre (Bongrand, 1999). The smaller the dissociation constant, the more tightly bound the ligand is, or the higher is the affinity between ligand and receptor. The dissociation constant for a particular ligand-receptor interaction can significantly change with environmental conditions (e.g. temperature, pH and salt concentration). The effect of different environmental conditions is to modify the strength of the intermolecular interaction between the ligand-receptor pair.

3.4 Description of bond formation and k_{on}

The rate of binding soluble (three-dimensional binding) or surface-attached (two-dimensional binding) ligands influences the efficiency of cell surface receptors. The conventional formalism used to describe 3D reactions cannot be used to account for (2D) interactions between surface-attached molecules. This point is considered in the well known Bell paper (Bell, 1978), which describes the association between two

molecules. Before binding, a diffusion-limited phase is necessary to bring the reactive sites into contact:

$$L + R \rightleftharpoons LR \rightleftharpoons C \tag{3.6}$$

The first step describes the initial contact between the molecules L and R with the formation of a transient complex LR which precedes the final complex C. In this first relation, the velocity of bond formation between proteins depends on the distance between them and consequently, on the membrane diffusion of the two surfaces where proteins are anchored (2D diffusion). The formation of the final complex C, described by the second step, can be expressed by the forward rate k_{on}. To describe the kinetics of the interaction which leads to the formation of the product C, it results then necessary knowing that the bond lifetime and the force resistance are critical parameters which play an important role.

Many authors emphasized the importance of the association rate and its suitability to account for molecular interactions. Indeed, the receptor efficiency was demonstrated to be dependent on the association rate in a variety of situations: integrin activation (Vitte et al., 2004), antigen-antibody interaction (Foote & Milstein, 1991) or tethering of leukocyte to the vessel walls mediated by selectins (Lawrence & Springer, 1991; Dwir et al., 2000). The probability of bond formation is dependent on the encounter time t_e and it can be classically expressed as follows:

$$P(t_e) \sim 1 - \exp(-k_{on} t_e) \tag{3.7}$$

Nevertheless, the association rate does not completely describe the bond formation under all conditions. In some cases a minimum duration time t_0 is necessary to form the bond (Robert et al., 2009), modifying the expression for the bond formation probability as follows:

$$P(t_e) \sim erfc(t_0/t_e)^{1/2} \tag{3.8}$$

In the case of ICAM-1 – anti ICAM-1 interaction, a value for the minimal contact time was estimated being t_0=6 ms (Robert et al., 2011).

3.5 Description of bond rupture and k_{off}

When an interaction between proteins takes place, the bond lifetime can be described by the reverse rate k_{off}. This parameter is a function of the force which is applied on the bond, as already expressed by Bell (Bell, 1978):

$$k_{off}(F) = k_{off}(0)exp(xF/k_BT) \quad (3.9)$$

where $k_{off}(F)$ is the dissociation rate when a force F is applied, $k_{off}(0)$ is the off-rate in absence of force, x represents the interaction range with a dimension of length, k_B is the Boltzmann constant and T is the absolute temperature.

However, this simple framework is not sufficient for many interactions. During the last decades, important progress was made in measuring interactions between surface-attached adhesion receptors in presence of forces at the single-molecule level, leading the following conclusions:

i. In the simplest cases, the dissociation rate of a ligand-receptor bond increases exponentially in presence of a disruptive force, as predicted by Bell (Chen & Springer, 2001; Dudko et al., 2008). Bond rupture could be modelled following the prediction of Kramers (Kramers, 1940), namely as the passage of a single potential energy barrier in an unidimensional reaction path.
ii. in many cases, such as streptavidin-biotin (Merkel et al., 1999), antigen-antibody (Pierres et al., 1995) or integrin-ligand (Zhang et al., 2002) interaction, bond rupture seemed to involve the passage of several energy barriers, implying the presence of a multiplicity of bound states for a given ligand-receptor couple. This might explain the time-dependent strengthening of several bonds, including streptavidin-biotin (Pincet & Husson, 2005).
iii. The studies of selectins behaviour while they rolls on leukocytes, led to the discovery of "catch bonds", in which the dissociation lifetime increases with tensile force applied to the bond. Examples were provided by Marshall (Marshall et al., 2003) in the case of P-selectin-PSGL-1 interaction and Thomas (Thomas et al., 2002) for lectin-sugar bond. However, a recent work of Zhu (Zhu et al., 2008) provided experimental evidence that a disruptive force might

strangely decrease the lifetime of L-selectin ligand interaction, as predicted by eq. (3.9), although this association was considered catch-bond. Indeed, the catch-bond phenomenon is not fully understood yet. A possible feature is that bond rupture may not follow an unidimensional path but an alternative rupture path by deforming a multidimensional energy landscape (Evans et al., 2004).

Chapter 4

Single molecule methods

Many biological reactions are extremely complex and their comprehension through the use of conventional biochemical techniques is difficult. Studying one biological macromolecule at a time clearly allows us to look at these molecules in action. But, at present, although single-molecule techniques applied on biological processes are growing very fast, they are still difficult to master. It is possible to make a distinction between these techniques based on the detection and manipulation of individual molecules (Ha & Selvin, 2008).

- In a first class of techniques where the manipulation of molecules is allowed, we have laminar flow chamber, force application via atomic force microscopy (AFM), biomembrane force probe (BFP) to cite the most representative ones. The last two techniques are force-based methods, which can give an estimation of the frequency of adhesive events and the force necessary to break a bond. The laminar flow chamber is a technique working at constant force and able to measure the frequency of adhesive events and the bond lifetime.
- In a second class, which includes techniques able to detect and follow in real time (but not manipulate) individual molecules, in addition to imaging by AFM, there are predominantly optical techniques such as single-molecule fluorescence (SMF) and semiconductor quantum dot emission, to cite the most common. Single-molecule fluorescence allows us to detect and localize molecules with

about 1.5-nm precision (Yildiz et al., 2003).

4.1 Laminar flow chamber

4.1.1 Principles

Laminar flow chamber is a widely used tool in cell adhesion studies either at the cell scale or at the single molecule scale. It is a versatile tool in understanding the mechanisms of proliferation, adhesion, and metastasis of cancer cell. Many researchers used it to investigate the dynamic adhesion of cells under a definite shear stress (Ling et al. 2003; Rinker et al., 2001). Kaplanski et al. (Kaplanski et al., 1993) monitored the motion of human white blood cells along a surface coated with activated endothelial cells in presence of a very low shear rate. In particular, some studies have been carried out to study leukocyte receptor-ligand interactions (Taite et al., 2006), interactions between selectins or integrins and their ligands (Alon et al., 1995; Wiese et al., 2009; Wayman et al., 2010), or biotin-streptavidin interaction (Agarwal et al., 2009; Pierres et al., 2002).

The laminar flow chamber is a technique that allows us to quantify the physical parameters involved in the interaction between biological molecules on surfaces. This technique provides a method to measure the association and dissociation kinetics of individual bonds. Additionally, it is possible to investigate the behaviour of the bond when a force is applied on it.

The laminar flow chamber is an enclosed space where a flux is imposed by flowing a liquid at a desired velocity. When the flux is sufficiently slow the flow become laminar and the flux velocity is parallel to the chamber floor. On the walls of the chamber this velocity is zero, and far from them its value is given by a first order of approximation (Pierres et al., 1995):

$$v(z)=Gz \tag{4.1}$$

where z is the distance from the walls and G is a constant called wall shear rate and

expressed in s^{-1}. The force T exercised by the flux per surface unit is given by:

$$T=\mu \times G \tag{4.2}$$

If the viscosity μ is expressed in Pa/s, T is expressed in N/m² The shear rate in a chamber of dimension $L \times l \times H$ and for a given flux Q will be:

$$G=6Q/lH^2 \tag{4.3}$$

A model for cell movement in a flow can be described by using microspheres. When the sphere is many radii distant from the walls, its velocity is equal to the flux velocity, but when it comes close to the walls the thin layer of flux between the microsphere and the walls resists to a deformation making the microsphere slowing down.

When a microsphere with a radius a is fixed to the floor of the chamber, it is subjected to an hydrodynamic force f which tends to detach it and to a torque force Γ. These are given by:

$$f\approx 32\mu a^2 G \tag{4.4}$$

$$\Gamma\approx 4\mu a^3 G \tag{4.5}$$

Because of a lever effect, the tensile force F exerted by the flux on the bond holding the microsphere will be:

$$F\approx(f+\Gamma/a)(a/2\lambda)^{1/2} \tag{4.6}$$

where λ is the length of the bond (Pierres et al., 1995).

It has to be remembered that this modelling is not perfect for describing cells. Indeed, a force of friction has to be added to describe cell movements due to asperities and protrusions on cell surface which give an elongated shape to cells compare to spheres (Tissot et al., 1992).

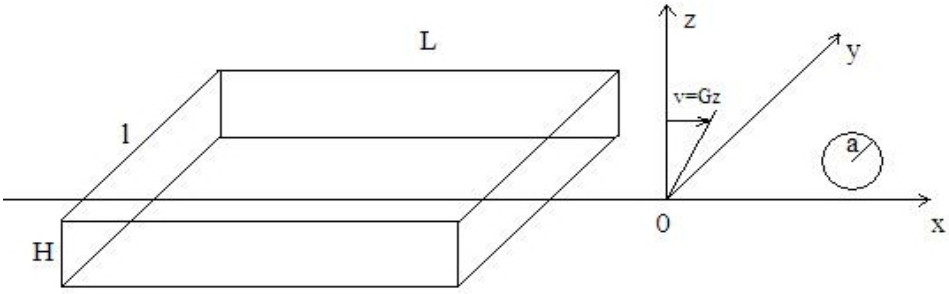

Figure 4.1 Principle of flow chamber. The flux velocity v is parallel to the axe Ox of the chamber. Close to the wall, v is a linear function of the z coordinate. The derivative dv=dz is the shear rate; *a* is the radius of the particle in the flow (Robert, thesis 2009).

The aim of a flow chamber experiment is to detect bonds between molecules attached on the microsphere surface and on the chamber bottom surface. The weak hydrodynamic traction (tens of pN) exerted on the bond after bead stops, together with the thermal stress causes the rupture of the bond. The flow chamber allows us to measure the bond lifetime, by analysing the duration of bead arrest. During a flow chamber experiment, a huge number of microsphere trajectories and arrests are recorded and analysed. If the bond rupture is a simple monophasic reaction:

$$P(t) = exp(-k_{off}t) \tag{4.7}$$

The curve obtained by plotting P versus t on a semi-log scale is a straight line, the slope of which is the dissociation rate, k_{off}. In real life, survival curves (P versus t) have non zero curvature and the analysis of these curves can give information on the rupture mechanism and the energy landscape (Pierres et al., 2002).

It is possible to define a spatial frequency of arrests as a ratio between the total number of arrests and the total distance covered by the microspheres after their sedimentation in the chamber. When beads reach the equilibrium after sedimentation on the chamber, the particle distance h from the surface follows a Boltzmann distribution. If the interaction force between bead and surface is negligible, the mean value <h> follows:

$$h=k_BT/mg \tag{4.8}$$

where k_B is the Boltzmann constant, T is the temperature of the system, m is the mass of a particle and g is the acceleration of gravity. The temporal frequency of arrests is defined as the ratio between the total number of arrests and the total duration of bead displacements.

4.1.2 Measure of kinetics of single bonds

Measure of k_{on}. The flow chamber is able to provide information on bond formation by measuring a related parameter, the adhesion frequency. However, it must be emphasized that single bond formation is more difficult to study than bond dissociation for at least two reasons:

- Studying bond formation requires us to generate multiple intermolecular contacts and to perform many checks to determine the proportion of contacts.
- Bond formation is more dependent on molecular environment than bond rupture. It can depend on the topography of the surfaces where ligands and receptor are attached (Brunetti et al., 2010; Gentile et al., 2010), on the valency of molecules (Haun & Hammer, 2008), on the molecular orientation and length (Huang et al., 2004) and on the lateral mobility of the molecules involved in the interaction (Chan et al., 1991). An exact knowledge of the conditions of bond formation is usually hard to reach and strong approximations are required to derive molecular association rates from adhesion frequencies measured on surface-attached molecules.

Laminar flow chambers can easily determine the average frequency of particle or cell arrest per unit length of trajectory or per unit time of observation. When interpreting the results, one has to observe that (Pierres et al., 2008):

1. if binding efficiency is high, the adhesion frequency represents the number of encounters between active molecules. Thus, it represents a geometrical rather than a kinetic parameter. In this case, the adhesion frequency *per unit length* should be weakly affected by limited variations of the flow.
2. Conversely, when binding probability is proportional to the encounter time (the time during which the molecules are close enough to form the bond), adhesion frequency *per unit time* should be weakly affected by limited variations of the flow. Adhesion frequencies are highly dependent on the definition of binding events and any detailed analysis requires a correction to make arrest detection independent of the shear rate.

Measure of k_{off}. Flow chamber is an interesting tool to investigate the bond rupture of ligand-receptor interactions. The primary output of data processing is related to all binding events together with their duration. This allows straightforward derivation of detachment curves displaying the logarithm of the proportion of binding events lasting for a time t as a function of t. If binding events are mediated by single bonds with *monophasic detachment kinetics*, unbinding curves appear as straight lines, the slope of

which is equal to the dissociation rate k_{off}. However, non linearity is a frequent occurrence as a possible consequence of different phenomena:

- additional bond formation may occur after initial particle arrest, resulting in progressive strengthening of attachment (Kaplanski et al., 1993);
- a single bond may display multiphasic behaviour with a time-dependent strengthening due to the passage of sequential barriers on the energy landscape (Pincet & Husson, 2005);
- particle-to-surface attachment may be mediated by several bond species with different dissociation rates.

In order to avoid some of these problems, one has to be sure of measuring single-molecule interaction. For this reason, the density of ligands on the coverslip or receptors on the bead surface has to be sufficiently low. In this situation, the formation of multiple bonds is unlikely. To test this condition, different concentrations of molecules are exploited during flow chamber experiment: if the frequency of arrests is proportional to the molecule density and the dissociation constant k_{off} does not change, the bond lifetime is related to the same type of events, meaning that the observed arrests are due to single molecule bonds.

The pioneering studies with laminar flow chamber were made on selectin-mediated adhesion (Kaplanski et al., 1993; Alon et al., 1995), followed by more recent studies (Sarangapani et al., 2004; Wayman et al., 2010). In the last decade, with laminar flow chamber the k_{off} was measured in case of monocyte adhesion to vascular endothelium (Rinker et al., 2001) and streptavidin-biotin interaction (Pierres et al., 2002).

4.2 Atomic Force Microscopy (AFM)

Nowadays, the most widespread single-molecule technique is atomic force microscopy (AFM). The AFM is based on the principle that a very soft cantilever with a tip that is moved to a surface, can sense the roughness of the surface and deflect by an amount which is proportional to the distance between the tip and the surface.

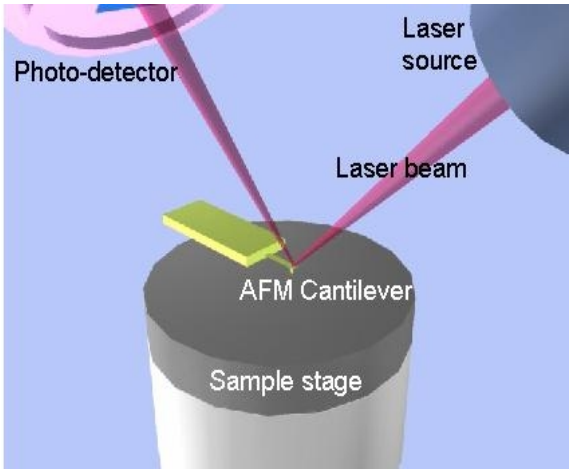

Figure 4.2 Atomic Force Microscope (AFM) – A laser is reflected off the back of a cantilever with a sharp tip and detected by a photodiode detector. AFM produces a topographical image. When the cantilever tip is deflected due to the forces between the tip and surface, the laser is reflected differently and the detector senses the difference in topography.
(http://npl-web.stanford.edu/user/files/www/afm0.jpg)

The most important application of the AFM is imaging, where it can work in various modes: contact mode, tapping mode and jumping mode. For example, in the tapping mode the tip is made to oscillate close to the sample surface. The amplitude of the oscillation is recorded and controlled by a feedback mechanism that keeps such amplitude constant. When passing over a bump the amplitude decreases, so the distance between tip and surface is increased to keep the amplitude of oscillation constant. On the contrary, when passing over a depression the tip is moved to the surface. This mode has the advantage that the transverse motion of the tip along the surface is not influenced by shearing and frictional forces, avoiding damage to the sample and noisy interference effects. A map of the distance of the tip from the sample provides an accurate topographic image of the surface (González-García et al., 2010; Peressadko et al., 2005). AFM has been also used to characterize the surface treatments (Eske & Galipeau, 1999). Other modes are preferable depending on the particular system.

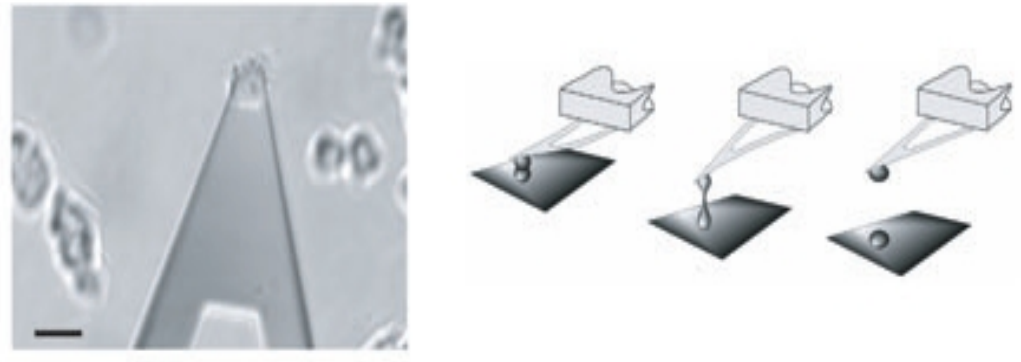

Figure 4.3 Attachment of living cells by means of receptor-ligand interactions. By applying a repulsive contact force between the cantilever-mounted cell and a target cell at the bottom of a Petri dish, and then retracting the cantilever from the target cell (right schematics), specific cell-cell adhesion forces can be measured. Scale bar, 20 μm. (Hinterdorfer & Dufrêne, 2006)

The AFM is also used to manipulate and exert mechanical force on individual molecules. A surface is coated with the molecules to be manipulated and the AFM tip is coated with molecules that can bind to the ones on the substrate. By moving the tip to the substrate, a contact with one of the molecules adsorbed on the substrate is made. The motion of the tip is controlled by a piezoelectric stage which allows to reach a sub-nanometer resolution. Retraction of the tip at constant speed allows to measure its deflection in real time, providing a measure of the force acting on the molecule as a function of its extension. The AFM covers forces in the 20 pN–10 nN range, depending on the stiffness of the cantilever. AFM measurements in force mode were performed on avidin-biotin bonds (Moy et al., 1994; Florin et al., 1994; Lee et al. 1994), antigen-antibody (Hinterdorfer et al., 1996) or cadherins (Baumgartner et al., 2000).

Although AFM is a very versatile and powerful tool, some points of caution are warranted for manipulating single molecules (Neuman & Nagy, 2008):

- the presence of undesired interactions between tip and substrate (van der Waals, electrostatic and adhesion forces) and the non-specificity of the attachments that often occur between tip and substrate;
- the difficulty in controlling the specific location of the attachment between the tip and the molecule. Spatial and force resolution in the AFM are limited by thermal fluctuations. Consequently, the signal-to-noise ratio for the force is small for values of just a few tens of pN (weak interactions), showing the

limitations of AFM. In contrast, AFM is ideal to investigate strong to covalent interactions.

4.3 Biomembrane Force Probe (BFP)

The biomembrane force probe (BFP) is a technique developed by Evans and collaborators (Evans et al., 1991). The principle of the BFP is similar to the AFM one for force measurement. it consists of approaching with two micropipettes with cells, or lipid vesicles, or microspheres, covered with suitable receptor and ligand molecules.

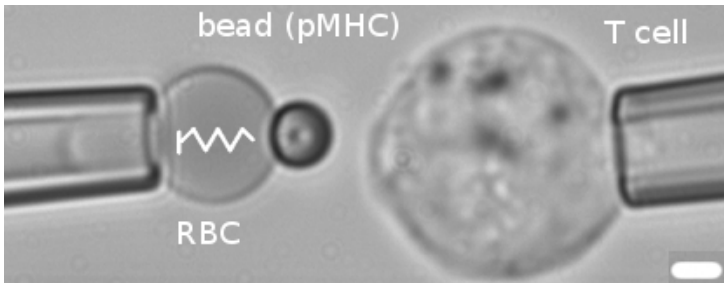

Figure 4.4 Image of Biomembrane Force Probe tool. A red blood cell is aspired by a micropipette (left) and a functionalized microsphere is fixed on its surface. A lymphocyte T is aspired by another micropipette (right). The micropipette on the left is displaced by a piezoelectric device, in order to make the microsphere in contact with the lymphocyte T. The red blood cell works like a spring and its deformations are measured after allowing the contact. P.-H. Puech, 2008.

As shown in Fig. 4.4, a micropipette aspires a red blood cell which works like a spring. A microsphere functionalized with a receptor is fixed on the red blood cell. Another microsphere or a cell functionalized with the suitable ligand is attached on the second micropipette. The two micropipettes are mounted on micromanipulators which allow their displacement using a piezo translator stage. After the contact between the two microspheres is made and bonds are formed, the first pipette is pulled out under microscopic control. The applied force results in the red blood cell deformation and it increases linearly when the velocity of the moving micropipette is constant. A spherical shape of the cell is recovered when the last bond is ruptured. Thus, the experimental parameter which is measured with this technique is the *unbinding force* rather than the bond lifetime (Evans et al., 1991). The interest of this procedure is that the stiffness of

the spring depends on the red blood cell surface tension and it may be varied in a wide range by controlling the sucking pressure applied through pipettes. The cell can indeed be subjected to a distractive force ranging from less than 1 to 100 pN.

The BFP can be used to apply a very wide range of loading rates (Merkel et al., 1999) and it has been mainly used to study molecular interactions at single molecule level, such as E-cadherins (Perret et al., 2004; Bayas et al., 2006) bonds or P- and L-selectin-PSGL-1 (Evans et al., 2004; Evans et al., 2001).

4.4 Single Particle Tracking (SPT)

Single-particle tracking (SPT) exploits the fact that the location of an isolated particle can be measured with a higher accuracy than the Rayleigh limit (typically around 200 nm). By attaching fluorescent molecules to proteins it is possible to detect the light emitted by this fluorophore and follow its trajectory. Fluorophores are excited from their ground state by absorbing light from an external light source. In this situation, a valence electron jumps into a higher energy excited state. When this electron returns to its ground state, a quantum of light is emitted.

Single-particle tracking is a powerful tool to study:

1. ligand density on surfaces. Measuring the density of surface-attached ligands is an important issue for single-molecule studies. This parameter can influence the absorption of biological molecules, the activation of cells (Kim et al., 1996), the kinetics of bond because of the possibility to observe cooperative and multivalent bonds. As previously explained, for single-molecule experiment it is fundamental to check the density of ligand on the surface, since this parameter is firmly important in the estimation of the k_{on}.
2. Ligand lateral diffusion by following its trajectory. Protein within the cell membrane are expected to undergo Brownian motion, but if interactions with other membrane constituents or peripheral structures occur, a deviation from this behaviour is registered. The diffusive motion of molecules of interest at the surface of living cells or artificial membranes can be followed after labelling

them. In this frame, the diffusion dynamics of glycine receptors (Dahan et al., 2003), the confinement of immunoglobulin receptors (Simson et al., 1995) and confinement and jumps of a G-protein-coupled-receptor (Meilhac et al., 2006) where measured.

3. The kinetics of ligand-receptor bonds. In the absence of mechanical constraint, the molecules have a probability to unbind due to thermal fluctuations at the molecular interface. A quantitative approach to quantify the bond lifetime is to detect and follow single fluorescent ligands or fluorescent nanocrystals (quantum dots) bound to ligands, interacting with receptors. When the fluorescent signal disappears, the molecule has detached and the statistics of these events gives the bond lifetime, as found for cadherins (Baumgartner et al., 2003) (k_{off}~1 s) and neurexin-neuroligin (Saint-Michel et al., 2009), biotin-avidin (Wayment & Harris, 2009) or TCR-pMHC (Huppa et al., 2010) interactions. Thoumine and co-workers (Thoumine et al., 2008) observed the detachment from the cell surface of quantum dots conjugated to adhesion proteins (synCAM) and they calculated the k_{off} of the bond being on the order of $0.1 min^{-1}$.

A drawback related to SPT is the ever-presence of the noise during all the steps (Saxton, 2008): labelling, localization, connection of the dots and interpretation of the connected dots. In fluorescence labelling, the main sources of noise are dark states of the label and background fluorescence. Labelling is mainly an experimental problem, solved by using appropriate fluorophores. Problems related to the connection of the dots and to the interpretation of the trajectories may be solved statistically, by using algorithms which are able to take into account the merging and splitting of dots and the causes of their motion (pure diffusion, anomalous sub-diffusion, confined motion and directed motion).

Two works, which were focused on this problem, present improved algorithms to well detect and interpret trajectories from SPT images, introducing useful statistical approaches. The studies revolved round the possibility to track CD36 receptors, evaluate the lifetimes of clathrin-coated pits (Jaqaman et al., 2008) and map the mobility of the epidermal growth factor receptor on the cell surface (Sergé et al., 2008), by creating algorithms that are able to increase the density of particles that can be

tracked.

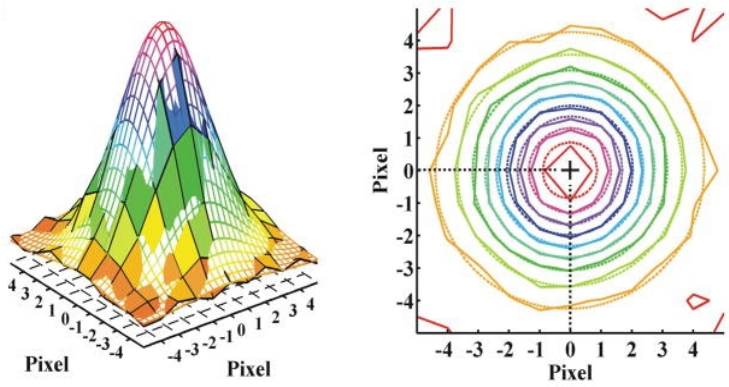

Fig. A single imaged fluorophore can be modelled by a two-dimensional Gaussian to determine its position with nanometer accuracy. The three-dimensional peak to the left shows the recorded intensity for each pixel as a coloured surface. A corresponding contour map is shown to the right (Walter et al., 2008).

Chapter 5

Importance of molecular environment in adhesive interactions

Ligand-receptor interactions and consequently adhesion processes are rather influenced by different factors and structures that surround the pair. This means that modification in the molecular environment may lead to changes in the kinetics and dynamics of bonds.

Huang and collaborators showed that the orientation and length of adhesion receptors such as P- and E-selectins influence their two-dimensional forward rate without consequently affecting the reverse rate and the stability of binding (Huang et al., 2004). A predominant role of environmental factors, such as surface topography and accessibility of active molecules to regions of contact, in determining forward rates of bond formation at cell interfaces was also demonstrated (Waugh & Lomakina, 2009). Thus, association rates of adhesion bonds may be strongly influenced by steric barriers between the surfaces and the reactive molecules in the contact region. Waugh's team postulated the necessity of available molecules and formation of “reaction zones” at the interface of adhesion sites that precedes bond formation (Waugh & Lomakina, 2009).
The study of simple systems such as single-molecule interactions on acellular surfaces is the basis for the investigation of more complicated system with interacting cells. When these "simple" interactions are well understood, it would be possible to put back molecules in a "biomimetic" context, to mimic and study more complicated mechanisms involved in cell-adhesion.

5.1 Regulation of cell adhesion by the cytoskeleton

The cytoskeleton is a dynamic three-dimensional structure that fills the cytoplasm and is made out of proteins. This structure acts as both muscle and skeleton, for movement and stability. The primary types of fibres comprising the cytoskeleton are microfilaments, microtubules, and intermediate filaments. It plays an important role in regulation, activation and adhesion.

As an example, integrin adhesion receptors link the ECM to the actin cytoskeleton and transmit biochemical signals and mechanical force across the plasma membrane. Integrin-mediated cell adhesion is enabled by cytoskeletal linkages. Inside-out signals to integrins originate from diverse plasma membrane receptors which presumably regulate integrins. This signalling is then modulated by cytoskeletal proteins that allow the activation of integrin-regulatory molecules and the control of their nearness to integrin cytoplasmic tails (Calderwood et al., 2000). In the case of T cells, it is known that to become activated, they must efficiently recognize antigen-presenting cells or target cells through several complex cytoskeleton-dependent processes, including integrin-mediated adhesion. A regulated cytoskeletal framework provides to recruit molecules that regulate adhesion and necessary for T-cell development, activation and proliferation (Billadeau et al., 2007).

5.2 Role of glycocalyx in modulating cell adhesion

Glycocalyx is defined as a set of extracellular polymeric materials (glycoproteins), glycolipids and sugar residuals with a variable thickness. Only identical twins have chemically identical glycocalices; everyone else is unique. The glycocalyx is used by the organism to discriminate between its healthy cells and foreign organisms, transplanted tissues, or diseased cells. The glycocalyx also includes some cell-adhesion molecules that enable cells to adhere to each other, thus playing an important role on cell-adhesion (Robert et al., 2006), and guide the movement of cells during embryonic development.

The anti-adhesive role of glycocalyx was largely demonstrated: cell-adhesion is enhanced by removing its constituents (Stockton et al., 1998) and conversely, increasing glycocalyx leads to a decrease in the adhesion (Wesseling et al., 1996). Different parameters and properties of glycocalyx can play a role on cell adhesion: thickness, viscosity, elasticity, area of surface were adhesion molecules are attached and shear rate in presence of flow.

The effect of glycocalyx on adhesion molecules is not well known yet when working with single-molecule bonds. However, some progresses on this studies were done. Indeed, Robert et al. (Robert et al., 2008) used hyaluronan layers to mimic the repulsive role of glycocalyx on the interaction between Fc-ICAM-1 and anti ICAM-1 in a single-molecule study. They demonstrated that by increasing the amount of hyarulonan and so the thickness of repulsive layer, the bond association rate decreased although the bond lifetime was not affected.

5.3 Effect of valency on ligand-receptor interaction

Many biological functions are based on multivalent interactions between couples of ligands and receptors, giving rise to stronger bonds compare to the weak individual ones formed by a single ligand-receptor pair. “Multivalent bonds feature prominently in a variety of biological processes, such as activation of T cells and intercellular adhesion” (Sulchek et al., 2006). Therefore, understanding and exploiting the characteristics of multivalency to control the strength of binding in multivalent biochemical systems is very important. The benefits of these studies could include:

- improvement of understanding the binding mechanism of antibodies;
- opportunity of modulating this binding, with the possibility for application in research and clinical immunology;
- development of new approaches to management of infectious disease;
- more efficient design of receptor-targeted ligands and drug leads;
- new reagents and processes useful in biochemistry and biology research.

Saint-Michel et al. (Saint-Michel et al., 2009) demonstrated the different kinetic

behaviour of monomeric and dimeric neurexin in absence of force, simply analysing the neurexin-neuroligin interaction. They put ligand-coated quantum dots on receptor-coated cell surface and looked at the progressive reduction of the number of fluorescent particles on the surface. In this way, they could have an estimation of the kinetic parameters of this ligand-receptor interaction.

The "avidity", used to describe the strength of bonds, of cellular adhesive interactions is a combination of the affinity of individual ligand-receptor bond and the valency, which is the total number of bonds formed. The concept remains still qualitative and not fully understood, despite its importance in immunology.

ICAM-1 molecule is a ligand for LFA-1 and Mac-1 integrins, making it an important player in lots of immune and inflammatory processes. A model for the entire structure of ICAM-1 has been built by Yang et al. (Yang et al., 2004). This crystal structure provided a basis for dimerization of ICAM-1 on the cell surface. Different studies have been conducted on the different behaviour between a monomeric and a dimeric ICAM-1 (mICAM-1 and dICAM-1 respectively). It was demonstrated that ICAM-1 dissociation from high affinity LFA-1 was about 10-fold faster for monomeric than dimeric ICAM-1: k_{off}=0.002 s^{-1} for dICAM-1 and 0.03 s^{-1} mICAM-1 (Sarantos et al., 2005). These results, obtained with flow cytometry, are also comparable with dissociations detected previously by surface plasmon resonance of 0.0016 s^{-1} for dimeric and 0.022 s^{-1} for monomeric ICAM-1 binding to immobilized high affinity LFA-1 (Jun et al., 2001b). The value for mICAM-1 binding affinity is also in agreement with Jun et al. The association rate and the stability of the bond between neutrophils and ICAM-1 were also measured. Although the rate of adhesion was the same for mICAM-1 and dICAM-1, adhesion stability showed a strong dependence on the bond valence: stable adhesion was solely observed when neutrophils bound dICAM-1 beads (Sarantos et al., 2005). In addition, it was formally shown on ICAM-1 that dimerization was not required to assemble a full binding site (Jun et al., 2001a).

Single bond rupture was studied not only by subjecting molecules to a constant force (usually with a flow chamber), but also with a steadily increasing force ramp in AFM or BFP. Sulchek et al. (Sulchek et al., 2006) used AFM to measure the effect of multivalency on attachment mediated by antibodies and MUC-1 antigens. They

observed that forces were shared by parallel bonds, and the k_{off} was about 40-fold lower with double bonds than with single bonds. Evan's team (Evans et al., 2010; Kinoshita et al., 2010) used a BFP to compare single and double bonds formed by ICAM-1 and LFA-1. They concluded that forces were equally shared by divalent bonds.

5.4 Influence of surface topography

Cell adhesion depends on different factors and one of these is the topography of the surfaces which are involved. Since the focal adhesion of cell is in the range of 5-200 nm, it is likely that nanoscale features may strongly influence these small cellular components. Indeed, it was demonstrated that nanostructured gold surfaces can modulate neuron behaviour depending on surface roughness (Brunetti et al., 2010). An AFM study showed that the distribution of focal adhesion (a complex involved in triggering cellular responses) is strongly affected by the size of surface nanostructures (González-García et al., 2010). This means that not only the kinetics of ligand-receptor interaction is important, but also how effectively the surfaces present these molecules. Carrier stiffness or surface roughness lower the 2D affinity, the forward rate, but not the reverse rate. This has been widely demonstrated by two teams: i) in case of adhesion mediated by a CD16b receptor on three different cells with different surface roughness, such as red blood cells (RBC), Chinese hamster ovary (CHO) and K562 (Williams et al., 2001); ii) in case of P-selectin – PLSG-1 interaction on three carrier systems like RBC, human promyelotic leukemia HL-60 and polystyrene beads (Wu et al., 2007).

Studies on effect of surface topography where also conducted to determine the distribution of adhesion molecules on the surface. Hocdé et al. (Hocdé et al., 2009) performed some measurements of fluorescence intensity aimed at localizing L-selectins and β_2 integrins on microvillus' surface: the first are recruited on the tips of microvilli while the latter are sequestered away from tips.

However, the results for cell adhesion on rough surfaces remain still controversial. Indeed, some studies have shown a decrease in proliferation and adhesion with an increase in surface roughness (Kunzler et al., 2007); some others have

documented exactly the opposite (Deligianni et al., 2001; Webster & Ejiofor, 2004); finally, in other works it has been observed that moderately rough substrate enhances the adhesion (Gentile et al., 2010). This can be probably due to the increase of the surface energy of adhesion (typically associated with moderately rough substrates and the non-uniform surface adsorption) and preferential conformation of proteins over non planar substrates, as mathematically shown by Decuzzi and Ferrari (Decuzzi & Ferrari, 2010).

To represent roughness on surface, mainly three different mathematical approaches are possible:

1. Hemispherical asperities (Cooper et al., 2001)
2. Fractal surfaces (Gentile et al., 2010)
3. Fourier transform (Peressadko et al., 2005)

A comparison between these three mathematical methods showed that the Fourier transform is probably the best framework to represent roughness, being able to accurately reproduce many rough surfaces in agreement with the experimentally observed adhesion forces measured with the AFM (Eichenlaub et al., 2004).

5.5 Effect of ligand lateral diffusion on bond kinetics

The function of cell surface receptors is to mediate the exchange of information between cells and their environment. In the case of adhesion receptors, their spatial distribution and diffusion are important to their function. Therefore, it is fairly important to understand the mechanisms which regulates the above-mentioned properties. Different experiments apt to characterise the lateral mobility of adhesion ligands or receptors have shown common mechanisms that control their function and consequently cellular behaviour. It is then clear that diffusion plays a vital role in many membrane-related functions including adhesion (Dustin et al., 1996). The ability of adhesive ligands to diffuse laterally is pivotal for the formation of intercellular adhesion, whose strength should increase with time. Adhesion can be increased by ligand lateral mobility in two ways: i) first, increased ligand motion allows receptors to move to areas of high

ligand density, increasing the number of bonds formed; ii) second, translational and rotational diffusion can improve alignment between ligand and receptor, increasing the probability of bond formation (Kucik et al., 1996). Different studies have shown that the diffusion of a ligand enhances cell adhesion by allowing ligand accumulation into the cell contact area, and by raising the rate of ligand-receptor bond formation (Chan et al., 1991; Thid et al., 2007). Recently, Yu and co-workers (Yu et al., 2010) studied the effect of clustering and mobility of integrins on adhesion, under flow conditions. Their results indicate that integrin clustering along with their continued motion are pro-adhesive under flow conditions, activating adhesion even in absence of increased integrin expression or integrin conformational changes. Although many studies of single molecule interactions in adhesive processes showed that the lateral mobility of ligand enhance the adhesion, English and Hammer. (English & Hammer, 2005) developed a simulation method (BRAD) to study the virus-cell interaction. Membrane proteins diffusion increased from 10^{-11} to 10^{-9} cm^2/s showing a little effect of mobility on the virus attachment on subsecond timescales. The fraction of viruses that bind with diffusing proteins was the same as in case of fixed proteins, meaning that the diffusion of proteins does not play a role in the virus-cell encounter.

To generate a model of cell surface and consequently study molecular interaction at the interfaces to describe cell-cell or cell-ECM interactions, supported lipid bilayers (SLB) have been extensively used. The key features are that the individual lipid molecules on SLB are mobile and anything linked to them in the upper leaflet retains this mobility. Anchoring ligand on SLB allows to study the 2D affinity and kinetic rates of ligand-receptor interactions in presence of ligand lateral diffusion (Fenz et al., 2009; Smith et al., 2008).

Chapter 6

Main objectives

Cell adhesion is a fundamental biological process mediated by specific molecular bonds between ligands and receptors attached to surfaces. The formation and rupture of these bonds depend on the kinetic and mechanical factors (distance between binding partners, force applied on bond, diffusion of molecules) and, as it has been recently observed, on the topography of the surfaces.

The goal of the present work is to quantify the effect of these parameters starting with antigen/antibody as a model system and measuring the binding and unbinding kinetics using the laminar flow chamber technique. The aim is to observe how the ligand-receptor interaction can be modified by tuning the molecular environment, by modulating

i. the multivalency of the molecules involved in the bond formation, studying monomeric and dimeric molecules in the adhesion, knowing that *in vivo* adhesion receptors often present a dimerized structure;
ii. the topography of the surface. It has been already shown that adhesion receptors are influenced by the surface topography, although the results are still controversial. We performed adhesion experiments varying the roughness of the substrate where investigated molecules are attached, knowing that a systematic comparison between them could show differences either in the adhesion frequency or in the detachment of the ligand-receptor bonds;

iii. the mobility of the surface, comparing an immobile system with a mobile one using fluid supported lipid bilayers (SLB). Recent results in the laboratory show that the binding efficiency scales non linearly with the encounter duration (Robert et al., 2009); in other words, there is a minimal time t_0~6 ms required to form the bond. To test this prediction, ligands where put on supported lipid bilayers to investigate how the diffusion (coefficient D) can modify the adhesion through the relationship:

$$t \sim L^2/D \tag{6.1}$$

where L is the molecular length and t is the diffusion time. If the diffusion time is smaller than this minimal contact time, the probability to have the formation of the bond should be lower then without diffusion.

In order to investigate these three aspects of the effects of molecular environment on ligand-receptor interactions, flow chamber experiments were performed. Using this technique, the kinetic parameters of molecular interactions between surface bound molecules were studied, as well as the effect of forces applied on the bonds. The flow chamber allows us to work at single-molecule level, yielding more information compared to the usual biochemical techniques that work with *ensembles*.

In addition, fluorescent experiments were carried out to determine i) the ligand density on surfaces, knowing that this parameter is important in the estimation of the association rate; ii) the diffusion of lipids forming supported bilayers, and molecules anchored on them; iii) the kinetic parameters of the ligand-receptor interaction at longer timescale than in flow chamber and in the absence of force.

All these techniques were employed in the study of acellular systems, were the molecules were attached on surfaces such as glass substrates for ligand, and microsphere or quantum dot surfaces for receptor.

Materials and methods

Chapter 7

Functionalization of surface

7.1 Constraints imposed by single molecule experiments

During measurements of single molecule adhesion with laminar flow chamber, some of the arrests of microspheres on the surface may not due to an interaction between the ligand and receptor couple under study. These unspecific interactions between the particles and the surface of the chamber stop particles. From the detection used, it is not possible to discriminate between specific and unspecific arrests. As a consequence, at least one negative control has to be used to measure the fraction of unspecific arrests. Hence, the adhesion frequency is estimated for both the negative control and the one related to the couple ligand-receptor. Then, by subtracting the adhesion frequency of the negative control from the test's one gives the specific adhesion frequency.

Values of arrest duration are used to compute the k_{off}. The ratio between specific and unspecific adhesion frequency has to be sufficiently high in order to measure the k_{off}. However, working at single molecule level in laminar flow chamber means dealing with a very low ligand density on one surface, in order to avoid possible multiple bonds. In this situation, the number of detected arrests won't be very high, since the molecules are quite sparse on the surface. This leads to a difficulty in the measurement of a sufficient ratio between specific and unspecific adhesion frequency. Then, it is often

difficult to find experimental conditions which provide an unspecific adhesion frequency significantly lower than the specific one. The minimal desired ratios are equal to 3. However, two main factors are able to increase this ratio:

1) *Increasing the specific adhesion frequency by helping the bond formation.*
   - The first way could be to *sterically* act on the couple through the functionalization of surfaces which causes ligand and receptor to orient themselves in order to make the bond sites accessible.
   - Second, by playing on the *number* of possibly interacting couples. Since the ligand density of one of the two surfaces has to be limited in order to ensure a single bond each time, the other surface has to present high receptor density to obtain a reasonably high specific adhesion frequency. In the case of microspheres, the density is determined by the coupling protocol of the provider, while for the other surface, the density is measured by labelling the ligand with a fluorophore and looking at it in fluorescence.
2) *Decreasing the unspecific adhesion frequency by lowering the possibility of non specific interactions.* The surface passivation aims for decreasing the possibility of non specific interactions. Surfaces which allow the adsorption of proteins are passivated by saturation through a protein which usually is bovine serum albumin (BSA). BSA is also systematically used to prepare surfaces for flow chamber trials and inside the flow which fills the chamber.

7.2 Cleaning of slides

The surface of prepared slides constitutes the lower face of the laminar flow chamber where beads are sedimenting close by. We used glass coverslips (Hoechst, Germany) for flow chamber experiments, ligand density measurement in epi-fluorescence and TIRF experiments. They have an area of 24*24 mm², a thickness of 170µm with a small tolerance in thickness variation equal to 10µm. However, the comparison between smooth and rough substrates was made by using different glass slide types: smooth or etched cover glass slides, with dimensions of ~75x25x1 mm

(Marienfeld, Lauda-Königshofen, Germany).

The cleanliness of slides is very important to allow an effective and reproducible functionalization. To clean and keep the slides in the best conditions it was used a support made in teflon which is not sensible to the washing solution and in which it is possible to put nine slides simultaneously (Fig. 7.1).

First, slides were three times washed with pure ethanol and profusely rinsed with deionized Milli-Q water (18.2 MΩ of resistivity). The second step was realised by dipping the slides in 100ml of "piranha", a solution of two-third of H_2SO_2 (Sigma-Aldrich, France) and one-third of preheated H_2O_2 at 50% (Sigma-Aldrich, France), which leads to an immediate oxidation of glass slides. The reaction was prolonged for ten minutes. The washing solution was then thrown after removal of slides, which were rinsed with five litres of Milli-Q water.

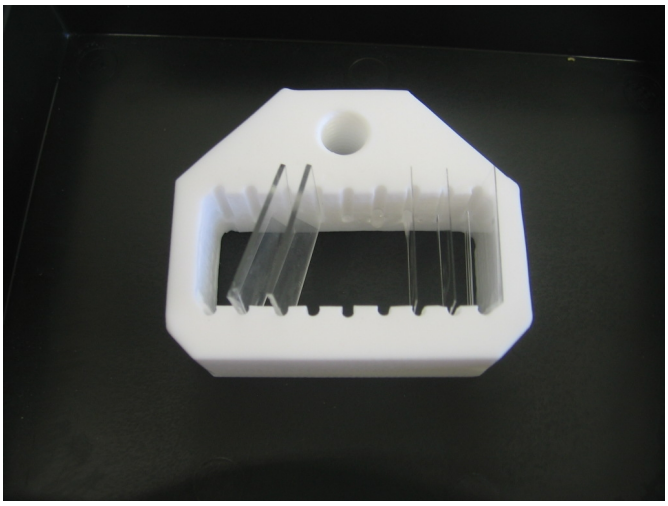

Figure 7.1 Support for slides made in teflon. On the left two cover glass slides, with dimensions of ~75x25x1 mm (Marienfeld, Germany). On the right three glass coverslips (Hoechst, Germany) with an area of 24*24 mm², a thickness of 170±10 µm.

Just before being used, slides were taken out of the support, with a pair of tweezers (VWR, France) previously cleaned with ethanol and rinsed with Milli-Q water. Each slide was then put in a teflon box (Fig. 7.2). These boxes present nine small squares relief on the bottom which maintained the slide far from the internal box surface. They were washed at high temperature with a solution of soap for glasses at 2% (Hellmanex, Hellma, Germany) in an ultrasonic bath and then rinsed with deionized

water after each use (Robert, thesis 2009).

Figure 7.2 Teflon boxes, designed by Philippe Robert, used as support of the slides during coating and rinsing. In this picture one can clearly see the nine small squares on the bottom of the boxes which prevent any contact between the slide and the surface of the box.

7.3 Grafting of immobile ligands on glass

7.3.1 ICAM-1 vs anti ICAM-1 on *smooth* substrates

For the laminar flow chamber experiments related to the couple of antigen-antibody constituted by ICAM-1 – anti ICAM-1, ICAM-1 was used to functionalize surfaces and anti ICAM-1 for beads. The functionalization has been made always at room temperature.

In order to study the effect of divalency in the ligand-receptor bonds, a comparison between a monomeric ICAM-1 (mICAM-1) and a dimeric ICAM-1 (Fc-dICAM-1), was done (Fig 7.3).

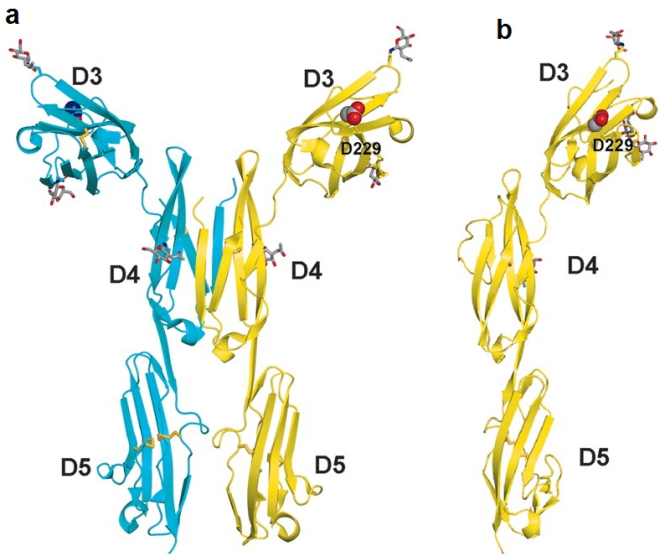

Figure 7.3 Diagrams of ICAM D3–D5 crystal structures. (*a*) The dimeric ICAM-1 D3–D5 structure. (*b*) The monomeric ICAM-1 D3–D5 structure, shown in the same orientation as the right monomer of dimeric D3–D5 in *A*, after superposition on D4. The side chain of the key $\alpha_M\beta_2$ binding residue in D3, is shown with large spheres. (Chen et al., 2007).

The first one presents a polyhistidine tag at the C-terminus while the second one is a chimera with an Fc fragment of human IgG1 at the C-terminus in which is fused the polyhistidine tag. Both of them were provided by Sinobiolocal Inc. (Beijing, China).

Glass coverslips were coated step by step as follows, at room temperature:

1. 200 µl of poly-L-lysine solution (PLL 300 kDa, Sigma-Aldrich, France) at 50µg/ml (solvent=0.2 µm-filtered phosphate buffer at 10^{-2}M and pH 7.4 with 0.01% of sodium azide).
2. 200 µl of glutaraldehyde (Sigma-Aldrich, France) at 25 mg/ml in a 0.2 µm-filtered borate buffer at 10^{-1} M and pH 9.5 with 0.01% of sodium azide. Glutaraldehyde covalently binds lysine residues.
3. 200 µl-solution of mouse anti histidine tag IgG1 monoclonal antibody (AbD Serotec, Oxford, UK) at 1µg/ml in order to covalently bind the PLL.
4. In order to passivate the aldehyde residues which did not react before, coverslips were incubated for one hour with 200 µl of glycine (Sigma-Aldrich) solution at 0,2 M in a phosphate buffer at 0.1 M and pH 7.2 with 0.01% of sodium azide.
5. 200 µl of mICAM-1 or Fc-dICAM-1solution at different concentration: 0.01

µg/ml, 0.02 µg/ml, 0.04 µg/ml and 0.08 µg/ml.

6. Finally, 200 µl of 0.2 µm-filtered BSA solution (Sigma-Aldrich, France) at 1 µg/ml. BSA inhibits unspecific interactions between the surface and the beads. After 30 minutes of incubation, slides were rinsed four times.

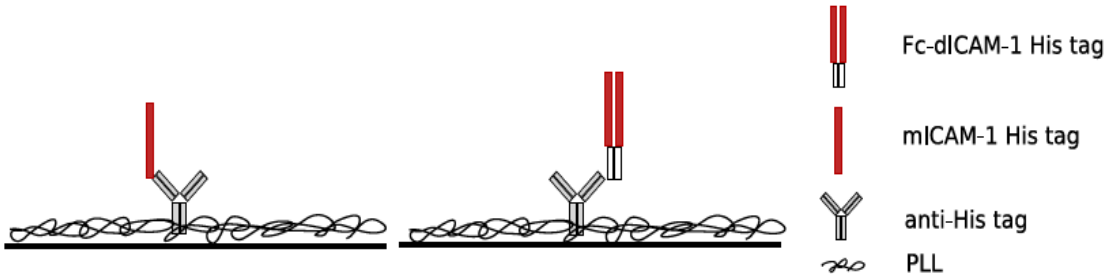

Figure 7.4 Schema of ICAM-1 – anti ICAM-1 construction. Glass coverslip is functionalized with PLL, anti-his tag antibody and mICAM-1 or Fc-dICAM-1.

When it is not specified, the buffer in which the reagents are dissolved is PBS at 0.1 M and pH=7.4. The incubation time for all the solutions was 30 minutes, except for glycine (1 hour). After each step, slides were rinsed four times with PBS (Fig. 7.5).

Figure 7.5 Rinsing of a slide inside its teflon box. The rinsing is performed by adding ~8 ml (volume of the box) of PBS inside the box and then throwing it.

7.3.2 ICAM-1 vs anti ICAM-1 on *rough* substrates

Topography of the surfaces which are involved in the cells processes can influence the bond between ligand and receptor. In order to study this effect more in detail, a comparison in the adhesion between molecules anchored either on smooth or on rough surfaces was done.

Rough glass slides were provided by Dr. Paolo Decuzzi from University of Texas (Huston, USA) with different roughness: 50 nm, 70 nm and 700 nm. Roughness of these samples was realized by following the procedure written in Gentile et al. (2010). In brief, glass surfaces were wet etched in a solution with ¼ of KOH and ¾ of H_2O at constant temperature of 70°C and at different times to reach different levels of roughness. The average surface roughness R_a and the root mean square roughness R_{rms} were measured over multiple regions of the substrates starting from the definition

$$R_a = \int_l \left| z(r) \right| dr/l \tag{7.1}$$

and

$$R_{rms} = \left(\int_l z(r)^2 \, dr/l \right)^{1/2} \tag{7.2}$$

where l is the sampling length and z(r) is the profile of the surface along the r direction, measured using AFM operating in tapping mode. Then, these surfaces were coated as explained in §7.3.1.

7.3.3 pMHC vs anti HLA

The study of the couple pMHC – anti HLA was done, together with the previous system of ICAM-1 – anti ICAM-1, in order to investigate the role of ligand lateral diffusion. By anchoring these molecules on the same fluid substrate, one can suppose that their diffusion follow the diffusion of lipids, so that the diffusion coefficient is the same for pMHC, ICAM-1 and lipids. Since the pMHC molecule is shorter than ICAM-1, according to the relation (6.1), its diffusion time should be smaller and an effect on the bond formation should be more evident.

A comparison between a fixed system and a fluid one was then executed. The

functionalization for pMHC is similar to the one for ICAM-1 – anti ICAM-1 and always at room temperature. Glass coverslips were covered with

1. 200 µl of PLL (Sigma Aldrich) solution at 50µg/ml in 0.2 µm-filtered phosphate buffer at 10^{-2}M and pH 7.4 with 0.01% of sodium azide;
2. 200 µl of glutaraldehyde (Sigma Aldrich) solution at 25 mg/ml in a 0.2 µm-filtered borate buffer at 10^{-1} M and pH 9.5 with 0.01% of sodium azide;
3. 200 µl-solution of BSA/biotin BSA (Sigma Aldrich) with a ratio 9:1 and at 100 µg/ml of concentration.
4. 200 µl of glycine (Sigma-Aldrich) solution at 0,2 M in a phosphate buffer at 0.1 M and pH 7.2 with 0.01% of sodium azide.;
5. 200 µl of streptavidin (Sigma Aldrich) at 10 µg/ml;
6. 200 µl of biotin R65 pMHC solution at different concentrations: 0.01, 0.02, 0.05, 0.5 µg/ml. The pMHC molecules are provided by Dr. Milos Aleksic (van der Merwe's laboratory, Oxford);
7. 200 µl of 0.2 µm-filtered BSA (Sigma-Aldrich) solution at 6%.

When it is not specified, the buffer in which the reagents are dissolved is PBS at 0.1 M and pH=7.4. Again, the incubation time for all the steps was 30 minutes, except for glycine (1 hour). After each step, slides were rinsed four time with PBS.

7.4 Grafting of mobile ligands on glass

To compare the effect of mobility in ligand-receptor interaction, the differences in adhesion between an immobile system, where coverslips were functionalized as described in §7.3.1 and a fluid one, were observed. In this last case, ligands were freely diffusing, since they where anchored in supported lipid bilayers (SLB) previously deposited on glass coverslips by Langmuir- Blodgett-Schaefer technique.

The comparison was made for two different couples of ligand and receptor: ICAM-1 – anti ICAM-1 and pMHC – anti HLA.

7.4.1 Langmuir-Blodgett-Schaefer technique

An amphiphilic molecule (or surfactant) is composed of two parts: a non-polar tail, like hydrocarbon chains and a polar head group. Irving Langmuir has demonstrated that amphiphilic molecules, such as fatty acids and their metal salts, have the ability to form stable monolayers at the air-water interface. The molecules in the monolayer have the hydrophilic head which is submerged into the water, and the hydrophobic tail that repels water. So that, the tail and therefore the whole molecule, tend to be orientated normally to the surface. This is perfectly obtained when the surface pressure becomes sufficiently high (Richardson et al., 1995).

Langmuir-Blodgett films are multilayer films where each layer is only a single molecule in thickness. They are formed by depositing single monoloyers on a substrate, one after the other.

Monolayer formation. Most of the surfactants that form monolayers are first dissolved in a proper solvent (often chloroform) and successively brought onto a subphase defined as the substance on which the monolayer is going to be formed. The most common subphase is Milli-Q water. This low ion-content ensures that the surfactant polar head will not be hybridized with minerals contained in natural water and therefore the properties of the monolayer are not modified.

At the air-water interface, water molecules undergo the action of lateral and downward cohesion forces. Because of a net force pulling them inwards, the molecules migrate from the surface to the bulk where no net force acts, until the number of surface versus bulk atoms is minimized and the equilibrium state is reached. This initial diffusion of molecules decreases the mean atomic separation and therefore increases the intermolecular force at the surface (Gengler thesis, 2010). The force acting on any surface is called surface tension γ: it is constant at equilibrium at a solid-gas interface but decreases when the temperature increases. Surface pressure is defined as the difference between the surface tension of pure subphase and the same subphase covered with molecules.

The injection of few micrograms of surfactant at the air-water interface will

make molecules spread over the available surface area. When an external force is applied on those floating molecules, their positions in the water will be affected and finally, if compression is sufficient, a solid film will be created. This compression of the monolayer goes through several phase transitions which are two-dimensional analogues to gas, liquid and solid states of matter (Adamson & Gast, 1997). The phase diagram of a given surfactant can then be identified simply by measuring an isotherm, *i.e.* pressure versus area per molecule at constant temperature (Fig.7.6).

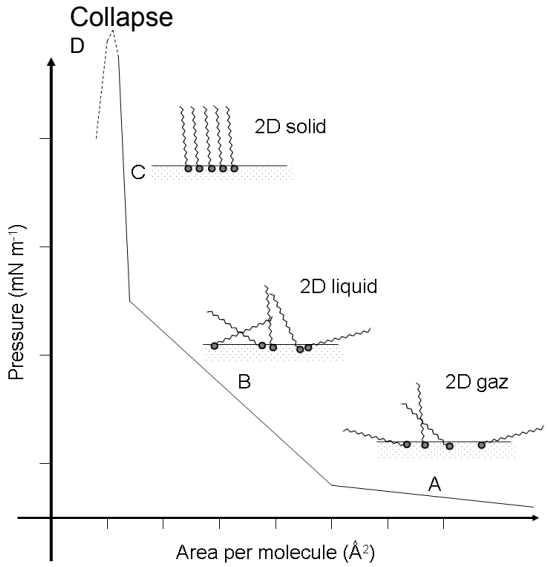

Figure 7.6 Example of isotherm showing all the transition phases that the lipids can follow by changing the pressure of these molecules. **A:** gas phase with not oriented molecules and far from each other. **B:** liquid phase with more packed molecules. **C:** solid phase where molecules are densely packed and well arranged. Formation of the monolayer. **D:** collapse after which the pressure decreases and one can observe the local formation of multilayers. Picture from Régis Yves Norbert Gengler thesis (2010, Zernike Institute for Advanced Materials, University of Groningen, the Netherlands.)

- *2D gas state formation*. Just after the dispersion of the molecules on the surface and the evaporation of the solvent (chloroform), a 2D gas state is formed with large distances between the molecules. If one compresses the molecules, it is possible to reach the 2D pressure of the surfactant of ~1 mN/m.
- *Gas-liquid transition*. Further compression leads to a first transition from gas to liquid in which the molecules are arranged in a more coherent way but still quite distant from each other.
- *Liquid-solid transition*. By going on with the compression, a next phase

transition (liquid to solid) is visible; at this stage the molecules are densely packed and any further compression leads to a rapid increase in surface pressure.

- *Collapse*. Applying more pressure to the monolayer induces a collapse. When this phase is reached, a decrease in pressure is visible and the monolayer becomes locally a multilayer. This is the reason why the state chosen for the film deposition is therefore the solid state (monolayer).

Equipment. A film balance consists mainly of four elements (Fig.7.7):

1. the trough made in teflon, where the lipid solution is spread together with the subphase;
2. the pressure sensor or Wilhelmy plate, which measures the change in surface pressure after addition of a surfactant. The principle is rather simple: a very thin filter paper is partially immersed in water. One can deduce the surface pressure simply by measuring the change of force acting on the paper with and without a molecular film present at the surface. This force, registered as an increased weight, is then measured by a very sensitive microbalance (typical sensitivity of about 0.01 mN/m);
3. a mobile teflon barrier, to compress the film until the desired pressure is reached. The barrier motors is automatically controlled by a sophisticated feedback mechanism, in order to keep the surface pressure constant;
4. a dipper, that allows for controlled immersion and extraction of the substrate.

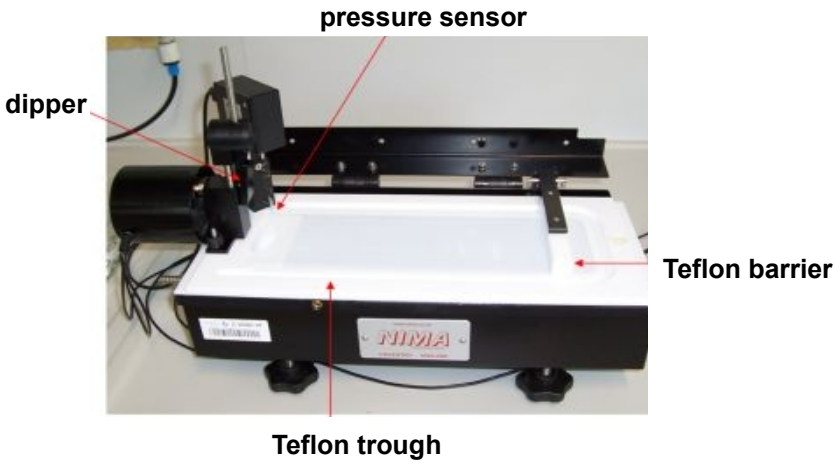

Figure 7.7 Film balance for Langmuir-Blodgett-Schaefer films, showing all the components: the teflon trough on which the lipid solution is dropped; the dipper which allows to immerse and extract the glass coverslips where the lipid layers are deposited; the mobile teflon barrier that compresses the film until the right pressure is reached; finally, the pressure sensor that measures the pressure exerted by the solution on the thin filter paper.

The trough used for this work was a NIMA Langmuir-Blodgett trough, controlled by a software developed by the provider and running on a computer.

Methods. The method used in this work for deposition of bilayer on solid substrates is the Langmuir-Blodgett-Schaefer:

1. For the first layer deposition it was used the Langmuir-Blodgett technique. The lipid mixture, dissolved in chloroform, is dropped onto the water surface and an hydrophilic glass substrate is immersed in the trough with the dipper. The chloroform evaporates, leaving an oriented lipid monolayer. The mobile teflon barrier compresses the monolayer until the desired surface-pressure is reached. The substrate is then drawn slowly up and the surface perpendicular to the water-surface is coated with the adsorbed lipids which form a monolayer: this is the first layer of the bilayer (Fig. 7.8). At the same time, the surface-pressure is maintained by a feedback mechanism that closes the barrier when necessary.

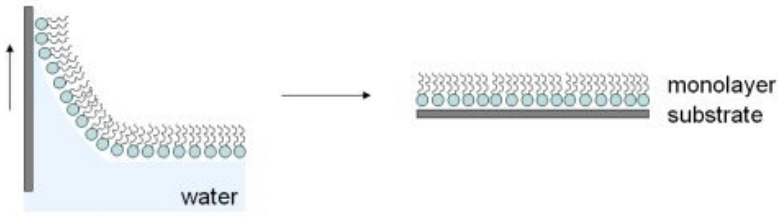

Figure 7.8 Langmuir-Blodgett deposition on solid substrate. The glass slide is slowly pulled up from the solution with lipids and the monolayer is adhering on it. This also called vertical deposition (picture from Jülich Research Centre website).

2. The second lipid layer was deposited with the Langmuir-Schaefer technique. Again, the lipid mixture is dropped onto the water surface and the desired surface-pressure. The substrate, previously coated with a monolayer is pressed horizontally through the water surface and the second lipid monolayer is transferred (Fig. 7.9).

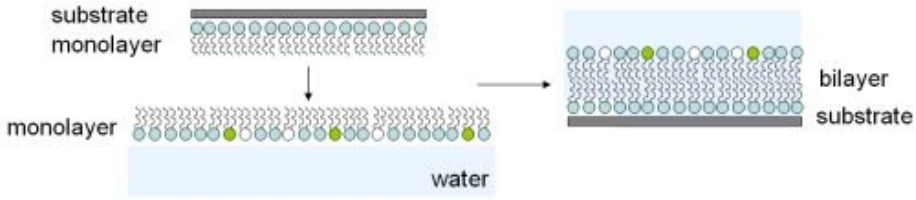

Figure 7.9 Langmuir-Schaefer deposition on solid substrate. The glass slide with the first monolayer is horizontally dipped into the liquid solution in order to ensure the adhesion of the second layer through the lipid tails. This technique is also called horizontal deposition (picture from Jülich Research Centre website).

7.4.2 ICAM-1 – anti ICAM-1 functionalization

The deposition of supported lipid bilayers (SLB) was realized on clean glass coverslips. The first monolayer was done by using the Langmuir-Blodgett vertical method, while the second layer was deposited by the horizontal method (Langmuir-Schaefer). All lipids were purchased from Avanti Polar Lipids (Alabama, USA). The film deposition was performed at a temperature of 25°C and a surface pressure of 25 mN/m. The lipids used for the SLB deposition were all phospholipids (Fig.7.10), a class

of lipids which represent the major component of all cell membranes.

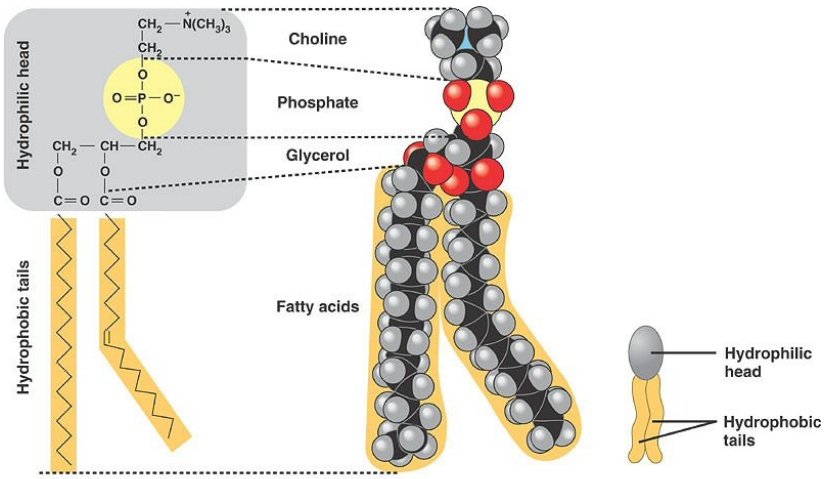

Figure 7.10 Schematic representation of a phospholipid. The glycerol portion of the molecule is between the two fatty acids (below) and the phosphate group with some methyl and amino groups (above). (http://kvhs.nbed.nb.ca/gallant/biology/phospholipid_structure.jpg)

The lipid mixture, dissolved in chloroform, used for the SLB was the following:

- DOPC (1,2-dioleoyl-*sn*-glycero-3-phosphocholine) or DPPC lipids (1,2-dipalmitoyl-*sn*-glycero-3-phosphocholine) as matrix, at 1mg/ml in chloroform. Bilayer formed with DPPC lipids are not fluid at room temperature, so they were used as negative control in the comparison with bilayers constituted by the fluid DOPC lipids. This difference is due to the fact that the DOPC lipid has 18 carbons and one double bond, while the DPPC has only 16 carbons and no double bond. Indeed, the double bond has an important role in determining fluidity: a cis- double bond strongly increases fluidity.
- DMPE peg 2000 lipids (1,2-dimyristoyl-sn-glycero-3-phosphoethanolamine-N-[methoxy (polyethylene glycol)-2000]) to sterically decrease the possibility of unspecific binding, at 0.3% of the mole of matrix lipids;
- fluorescently labelled bodipy C12 (4,4-difluoro-4-bora-3a,4a-diaza-s-indacene) from Molecular Probe (Invitrogen) at 0.1% of the mole of matrix lipids, to measure the fluidity of the bilayer by recovery after photobleaching;
- NTA DOGS lipids (1,2-di-(9Z-octadecenoyl)-*sn*-glycero-3-[(N-(5-amino-1-carboxypentyl) iminodiacetic acid)succinyl] (nickel salt)) at concentrations

which varied from $0.4x10^{-4}$% to 10^{-4}% of the mole of matrix lipids, to bind his tagged proteins. These concentrations allow to have a density of NTA lipids of 1 lipid every 10^6 DOPC lipids, namely ~1 lipid/μm^2.

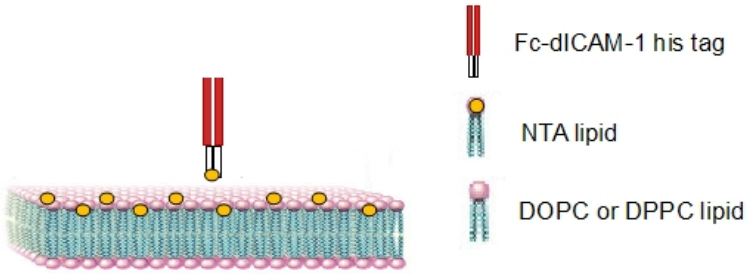

Figure 7.11 Schema of ICAM-1 – anti ICAM-1 construction on supported lipid bilayers for flow chamber experiments. SLBs with DOPC as matrix and NTA DOGS lipids are deposited on glass coverslip and then functionalized with Fc-dICAM-1 his tag.

The fluidity of bilayer was checked after deposition by using continuous photobleaching (CP) in fluorescence to measure the diffusion coefficient of bodipy lipids. This technique will be later explained (§9.5.1).

Once the SLB was deposited on the slide, the sample was coated with:

1. 100 µl of a solution of BSA (Sigma-Aldrich) at 0.3%;
2. 250 µl of FcICAM-1 at 2.5 µg/ml in PBS (last step for flow chamber assay);

Slides were rinsed four times in PBS after each step whose incubation time was 30 minutes except for FcICAM-1 (45 minutes).

7.4.3 pMHC – anti HLA functionalization

SLB were deposited on clean glass coverslips by using the Langmuir-Blodgett-Schaefer technique. The lipid solution used to build the SLB was composed as follows:

- DOPC lipids at 1mg/ml;
- DOPE (1,2-dioleoyl-*sn*-glycero-3-phosphoethanolamine) cap biotin at concentrations which varied from 0.002% to 2%;
- fluorescently labelled bodipy lipids at 2 µg/ml in chloroform.

The film deposition was performed at a temperature of 25°C and a surface pressure of

25 mN/m. Immediately after deposition, the fluidity of bilayer was checked in CP to measure the diffusion coefficient of bodipy lipids.

Successively, slides were coated with:

1. 200 µl of a solution of BSA (Sigma Aldrich) at 0.5%;
2. 200 µl of streptavidin (Sigma Aldrich) solution at 1 µg/ml;
3. 200 µl of biotin pMHC R65 at different concentrations (0.01, 0.05 and 0.5 µg/ml) provided by Dr. Milos Aleksic (Anton van der Merwe's laboratory, Oxford);
4. 200 µl of BSA solution at 6%.

Incubation time for each step was 30 minutes and after each coating slides were rinsed four times with PBS.

Chapter 8

Laminar flow chamber

A laminar flow chamber is an *in vitro* device that can simulate *in vivo* fluid shear-stress on different cell types subjected to dynamic flow in their physiological environment. However, in this study a very low shear rate was used to apply low forces on bonds and monitor their formation and dissociation.

The flow chamber consists of a polymethyl methacrylate (PMMA or plexiglas) transparent distributor and a gasket (in our case this is represented by 4 layers of tape). A glass coverslip is fixed on top of the gasket by a screwed piece of aluminium. The distributor, forming one side of the parallel-plate flow chamber, includes inlet and outlet ports. The thickness of the gasket determines the height of the flow path. The glass coverslip forming another side of the flow chamber, can be coated with ECM proteins, vascular cells, or biomaterials of interest. Typically, the fluid enters one side of the chamber and leaves from an opposite side. The laminar flow chamber is capable of producing well-defined wall shear-stress in the physiological range of 0.01-30 dyn/cm^2. Shear stress is generated by flowing fluid through the chamber over the immobilized substrate under controlled kinematic conditions using a syringe pump. The fluid contains a suspension of cells or microspheres.

In case of flow chamber assays for the couple ICAM-1 – anti ICAM-1 on SLB, the chamber was round with teflon insert.

A

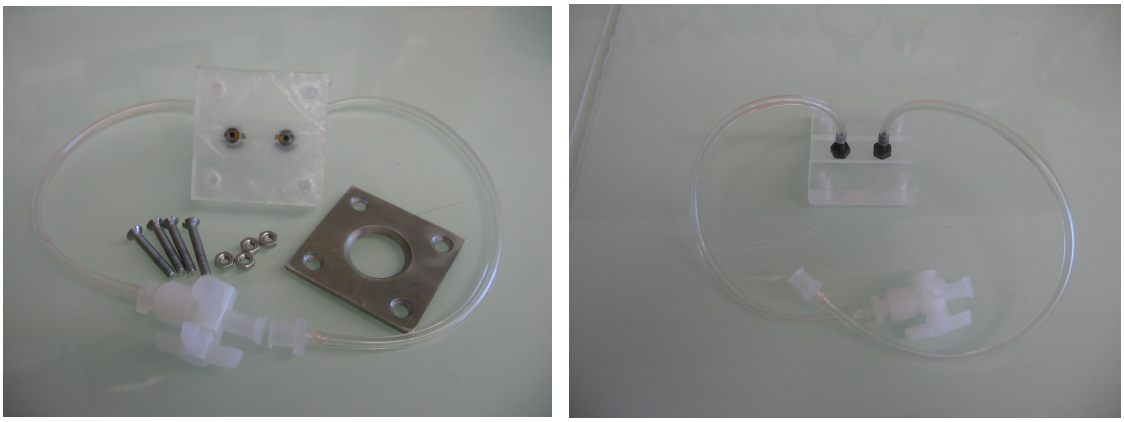

B

Figure 8.1 Pictures of the two models of flow chamber used for this project. A: a model realised in the laboratory by Philippe Robert, with dimension of 4x4x1 cm^3 and the polish bottom to improve the contrast. B: A modified round chamber with teflon insert used for supported lipid bilayer.

With this technique one can observed the sample at the microscope both in transmission and in fluorescence.

8.1 Beads functionalization

The microspheres used for flow chamber trials are paramagnetic polystyrene beads, charged with iron oxide, with 4.5 µm of diameter and 1500 kg/m^3-density

(tosylactivated Dynabeads M450, Invitrogen). Tosylactivated Dynabeads M-450 possess reactive sulphonyl esters that can interact covalently with proteins such as antibodies or other ligands containing primary amino or sulphydryl groups, increasing the number of covalent bonds with higher temperature and pH. These beads improve the orientation of the antibody they have bound, thanks to their slight hydrophobia.

Figure 8.2 Dynal MPC-E magnet. This instrument, which can support six tubes of 1.5 ml, allows to separate the pellet from the supernatant which is repeatedly removed.

The beads functionalization with two layers of antibodies followed the protocol suggested by the provider:

1. 25 µl of M450 Dynabeads, which correspond to 5 µg of microspheres, were put in a tube placed in a magnet (Dynal MPC-E, Invitrogen), in order to separate the beads from their solvent which was then removed.
2. Subsequently, the microspheres were rinsed twice with 1 ml of borate buffer at 10^{-1} M and pH 9.5 with 0.01% of sodium azide and put again in the magnet to discard the supernatant.
3. 30 minute of incubation at 37°C with 5 µg of rat anti-mouse Fc fragment antibody (AbD Serotec) in 1 ml of borate buffer took place. The physical adsorption of the ligand to the bead surface is rapid, while the formation of covalent bonds will need more time.
4. Afterwards, a solution of BSA with final concentration of 1 mg/ml was introduced in the tube and incubated for all night at 37°C with gentle tilting and rotation.
5. After the night, the microspheres were rinsed with 1 ml of PBS and put in the

magnet to separate the supernatant.

6. A solution with 10 µg of mouse anti-human ICAM-1 clone HA58 (eBioscience) or mouse anti-human HLA A2 (AbD Serotec) for test beads and mouse IgG1 K isotype control (eBioscience) or goat anti-histidine tag (AbD Serotec) for control beads in PBS was introduced in the tube to create the second layer of antibody on the surface of the microspheres. This incubation lasted 30 minutes at 37°C.
7. Then, beads were stored at 4°C with 0.1% of BSA and 0.1% of sodium azide and ready to be used.

When used supported lipid bilayer to investigate the role of mobility in the interaction between adhesion proteins, the M450 beads were coated both with one or two layers of antibody. In the first case, the followed protocol was the same as the one described above, but the step 1 was replaced by the step 6.

Fig.8.3 illustrates the interaction between the glass surface and the beads.

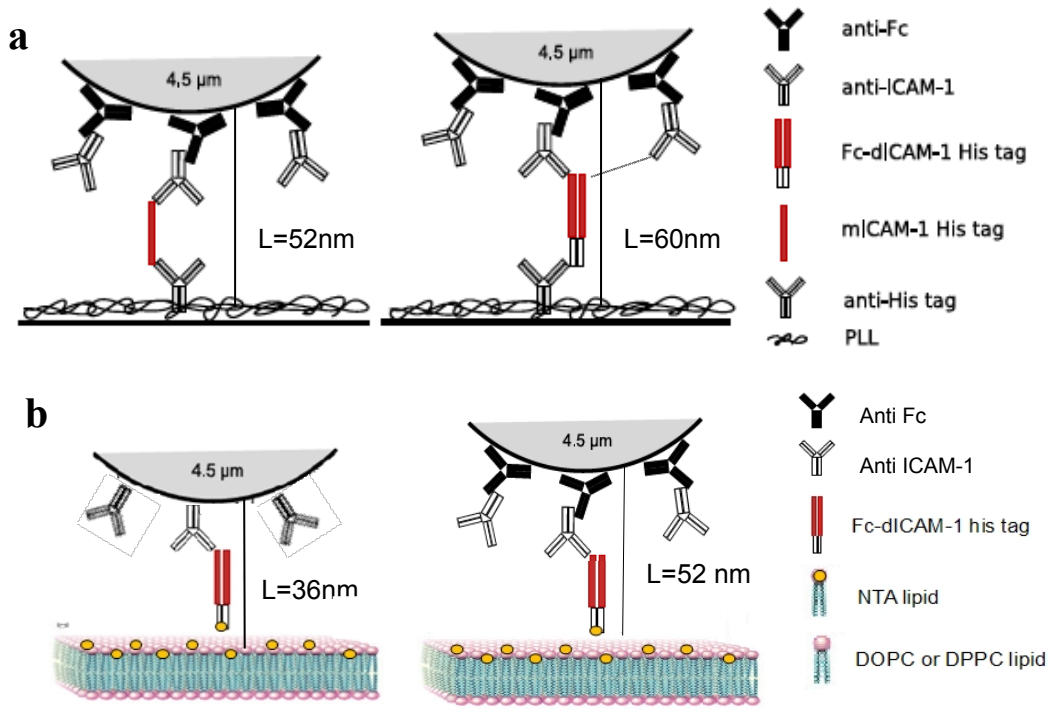

Figure 8.3 a: Scheme of ICAM-1 – anti ICAM-1 construction for flow chamber experiments. Glass coverslip is functionalized with PLL, anti-his tag antibody and mICAM-1 or Fc-dICAM-1. Beads are coated with an anti-mouse Fc fragment antibody and the anti ICAM-1. **b:** Scheme of ICAM-1 – anti ICAM-1 construction on supported lipid bilayers for flow chamber experiments. SLBs with DOPC as matrix and NTA DOGS lipids are deposited on glass coverslip and then functionalized with Fc-dICAM-1 his tag. Beads are coated with an anti-mouse Fc fragment antibody and the anti ICAM-1 (2 layers beads), or only with anti ICAM-1 (1 layer beads).

8.2 Realization of experiments

The flow chamber is mounted on an inverse optical microscope Zeiss Axio Observer D1 (Zeiss, Germany) or an Olympus CK40 (Olympus, Japan). The objectives which were used have a magnification of 10x and 20x (Olympus, Japan and Zeiss, France). A flux is pumped through a pipe on the flow chamber by a syringe mounted on a syringe pump Razel A-99 (Razel, USA) or an automatic syringe pump NE500 (ProSense B.V., Munich, Germany) controlled by a homemade program written in Labview. An other pipe allows the flow to exit the chamber. Through the syringe pump it is possible to vary the velocity of the flux and consequently the shear rate.

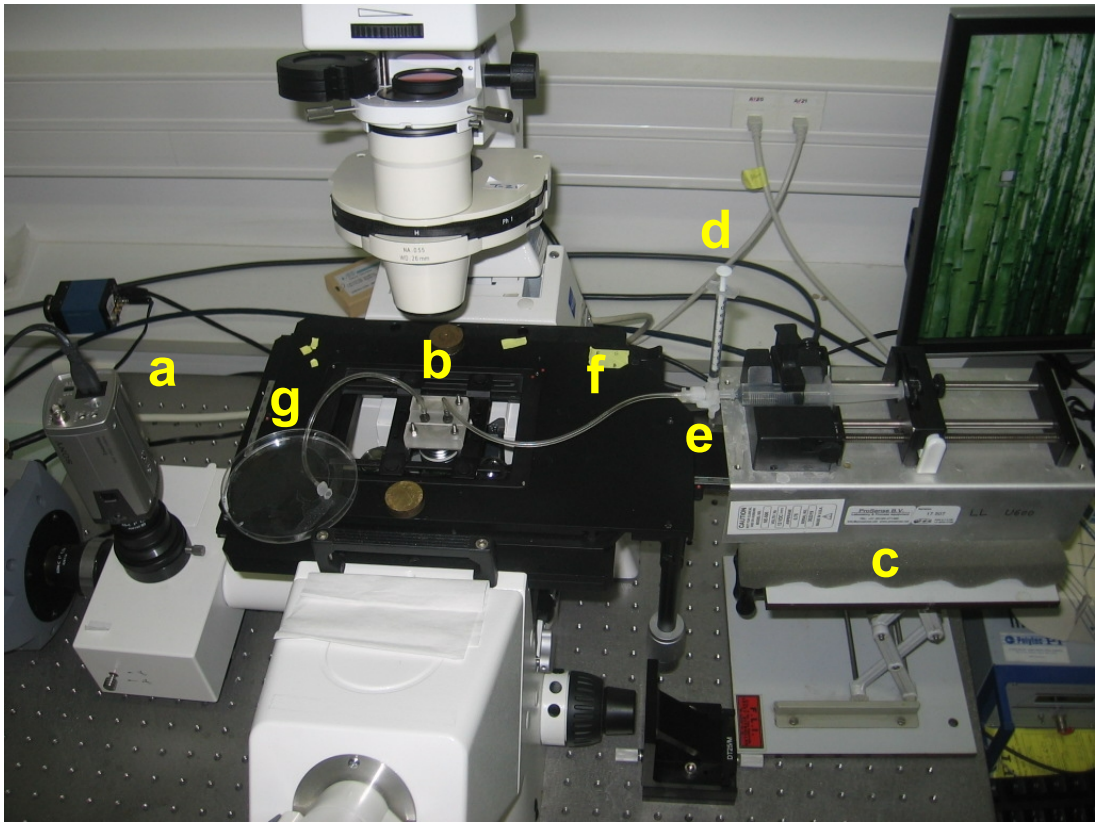

Figure 8.4 Flow chamber apparatus with the chamber mounted on an inverted microscope. **a:** standard video camera. **b:** chamber. **c:** syringe pump supporting a 10ml syringe with the flow solution (PBS+BSA). **d:** syringe used to inject the microspheres. **e:** valve with three entries/exits. **f:** pipe for the flow entry. **g:** pipe for the flow exit.

8.3 Acquisition of video signal

A standard video camera Sony N5 (Sony, Japan), is mounted on an inverse microscope in order to record the displacements of particles in flow. A pixelsize of 1 µm and 0.5 µm is achieved by using the two objectives defined above. The theoretical acquisition speed is 25 images per second. A process involving the signal acquisition features of the video camera allows to double the acquisition frequency of the camera. So that, it is possible to record an image in two series of lines: firstly, odd lines in 1/50 s, then even lines again in 1/50 s. The two half-images are assembled in order to form a total image each 1/25 s; this image is called interlaced. The separation in two half-images and the reassembly of their chronological interval allows to obtain an acquisition frequency of 50 images per second; this operation is the disinterlacing. The final acquisition frequency of this experimental set up is then 50 images per second.

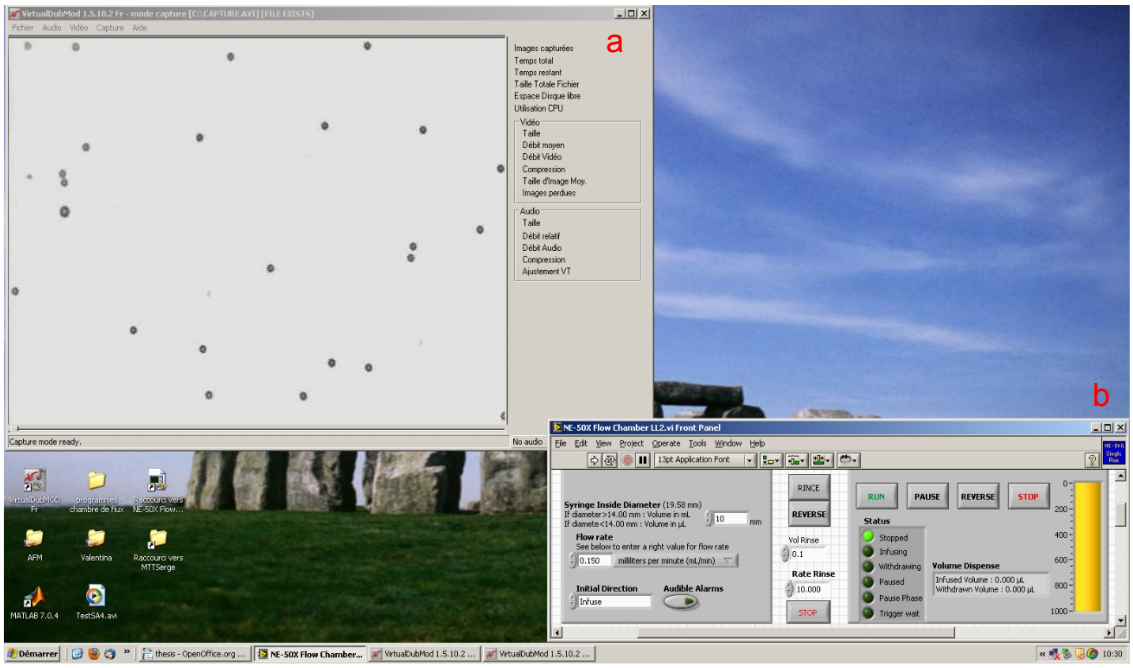

Figure 8.5 **a:** image of film where anti ICAM-1 coated beads are flowing on an ICAM-1 functionalized coverslip. The homogeneity of the surface is shown by the good contrast reached with VirtualDub. The dimensions of the image are 360x240 µm². **b:** window of Labview program which controls the syringe on the syringe pump.

8.4 Data storage and analysis

The analogical signal of the video camera is digitized through a computer equipped with a Win-TV card sold as TV signal receiver (Hauppauge, Germany). A freeware called VirtualDubMod, written for video mounting, allows to show the signal of the card, record it as video file, compress it in real time with the desired algorithm of compression and save it on the hard disk. The algorithm of compression used in the laboratory is the open source DivX 5.1.1.

The analysis of flow chamber data consists in measuring the displacement of microspheres from the recorded films. Indeed, it is possible to detect spatial and temporal coordinates of each particle starting from its trajectory, possibly adding other parameters such as the particle surface area. The contrast between the particle and the substrate is very important while the realization of the flow chamber experiment. Indeed, the substrate must be homogeneous while looking at it with the microscope. The method which has been used consists in detecting particles while they enter an observed area. An homemade software called Suitavi, written in the laboratory by the Professor Bongrand, is able to determine the position of particles from the films. It reads the compressed video file and detects the particle border through a luminosity contrast versus the background (Fig. 8.6a). The particle centre and the surface area are computed and the coordinates of the particle are recorded in the current image. The software executes such computations on the next images. At the end of this procedure, a folder is produced with one file for each detected particle, containing a table which reports image number, spatial and temporal coordinates and surface area for each image where the particle was detected. It is possible to speed up the process by using several computers in parallel.

From the table of spatial and temporal coordinates of each particle it is possible to represent the trajectory as a function of the time. This representation can be realized through a program written in the laboratory by Dr. Laurent Limozin using IgorPro software (Wavemetrics, USA). This program, called Arrestsuitavi, is able to establish the number of arrests observed and their duration along with the cover distance and the

velocity of the particles.

Beads trajectories are determined with a time resolution of 20 ms and a lateral one of 40 nm. An arrest is defined as a part of trajectory where the particle has a displacement shorter than a threshold distance set at 0.5 μm during 0.2 s, and the duration while the particle displacement verify this condition is called duration of arrest. Only the trajectories of settled microshperes whose height corresponds to the Boltzmann distribution at the equilibrium have to be considered (§4.1.1). For each trajectory one can estimate the velocity of the particle at every position in an interval of ten positions. Then an histogram of particles velocities is drawn (Fig. 8.6d). Thresholds for the minimal and maximal velocity are manually chosen at the tails of the distribution corresponding to the settled beads. The space (AF) and time (AF') adhesion frequency is computed as follow:

$$AF = N / \left(\sum_{k=1}^{N} d_k \right) \quad \text{or} \tag{8.1}$$

$$AF' = N / \left(\sum_{k=1}^{N} t_k \right) \tag{8.2}$$

where d_k and t_k are respectively the distance and the duration of the particles whose velocity belongs to the chosen interval of velocity, and N is the total number of arrests. The adhesion frequency can be measured either in mm^{-1} or s^{-1}.

Errors during the detection of arrests. The Arrestsuitavi program presents some extra functions to identify errors during the detection of arrests. A detected arrest has to meet a certain number of criteria on area and velocity before and after the arrest to be validated.

The velocity of the particle before the arrest. One has to take into account only arrests of settled microspheres whose height corresponds to the Boltzmann distribution at the equilibrium.

The velocity of the particle after the arrest. When a settled microsphere stops and an other microsphere passes on top of the previous one, the program wrongly detects the detachment of the fixed bead; hence, the arrest duration is false. The criterion for the velocity after arrests allows to detect these kind of situations identifying

when the velocity of the particle is too high for a settled bead. In this case, the arrest is taken into account for estimating the adhesion frequency but its duration is considered unknown and it is not included for the detachment curves.

The area of the particle has to be in a certain range of areas indicating the possible area of a single microsphere. This range is previously chosen. This criterion allows to detect situations where a followed bead stops because it encounters another fixed bead: the apparent area of the microsphere suddenly increases.

Errors during the detection of covered distances. When a moving microsphere gets in contact with either fixed or slower ones, the Suitavi software may assign its trajectory to them, altering the computation of the adhesion frequency. This is a frequent error due to the fact that Suitavi searches the current particle position downstream of its previous position. Thus, if a faster particle appears between the two positions, its trajectory will be considered as the sequel of the former particle. Arrestsuitavi owns a function able to detect such errors by assessing the similarity of the detected trajectories (Robert, thesis 2009)

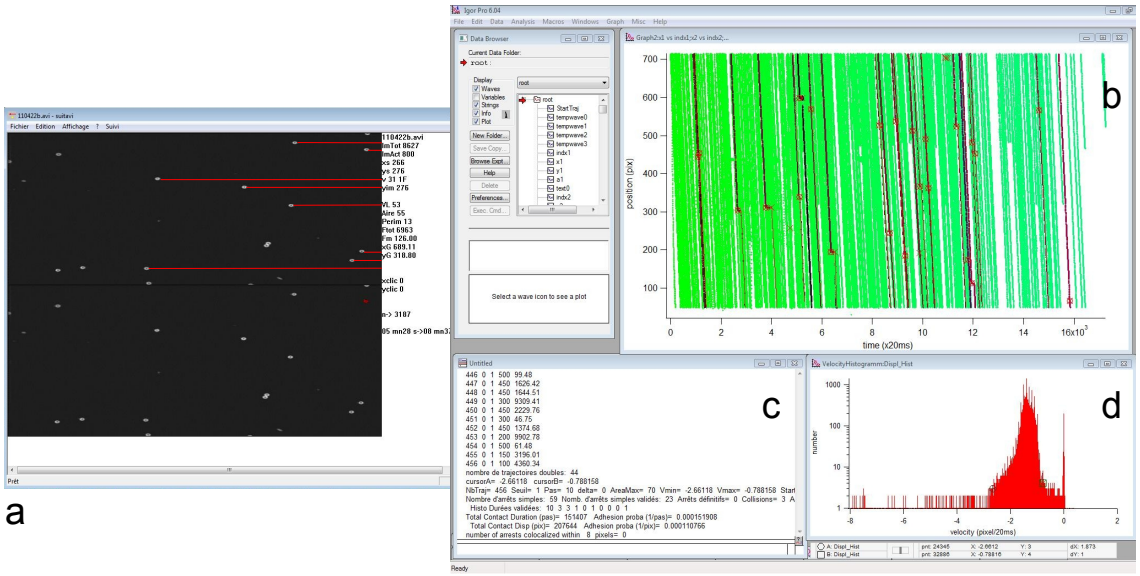

Fig. 8.6 **a:** window of Suitavi program working on Microsoft Windows XP Professional. The upper half image is formed by the even lines, the second half image is formed by the odd lines. The detected trajectories are represented by red lines on the upper half image. On the right, screen snap while using Arrestsuitavi for the trajectories analysis. **b:** representation of the microspheres' trajectories. **c**: command window of the software. **d:** histogram of beads velocity. The velocity is negative for convention. The value of the velocity at the peak on the left corresponds to the velocity of the sedimented beads, while the value of the velocity at the peak on the right, close to zero, represents the velocity of the arrested beads.

Chapter 9

Experiments in fluorescence

9.1 Epi-fluorescence microscopy

Fluorescence is the emission of light that occurs within nanoseconds after the absorption of light that has necessarily a shorter wavelength. The difference between the exciting and emitted wavelengths, known as the Stokes shift, is a critical property of fluorescence.

Fluorescence microscopy is often used to study properties of organic or inorganic substances. The principle is the following: a sample is illuminated with light of a specific wavelength which is absorbed by the fluorophores, causing them to emit light of longer wavelength (Swift & Trinkle-Mulcahy, 2004). The illumination light is separated from the emitted fluorescence through a spectral emission filter. Typical components of a fluorescence microscope are a light source, the excitation and emission filters, the dichroic mirror. The filters and the dichroic are chosen to match the spectral characteristics of the fluorophore used to label the sample under study. Most fluorescence microscopes in use works in epi-fluorescence where excitation and observation of the fluorescence are from above (epi–) the sample. The excitation light passes above (or, for inverted microscopes, below), through the objective lens and then onto the sample. The fluorescence in the sample generates an emitted light which is focused to the detector by the objective. Since most of the excitation light is transmitted

through the sample, only the reflected one reaches the objective together with the emitted light giving an improved signal-to-noise ratio. Another filter between the objective and the detector can discriminate and then filter out the excitation light from the fluorescent one. Since fluorescence microscopy requires intense, monochromatic illumination, the two main types of light source used are xenon or mercury lamp with an excitation filter, and lasers.

9.2 TIRF microscopy

Total internal reflection fluorescence microscopy (TIRFM) allows to use the unique properties of an induced evanescent wave in a limited region of a sample immediately adjacent to the interface between two media having different refractive indices. The most commonly used interface in the application of TIRFM is the contact area between an aqueous sample and a glass coverslip which supports the sample (Axelrod, 2008).

In the physical phenomenon of total internal reflection (TIR), a collimated light beam that comes from one medium to a second one, reaches the interface between the two media where it can be either refracted, or reflected, depending on the incident angle and the difference in refractive indices of the two media. A refractive behaviour of the beam light governed by the Snell's law:

$$n_1 \times \sin\theta_1 = n_2 \times \sin\theta_2 \tag{9.1}$$

where n_1 and n_2 are respectively the higher and the lower refractive index. θ_1 represents the angle that the incident beam forms with the normal to the interface, while θ_2 is the refracted beam angle. TIR is possible in situations in which the beam light comes from the medium with lower refractive index to the one with lower refractive index. When light strikes the interface of the two materials at a sufficiently high angle, called the critical angle ($\theta_c=\arcsin(n_2/n_1)$), its refraction direction becomes parallel to the interface. By increasing even more the angle the beam light is reflected entirely back into the first medium.

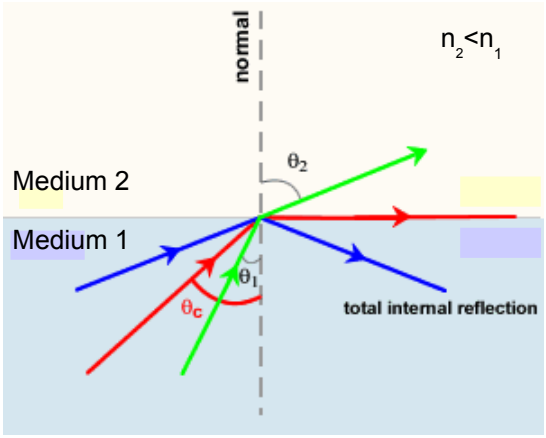

Figure 9.1 Representation of the refracted and reflected behaviour of a beam light which propagates through a medium with a refractive index n_1 to another one with a refractive index $n_2<n_1$. The green arrows show the refraction when the incident angle θ_1 is smaller than the refracted one θ_2. In red it is shown the behaviour of the beam when the critical angle θ_c is reached and the refracted beam is parallel to the interface. The blue arrows describe the the total internal reflection of the incident beam when the incident angle is bigger than θ_c.

However, the reflected light generates a highly restricted electromagnetic field adjacent to the interface which has the same frequency as the incident light. Since the field decreases exponentially from the interface, it penetrates to a depth of only approximately 100-200 nm into the sample. Confinement of the secondary fluorescence emission to a very thin region allows to avoid excitation of fluorophores in the bulk of the specimen, leading to a much higher signal-to-noise ratio compared to conventional epi-fluorescence. This enhanced signal level is the reason why TIRFM is extremely useful in any application requiring imaging of single molecules in samples having large numbers of fluorophores located outside of the optical plane of interest, such as molecules in solution in Brownian motion, or single protein trafficking in cells. TIRFM is an ideal technique to investigate both the mechanisms and dynamics of many proteins involved in cell-cell interactions (Lieto et al., 2003).

9.3 Quantum dots

Quantum dots (Qdot) are fluorescent nanocrystals capable to absorb light and re-emit photons at a different wavelength. They are atom clusters with 15 – 20 nm of diameter constituted by:

- a core made up of a semiconductor material (often cadmium mixed with selenium or tellurium);
- a semiconductor shell (zinc sulphide) surrounding the core and improving both the optical and physical properties of the material;
- an amphiphilic polymer coating which surrounds the core and the shell. It provides a water-soluble surface that can be modified depending on specific assay requirements.

Qdot's intrinsic brightness is many times higher than traditional organic fluorophores, and their photostability is many orders of magnitude greater. After absorption of a photon of light, Qdot fluorescence is due to the formation of excitons which typically exhibits a much longer lifetime (up to ~200 nanoseconds) than usual fluorophores do, a property that can be advantageous in long timescale detection studies. However, these nanoparticles are subjected to blinking, the property of turning continuously on and off which can often make difficult their detection and consequently the possibility of following them.

Fluorescent experiments with Qdot were here performed in order to estimate the ligand density on surface by simply counting the number of Qdot, to measure the diffusion coefficient of ligands on supported lipid bilayer by following the Qdot trajectories and to determine the dissociation rate of a bond at higher timescale than with flow chamber.

9.4 Measurement of ligand density on surface

To investigate the interaction between ligand and receptor in flow chamber, it is important to measure the density of ligand on the surface in order to ensure that one is

working at very low concentration and be able to study single molecule bonds. Density measurements were performed in fluorescence in two different ways: i) analysing the fluorescent signal of the labelled anti ICAM-1, or ii) counting the number of Qdot present on the surface.

9.4.1 Intensity measurements

To perform this type of measurement in epi-fluorescence, coverslips were coated as explained in §7.3. However, after the last step of BSA passivation, a 200 µl-solution of phycoerythrin (PE) mouse anti-human ICAM-1 clone HA58 (eBioscience, San Diego, California, USA) at 10 µg/ml was incubated on the surface for 30 minutes. The slides were then rinsed four times in PBS and covered with glass cover slides. Successively, the coverslips were put on an inverse microscope Axio Observer D1 (Zeiss, France), equipped with a 100x objective with numerical aperture (NA) 1.4 and observed through an Andor iXon camera running on iQ software (Andor, Belfast,UK). The signal detected from these slides was compared to the signals measured from a series of calibrated samples. These last samples were obtained putting 5 µl of PE anti ICAM-1 solution on coverslips which were then covered with glass slides, creating a space of 10 µm in height. The concentration of PE anti ICAM-1 was changed systematically, in order to have different intensities of signal, and the number of molecules in the volume was computed leading to the following densities: 0.1, 0.3, 0.9, 2.7 and 8 molecules/µm². Then, a comparison between the intensities of these calibrated samples with the test sample gave the density of molecules grafted to the surface.

9.4.2 Single-particle counting

In order to measure the surface density of ligands, single-particle tracking (SPT) in epi-fluorescence or TIRF was carried out. Slides were functionalized as described in

§7.3 and another step was done at the end: a 200 µl-solution composed by 10 nM of streptavidin Qdot (Invitrogen, Carlsbad, California, USA) with wavelength emission at 605nm, 10 nM of biotin anti ICAM-1 clone HA58 (eBioscience, San Diego, California, USA) for ICAM-1 – anti ICAM-1 interaction, or anti-human HLA A2 (AbD Serotec) for pMHC – anti HLA bond, and BSA at 6 µg/ml in PBS was added on slides.

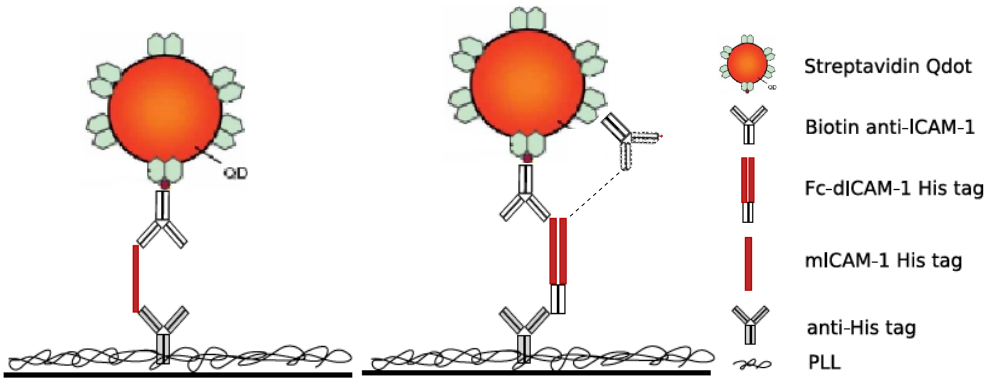

Figure 9.2 Schema of ICAM-1 – anti ICAM-1 construction for fluorescence experiments. Glass coverslip is functionalized with PLL, anti-his tag antibody and mICAM-1 or Fc-dICAM-1. 605 streptavidin quantum dots are coated with the biotin anti ICAM-1.

In case of TIRF trials, an inverted Axiovert 200M microscope (Zeiss) with a polarized laser (series 77, Lasos lasertechnik GmbH Zeiss, Jena, Germany) together with a 100x objective with NA 1.4 and a filter cube with excitation=458/10, dichroic=470 and emission=605/40 were used. Experiments were performed at a temperature of 20°C. Slides were coated as described in §7.3 and mounted on round chambers with a teflon insert (Fig.8.1B). The observation at the microscope occurred immediately after the injection of Qdot+anti ICAM-1 solution. For each sample a series of images for different fields was taken, in order to reach a satisfied statistics.

An inverted Axio Observer D1 (Zeiss) mounting a 100x objective with NA 1.4, and a filter cube for Qdot (Semrock, Rochester New York, USA) with excitation=435/40, dichroic=470 and emission=605/40 were used to realize epi-fluorescence trials. The functionalization of slides was the same as for TIRF experiments, but sample were incubated for 15 min with a Qdot+anti ICAM-1 solution, then rinsed four times in PBS before being observed in fluorescence. For each sample a series of images for different fields was taken.

Sequences of images were recorded with an iXon camera running on iQ software (Andor), at 10Hz frequency and using an exposure time of 100 ms. The density of Fc-ICAM-1 or ICAM-1 molecules lying on the surface was estimated by directly counting the number of Qdot through a multiple-target tracking (MTT) algorithm (Sergé et al., 2008). Slides functionalized without anti ICAM-1 were used as control and the real density of ligands on the surface was estimated as the difference between the number of Qdot on test slides and on control surfaces, working with a very high ratio specific/non specific.

The recorded films were then analysed by using the MTT algorithm, by introducing the following values: r_0=185 nm=2.3 pix is the radius of the two-dimensional Gaussian used to determine the Qdot position; I=3000 and I=1000 as threshold for the lowest, detectable particle intensity in case of epi-fluorescence and TIRF respectively. The different values of the intensity depend on the different background intensity of the two Andor camera used for the two fluorescent techniques. Indeed, the camera used for TIRF experiment has a lower background intensity (300) compared to the one used for epi-fluorescence (1000). In this way, it was possible to estimate and record the coordinates and the intensity of each dot as function of time. This parameters were then treated with IgorPro software in which some small home-written macros allow to check the reliability of the number of detected dots by superimposing them on the recorder images; the distribution of intensities and the signal-to-noise ratio by comparison with the background.

9.5 Measurement of diffusion coefficient

In realizing experiments to compare an immobile system with a fluid one where the molecules under study are anchored on SLB, it was necessary to verify the diffusion of lipids and ligands. To measure the diffusion coefficient of lipids, trials in Continuous Photobleaching (CP) were performed, while in case of diffusion coefficient of ligands, single molecules were followed with SPT.

9.5.1 Continuous Photobleaching for lipid diffusion

Before analysing the kinetics of ligand – receptor interaction in case of fluid system, it was fundamental to measure the diffusion coefficient of lipids constituting the SLB by using the Continuous Photobleaching.

The CP technique is based on the bleaching property (decrease in fluorescence intensity during fluorescence imaging) of some fluorophores. "Photobleaching is defined as the permanent destruction of fluorescence by a light induced conversion of the fluorophore to a chemically non-fluorescent compound" (Swift & Trinkle-Mulcahy, 2004). In fluid bilayers illuminated only in a limited area, bleached fluorophores can be replaced by fresh ones due to the diffusion.

After the deposition of supported lipid bilayers on coverslips as described in §7.6.2 and §7.6.3, the samples were put on an inverted microscope Axio Observer D1 (Zeiss) equipped with a 100x objective. A mercury lamp at 50% of power was used to bleach the samples. An iXon camera running on iQ software (Andor) was used to record 200 images of different fields for each samples. Since the used frame rate was of 10 Hz, the observation time of each field was of 20 s. The analysis of data followed the procedure described in (Fenz et al., 2009). Two parameters which are linked to the diffusion coefficient were measured: the bleaching rate of bodipy (B) and the intensity profile at the rim of the illuminated area, for the last recorded image of the sample (meaning after 20s of illumination). The field diaphragm of the microscope was opened to 80 µm, knowing that on time scale much smaller than R^2/D, changes in the centre intensity of the illuminated field are only due to photobleaching. In this situation, the average intensity in a small area of the image centre was measured and the coefficient B was estimated by using the following law as a model to describe the intensity behaviour as a function of time:

$$I(t)=I_0 e^{-Bt}+I_{Bg} \tag{9.2}$$

where I_0, I_{Bg} and B are fitting parameters. Once B was determined, it was easy to have an estimation of the diffusion coefficient D from the spatial intensity distribution. The

mean intensity curve *I(x)* was calculated from the intensity distribution averaged over a line with 4 µm of thickness drawn perpendicular to the edge of the field stop and fitted with a single exponential:

$$I(x)=I_0 e^{-x\sqrt{B/D}}+I_{Bg} \tag{9.3}$$

Twelve different lines were drawn and for each of them the average intensity was determined. Then, the mean value was calculated from them and a diffusion coefficient *D* for bodipy was extracted.

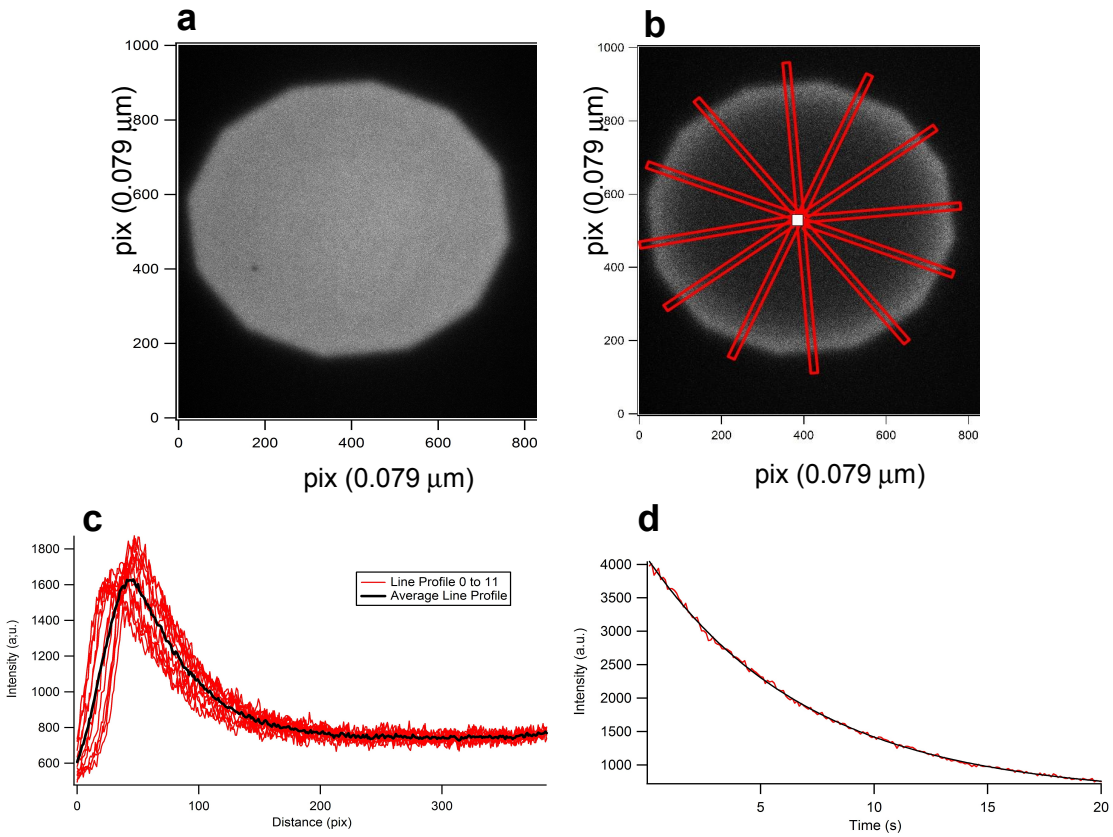

Figure 9.3 Example of CP analysis of SLB with fluorescent bodipy lipids. **a:** the fuorescent image of the area of the sample under study; **b:** the same area after 20s of exposition to the light. The image shows the central square from whose intensity profile **(d)** the bleaching rate B can be measured. The diffusion coefficient will be then estimated from the intensity profile **(c)** of the 12 red lines with 4 µm of thickness **(b)**.

The diffusion coefficient of lipids was measured after their deposition on coverslips, then after anchoring the ligands or the molecular chain and finally after flow chamber trials to asses the integrity of the bilayers and record a potential slowing down

of lipids due to the other molecules or possible damages caused by the flow.

9.5.2 SPT for ligand diffusion

If the diffusion coefficient for lipid was measured by Continuous Photobleaching, the estimation of this parameter for the ligands which are attached on SLB was done in TIRF and epi-fluorescence by single-particle tracking (SPT). Slides were functionalized as described in §7.4.2 and §7.4.3 for ICAM-1 – anti ICAM-1 and pMHC – anti HLA interactions, respectively. Then,

- for ICAM-1 – anti ICAM-1 bonds, 200 µl of a solution with anti ICAM HA58 at 10 µg/ml, Qdot 605 streptavidin conjugate at 1 nM and BSA 6% was added and samples were immediately observed in TIRF.
- For pMHC – anti HLA bonds, slides were incubated for 30 minutes with 200 µl of anti HLA A2 (Abd Serotec) at 10 µg/ml, before being rinsed; then 200 µl of Qdot 605 streptavidin conjugate at 1 nM and BSA 6% were added for 15 minutes. Samples were then rinsed and analysed in epi-fluorescence.

Qdots trajectories were followed by using the MTT algorithm which was appositely modified for the systems under study. The realisation of these type of experiments is analogous to the ligand density measurement with Qdot described in §9.4.2, but some modifications in MTT parameters and acquisition setting were done. The two-dimensional Gaussian radius and the threshold for the lowest, detectable particle intensity were not modified. However, as the system is mobile, a parameter related to the diffusion coefficient (r_{max}) was modified. Indeed,

$$D_{max}=r^2_{max}/4\tau \tag{9.4}$$

where D_{max} is the maximum diffusion coefficient that the Qdots can reach and τ is the exposure time set at 33 ms. The value of the maximum detectable diffusion coefficient was put at 0.5 µm²/s, since no faster Qdots were observed at first glance. Then, the r_{max} was 0.26 µm.

Once the position of each detected dot was recorded as function of time as well

as their fluorescent intensity, the analysis of data was carried out by using a small program written in IgorPro software to reckon the mean square displacement (MSD) of each dot. A distribution for the diffusion coefficient of each nanoparticle was obtained from the MSD:

$$MSD \sim 4Dt \tag{9.5}$$

A median value was estimated and assigned to the mobile Qdot.

Some problems of detachment were recorded during the pMHC – anti HLA A2 counting experiments. Indeed, the number of Qdots on the surface decreased with the time, leading to some difficulties in the estimation of the diffusion coefficient.

Results and discussions

Chapter 10

Study of effect of divalency

Some of the results of the present study on the effect of the divalency on the ligand-receptor interaction are described in the article *"Bond strengthening and force sharing strongly enhance the avidity of adhesion receptors subjected to forces"*, attached at the end of this manuscript.

The study of the effect of ligand divalency on the antigen-antibody couple is based on the comparison of the bond kinetics between the mICAM-1 and the Fc-dICAM-1. The two molecules are different from each other not only in terms of valence, but also in length. Indeed, the Fc-dICAM-1 has an Fc fragment which makes this molecule 8 nm longer than the mICAM-1. The study of the bond kinetics was performed both without any external force acting on the bond and in presence of a shear force in flow chamber.

10.1 Kinetics at zero force

10.1.1 Realisation of experiments

For the zero force case, the tool used to investigate the interaction between ICAM-1 and anti ICAM-1 was the SPT. The functionalization of the glass coverslips used as support for the molecular chain under study followed the protocol described in §7.3.1, where the slides were not rinsed after Qdot solution spreading. In this situation, SPT experiments were performed in order to detect the quantum dots put on the top of the molecular chain. As the signal from the background was high, due to the presence of Qdot in the bulk, TIRF microscopy helped to look only at the surface, being able to discriminate the signal coming from the surface to the one from the bulk. With this technique it was possible to detect the quantum dots on the surface, count them and analyse the dissociation of bonds by calculating the number of dots on the surface as function of time.

Two different concentrations of mICAM-1 and dICAM-1 were used: 0.02 and 0.04 µg/ml.

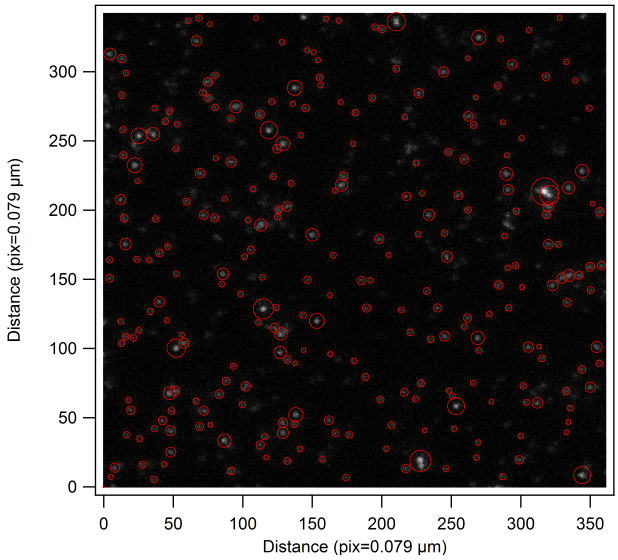

Figure 10.1 Image of Qdot in TIRF with 100x objective. The detected Qdots are circled in red. The dimension of the circle is function of the dot intensity. The Qdot are used here to study the bond rupture of the couple Fc-dICAM-1 – anti ICAM-1.

The experiments were performed in two steps:

1. after putting the Qdots on the surface, the sample was observed with the microscope and 10-image films were taken for different fields every 30 – 45 seconds. This step lasted 20 min.
2. The sample was rinsed and observed again with the microscope. 10-image films were recorded for different fields but the interval between them varied. For the first 15 minutes, the films were recorded every 30-45 seconds; then, this interval increased until 60 – 90 seconds, for other 15 minutes. Finally, a last set of films were recorded after a pause of 1 – 2 hours.

The films were then analysed with MTT algorithm in order to count the number of Qdots on the surface. The density of ligand on the surface was extrapolated by measuring the number of dots just before rinsing the samples. The same type of analysis was performed for negative control, i.e. samples without ICAM-1, obtaining from 10x to 100x lower values for density compared to the positive ones. Then, the specific ligand density was calculated by subtracting the density of the negative control from the positive one. These measurements gave the following results:

Density measured with Quantum dots (1/μm²)				
	mICAM-1		Fc-dICAM-1	
Concentration	0.02 μg/ml	0.04 μg/ml	0.02 μg/ml	0.04 μg/ml
TEST	0.15±0.03	1.03±0.07	0.38±0.03	0.91±0.08
CONTROL	0.036±0.004	0.06±0.03	0.025±0.10	0.063±0.048

Tab.10.1 Table showing the specific ligand density on surface for mICAM-1 and Fc-dICAM-1 at two different concentrations: 0.02 and 0.04 μg/ml. The values were estimated by counting the number of Qdots on surface from TIRF experiments. These are average values obtained over 3 experiments. The density is measured in $1/\mu m^2$.

10.1.2 Effect of divalency on k_{off}

Fig. 10.2 shows the number of Qdots as function of time in four different conditions: mICAM-1 at 0.02 and 0.04 µg/ml; Fc-dICAM-1 at 0.02 and 0.04 µg/ml.

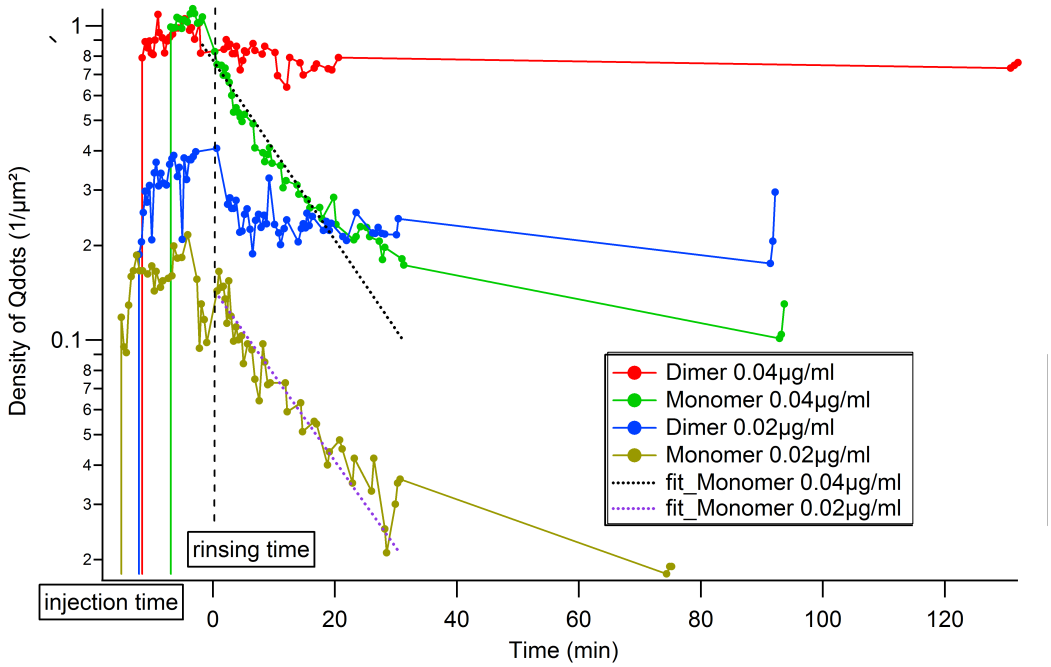

Figure 10.2 Detachment curves showing the density of Qdots on the surface as function of time. In red and blue the Fc-dICAM-1 curves for the two different concentrations (0.04 and 0.02 µg/ml respectively), and in green and gold the curves for mICAM-1 at 0.04 and 0.02 µg/ml respectively. Time t=0 is defined as the moment in which the slide is rinsed, and around 20 min after the injection of Qdot solution. As it is clear, the dimeric FcICAM is stable, while the monomeric one detaches. The dashed lines represent the exponential fit to measure the dissociation rate of the mICAM-1 (koff~15 min for both concentrations).

The dissociation time was measured by fitting the curves for the monomer with an exponential. It is clear, by looking at the curves, that the behaviour of the two types of molecules is extremely different. While the dimeric FcICAM-1 seems to be stable or slightly affected by time, showing always the same number of dots on the surface, the monomeric ICAM detaches with a long-term rupture time of ~15 min for both concentrations.

This behaviour suggests that some mechanisms of rebinding are present in the case of dimeric ICAM-1, which allow the molecule to detach less easily.

10.2 Kinetics in flow

The flow chamber allows the measurement of the dissociation rate of a bond between molecules attached to two different surfaces. Receptor-coated microspheres charged with iron oxide were driven along the ligand-coated surface by a hydrodynamic flow. The beads were subjected to different shear rates, resulting in the following velocities: 10, 22.5 and 37.5 μm/s.

10.2.2 Effect on k_{on}

The flow chamber experiments show a difference between mICAM-1 and dICAM-1 in terms of adhesion frequency. Figure 10.3 shows the adhesion frequencies as function of the bead velocities in the four investigated cases. Evidently, the curves for the longer molecule are visibly different to the ones concerning the mICAM-1, and this is true for both concentrations.

This behaviour can be explained simply by taking into account the difference in length (8 nm) between the two types of molecules, due to the presence of the Fc fragment in the dICAM-1. As demonstrated by Robert et al. (Robert et al., 2009), the adhesion of the pair ICAM-1 – anti ICAM-1 depends on the contact time between ligand and receptor. The shorter the molecule the smaller the contact time. From the experimental data, the predicted trend for the adhesion frequency of dICAM at 0.02 μg/ml was then estimated by applying the equation showed in the appendix of Robert et al., 2011:

$$FA = C\,erfc\left(\sqrt{t_{on}/t_e}\right) = C'\sigma_L\sqrt{\frac{L-z_0}{L+z_0}}\,erfc\left(\sqrt{\frac{vt_{on}}{\sqrt{L^2-z_0^2}}}\right) \qquad (10.1)$$

where C and C' are two constants, σ_L is the ligand density, L is the molecular length, z_0 is the height of the bead from the surface, v is the bead velocity and t_{on} is an intrinsic parameter of the bond. It showed a decrease compared to experimental data. Then, the

values of the adhesion frequency result to be closer to the mICAM-1 one (black curve in fig. 10.3).

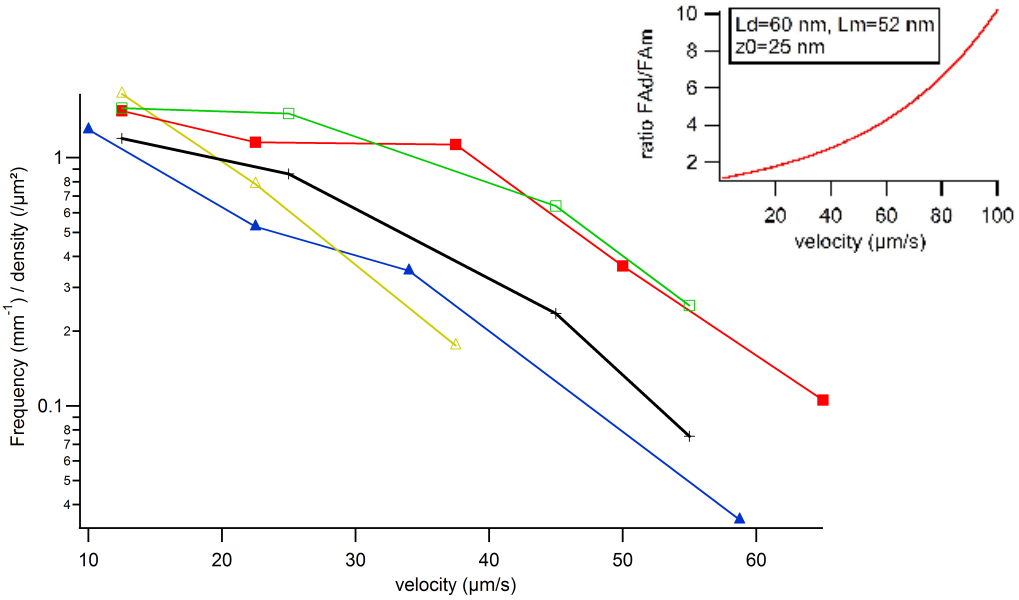

Figure 10.3 Adhesion frequency as function of bead velocity. The red and green curves with square symbols show the dICAM-1 behaviour in case of 0.04 and 0.02 µg/ml respectively. In blue and gold triangles the adhesion frequencies per unit length divided by the density (from Table 10.1), for mICAM-1 at 0.04 and 0.02 µg/ml respectively. The black curve represents the predicted behaviour of dICAM-1 at 0.02 µg/ml when the ratio between the experimental adhesion frequencies of dimer and monomer is taken into account (on the right)

10.2.2 Effect on k_{off}

The influence of dimerization on the ICAM-1 – anti ICAM-1 are well described in the paper *"Bond strengthening and force sharing strongly enhance the avidity of adhesion receptors subjected to forces"* attached at the end of this manuscript.

The laminar flow chamber was used to compare the lifetimes of single or double bonds when a pulling force ranging from 0 to 40 pN was applied on them. In order to estimate the dissociation rate, the detachment curves for the test and negative control were built for both the dimeric and monomeric ICAM-1. The bond survival fractions as function of time for the pooled negative control are shown in Fig. 10.4 for the different shear rates, while the detachment tests curves for dICAM-1 and mICAM-1 at the two

studied concentrations (0.02 and 0.04 µg/ml) are represented in Fig. 10.5. Although the number of performed experiments was high as well as the collected data, a selection was applied on these on the basis of the specific/non specific ratio. Only data with a $S/NS \geqslant 3$ (2.5 in case of monomer at 0.02 µg/ml) were kept and analysed. From Fig. 10.5 one can gather that the lifetime of dICAM-1 – anti ICAM-1 bond might be weakly affected by the force to which it is subjected. Conversely, the monomeric ICAM-1 shows an important decrease in the bond lifetime with the increasing force.

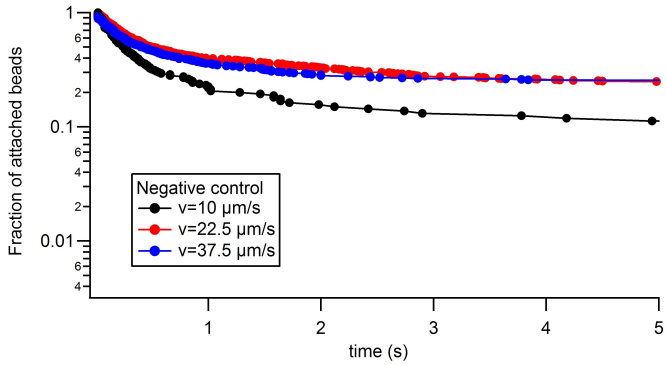

Figure 10.4 Detachment curves for pooled negative controls at three different shear rates.

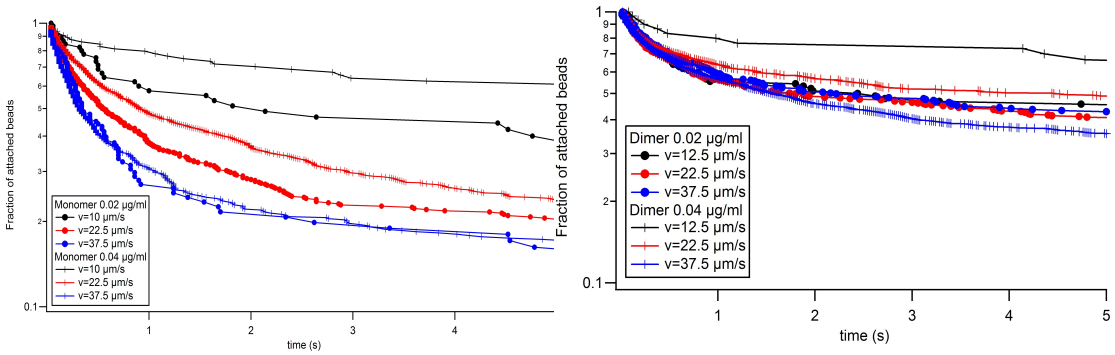

Figure 10.5 Detachment curves for mICAM-1 and dICAM-1 at the two concentrations. Raw data.

As the dimeric curves showed a similar trend for the two concentrations, they were pooled so as to reinforce the statistics. The same was done for the mICAM-1. In addition, the detachment curves were corrected by subtracting the negative ones, as already attempted by Kinoshita (Kinoshita et al., 2010). The results of this analysis are shown in Fig. 10.6.

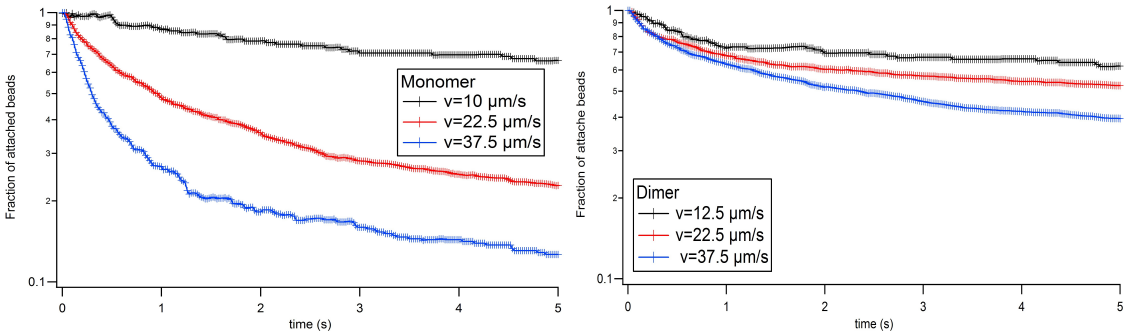

Figure 10.6 Detachment curves for mICAM-1 and dICAM-1 after correction (subtraction of negative control curves)

It is now more evident that both mICAM-1 and dICAM-1 bonds exhibits an initial dissociation rate dependent on the applied force. This is consistent with the Bell's formula (3.9). Additionally, a time- and force-dependent strengthening was observed, along with the higher stability of divalent bonds compared to the monovalent ones. This behaviour is in agreement with other studies conducted by Sarantos (Sarantos et al., 2005) and Jun (Jun et al., 2001b), where the bond lifetime of monomeric bonds was 10x lower than the dimeric one. As a matter of fact, the fraction of divalent attachments surviving at force of ~30 pN during 2.5 s was 2.5x higher than that of monovalent bonds.

In order to describe the strengthening dependence on time and force, a simple two-parameter function was used for measuring the survival fraction of bonds as function of time:

$$\frac{dN}{dt} = -k(F,t)\,N(t) \tag{10.2}$$

where

$$k(F,t) = \frac{k(F,0)}{1 + a(F)\,t} \tag{10.3}$$

$$N(t) = N(0)\left[1 + a(F)\,t\right]^{-\left(\frac{k(F,0)}{a(F)}\right)} \tag{10.4}$$

and *k(F,0)=k0*. From the experimental properties of single bonds it was possible to

predict the lifetime of double attachments subjected to pulling forces. The experimental monomeric data were fitted with the above-mentioned function (Fig.10.7), to estimate the two parameters *a* and *k0* (Fig.10.8).

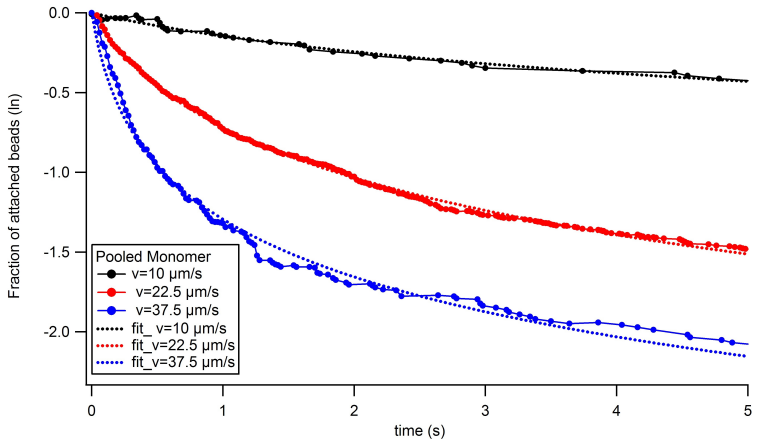

Figure 10.7 Detachment curves for the pooled monomer (lines with circle) with the two parameters fit (dashed lines) for three different bead velocities. This graph shows the good quality of the fit.

Subsequently, the same parameters were used in a simulation to better understand the dimeric behaviour. Thus, the experimental data of the divalent bonds subjected to a mechanical stress showed an intermediate behaviour of sharing and not sharing force between the two formed bonds. This leads to an increased bond strength already under small pulling force and at timescale ranging from milliseconds to seconds.

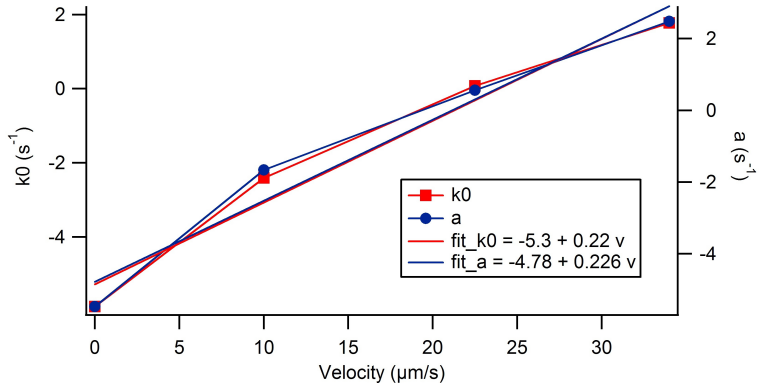

Figure 10.8 Monomer 0.04 µg/ml: estimation of the two parameters k0 and a of the model for the three velocities investigated in flow chamber and the zero velocity corresponding to the Qdots result.

10.3 Discussion

The comparison between monovalent and divalent ICAM-1 – anti ICAM-1 attachments was performed to understand the role of multivalency in adhesive interactions. The association and dissociation kinetics were studied in absence and presence of mechanical force. In the first case TIRF experiments were carried out, showing a different behaviour between the two different forms of ICAM-1. It has been demonstrated that the dICAM-1 remains stable for timescale ranging from minutes to hours. On the other hand, the bond lifetime of monovalent bonds was much smaller, showing detachment of bonds. Using TIRF, the density of ligand on the surface was measured for two different concentration of mICAM-1 and dICAM-1: 0.02 and 0.04 μg/ml. The results showed that the density was not proportional to the concentrations.

With laminar flow chamber the adhesion frequencies of monovalent and divalent bonds at different bead velocities were measured and compared. As a result, a difference between them was observed and explained by accounting for the different length of the mICAM-1 and dICAM-1. Indeed, from the experimental data, a predicted dimeric curve for the adhesion frequency was built. The formula (10.1) was used to compute the adhesion frequency setting the length at 52 nm (momomeric length) and considering the ratio between the 2 experimental adhesion frequencies. This resulting curve approached the experimental monomeric one.

At the same time, the stability of the bonds was investigated, leading to the first observation that, though monomeric and dimeric initial attachments depend on the applied force according to the Bell law (Bell, 1978), the divalent bonds are much stronger, as already predicted by other authors (Sarantos et al., 2005; Jun et al., 2001b) for ICAM-1 – LFA1 interaction. Moreover, a strengthening dependence on force and time was found and described with a two-parameter function. For divalent attachments, simulations along with experimental data exhibited an intermediate behaviour between simultaneous and subsequent formation of stressed divalent bonds. This leads to stabilization of the bond at millisecond-to-second timescale and under small mechanical forces of tens of pN. The amount of bond sharing is certainly dependent on the

molecular model and mode of coupling between sites and surfaces, therefore, it is difficult to compare our conclusions with others concerning this point, such as Evans and co-workers (Kinoshita et al., 2010) who concluded that forces are equally shared by divalent bonds. In any case, bond sharing was not very important in the force range used (low force) in this study. It might be more important if higher forces are used. In the light of this work, the high binding efficiency of many ligand-receptor interactions might be explained.

Chapter 11

Study of the effect of surface topography

As already known, the topography of surfaces interacting through adhesion proteins plays a pivotal role in the interaction. The study of this effect was done here by performing flow chamber experiments and comparing the bond kinetics in case of surfaces with different roughness. The couple of antigen-antibody used to investigate this phenomenon is constituted by Fc-dICAM-1 – anti ICAM-1. Ligand density measurements were carried out to ensure the single-molecule state and understand better if the molecules lie in specific region when anchored to rough substrates.

In order to compare the kinetics of the bond, ligands were spread on glass slides with three different level of roughness: two different type of rough slides (provided by Dr. Paolo Decuzzi from Texas University), and a smooth one.

11.1 AFM images of surface topography

The rough slides provided by Dr. Paolo Decuzzi had nominal roughness: R=50 nm and R=700 nm. These values were measured as described in §7.3.2 (and more extensively by Gentile et al., 2010), by computing the average surface roughness R_a and the root mean square roughness R_{rms}. However, AFM images of all the three surfaces

were taken in the laboratory by Dr. Zohair Mishal, in order to confirm the net topographic difference among them (Fig. 11.1).

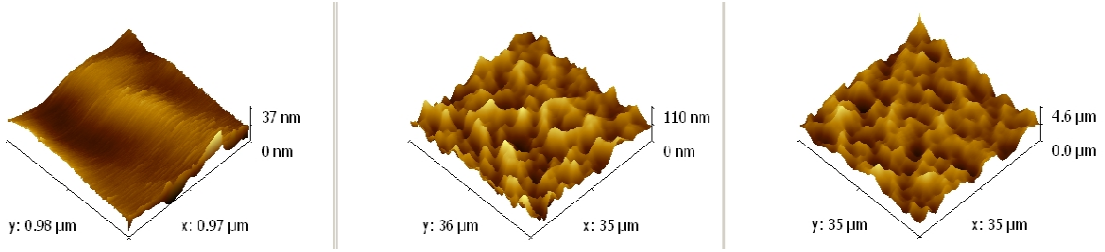

Figure 11.1 AFM images of the three substrates used to investigate the effect of surface topography on Fc-dICAM-1 – anti ICAM-1. Starting from the left: smooth surface, slide with R=50 nm and the last one with 700 nm of roughness.

The measurements were carried out at 25°C. Topographical imaging of the samples were performed with NT-MDT AFM (NT-MDT Co., Zelenograd Research Institute of Physical problems, Moscow, Russia), in contact mode with lateral scan rate of 1-1.5 Hz at 512 lines. The used AFM cantilevers had a nominal constant of 0.03 Nm^{-1} (Veeco). To estimate the roughness of the samples, the root mean square values of the surface height were measured by an AFM software (Gwyddion). All these measurements were taken for a central area of the sample over at least 0.5x0.5 μm^2, in order to avoid edge effects. The values found for the two rough substrates and the smooth one are the following:

- Rough 50 nm→(24.1±1.7) nm
- Rough 700 nm→(426.9±90.4) nm
- Smooth→(1.86±0.18) nm

11.2 Measurements for ligand density

Knowing whether roughness influenced coupling density is obviously important for interpreting the effect of roughness on adhesion. In order to measure the ligand

density on surface, intensity measurement and single-particle detection experiments in epi-fluorescence were performed, as described in §9.4.1 and §9.4.2.

11.2.1 Intensity measurement

The realisation of this experiment started with the preparation of five calibrated smooth coverslips, as in §9.4.1. Two smooth coverslips were functionalized following the procedure in §7.3.1, and §9.4.1 for the last step. The test was prepared with the concentration used for flow chamber experiments (0.04 µg/ml), while no Fc-ICAM-1 was put on the surface for the negative control. A comparison between the intensities of the five calibrated samples with the test sample gave the density of molecules grafted to the surface. The experiment was performed in epi-fluorescence and, for each sample, five images were taken, corresponding to different zones of the surfaces. For each image, the specific signal was calculated as follows:

$$I_{spec}=I_{sig}-I_{bgd} \tag{11.1}$$

where I_{sig} and I_{bgd} are the intensities of the sample and the background respectively. The same analysis was carried out for the test and the negative control. A difference between the two specific values was calculated, leading to the specific value for the test. The last was compared with the five previous calibrated intensities.

$$I_{spec(negative)}=I_{sig}-I_{bgd} \tag{11.2}$$

$$I_{spec(positive)}=I_{sig}-I_{bgd} \tag{11.3}$$

$$I_{spec}=I_{spec(positive)}-I_{spec(negative)} \tag{11.4}$$

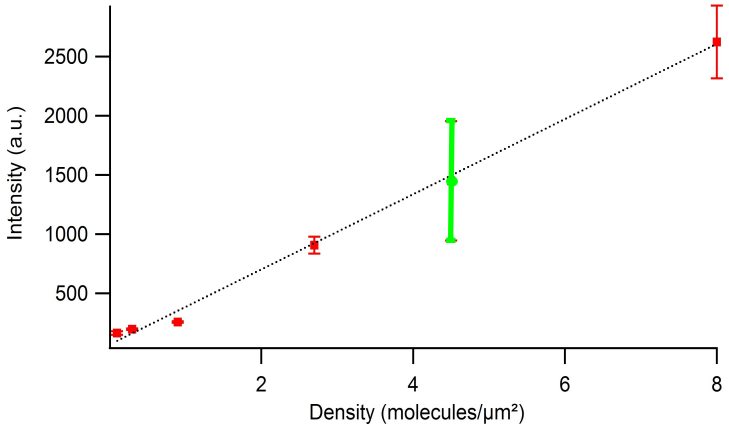

Figure 11.2 Intensity values as function of density with standard deviations. The red square represent the values for the five calibrated samples and the green circle is the specific intensity for the test.

Results for the calibrated samples and the test are shown in Fig. 11.2. By comparing the resulting intensity for the test with the calibrated slides, the density of ligand on the surface was computed, yielding ρ=4.5 molecules/µm2.

11.2.2 Single-particle counting

After having coated the slides as described in §7.3.2, a solution with Qdots and anti ICAM-1 was spread on them for 15 min before rinsing. The samples were then analysed in epi-fluorescence. The choice of this technique instead of TIRF is justified by the observation that the Fc-ICAM-1 is fairly stable, so it is not necessary to have anti ICAM-1 in the bulk to reach a kinetic equilibrium. The number of Fc-dICAM-1 was associated with the number of dots present on the surface. For each sample, 10 films related to 10 different sample fields were recorded. Each film was composed of 10 images taken with 10 Hz frequency. The number of Qdots was calculated for each film giving 10 values for a given sample. The average of these values gave the number of dots and consequently the number of ligands. This procedure was repeated for all the experiments and the final value for density was computed by averaging all the values coming from the different experiments. The results are showed in the Table 11.1.

Density (1/μm²)		
SMOOTH	ROUGH 50 nm	ROUGH 700 nm
1.70±0.26	2.19±0.14	1.98±0.12

Table 11.1 Table showing the ligand density on surface for Fc-dICAM-1 at 0.04 μg/ml for the three different substrates. The values were estimated by counting the number of Qdots on surface from experiments in epi-fluorescence. These are average values obtained over an high number of experiments. The density is measured in $1/\mu m^2$.

Results are very similar for all the substrates, showing that there is not a favoured surface topography for Fc-dICAM-1 absorption and that the presence of peaks and asperities does not influence the attachment of these molecules on rough surfaces.

11.3 Flow chamber experiments

The kinetic parameters were calculated by performing flow chamber experiments. The beads were functionalized with a first layer of antibody (anti – mouse Fc fragment), covalently bound to the bead surface. Then, a second layer was formed with anti – ICAM-1, or an isotype control (for negative control). The concentration of Fc-ICAM-1 used to coat the slide was always c=0.04 μg/ml. Lower concentration were tried leading to an unsatisfying ratio between the specific adhesion and the unspecific one. This showed that beads did not sufficiently adhere on the surface, meaning that the amount of ligand was too low. The bond kinetics was investigated employing different shear rates corresponding to different beads velocities.

Role of topography on k_{on}. According to the (10.1), the adhesion frequency for the three differently rough surfaces as function of the bead velocity was measured. The results are shown in Fig. 11.3 and in Table 11.2.

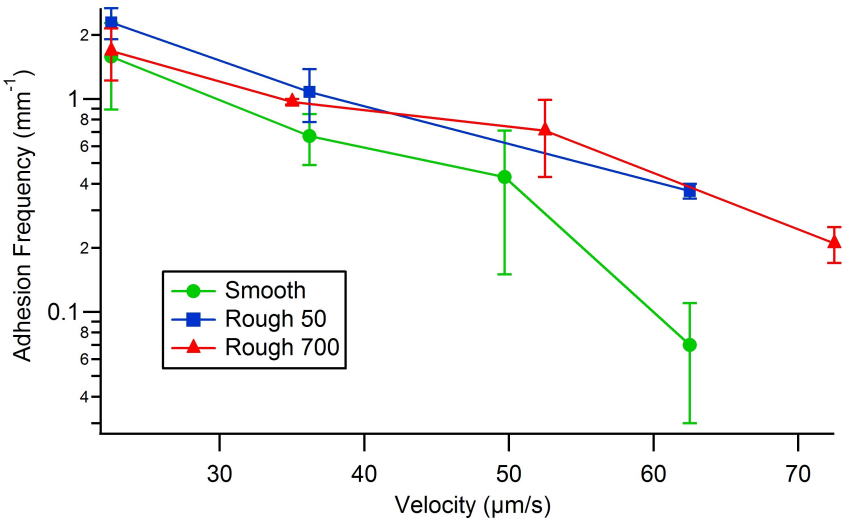

Figure 11.3 Curves representing the adhesion frequency as function of beads velocities for the three substrates: green for the smooth, blue for the 50 nm-rough and red for the 700 nm-rough surfaces.

Velocity (µm/s)	ROUGH 700			ROUGH 50			SMOOTH		
	Adh.Freq. (mm^{-1})	Nb arrests	S/NS	Adh.Freq. (mm^{-1})	Nb arrests	S/NS	Adh.Freq. (mm^{-1})	Nb arrests	S/NS
22,5	1,68±0,46	250	7	2,29±0,38	238	7,4	1,58±0,69	535	3,4
37,5	0,97±0,03	339	9,3	1,08±0,30	340	8	0,67±0,18	584	6,7
50	0,71±0,28	200	15,5				0,43±0,28	411	6,3
67,5	0,21±0,04	228	6,7	0,37±0,03	313	8,6	0,07±0,04	161	3,2

Table 11.2 Adhesion frequencies (with standard deviations) as function of bead velocity. The number of arrests and the ratios between the specific and the non specific adhesion frequencies measured for the three substrates with flow chamber are also on the table.

The adhesion frequency decreases when the beads velocity increases. It is fairly visible that there is not a significant difference in the bond formation between the three samples, except at the highest velocity, where the adhesion frequency of the smooth surface is smaller than in the other two substrates. It seems then that the k_{on} increases at high velocities due the rough surfaces. This suggests that the localisation of ligand on the surface and the contact area might be important parameters in the probability of bond formation.

From the table 11.2 it is also evident that the ratios between the specific and non specific signals are improved when rough substrates are employed. This show a role of the topography in decreasing the unspecific attachments, as the value for the test adhesion frequencies are very similar in the three cases. Again, the only deviation from this behaviour it can be observed at high velocity where the adhesion frequencies for the negative controls are the same (~0.02 mm^{-1}).

A difference behaviour in the bead velocity was recorded when using the 700 nm-rough slide and the smooth one. Indeed, for same values of flow rate, beads showed different values of velocity (Fig.11.4): the roughness slowed down the beads.

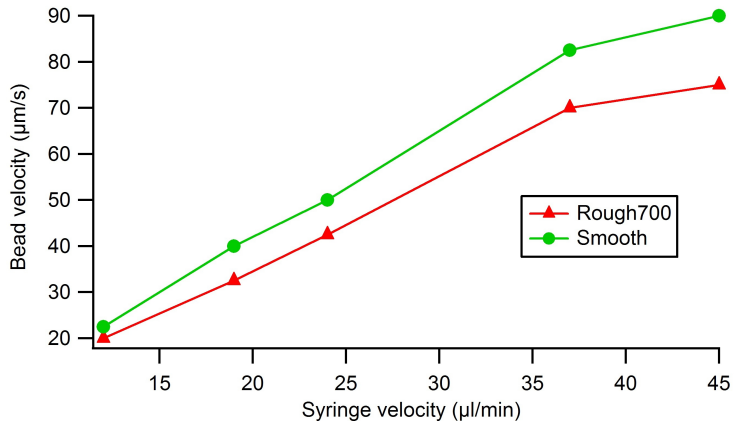

Figure 11.4 Bead velocity as function of flow rate for the 700-nm rough slide (red triangle) and the smooth one (green circle). The conclusion has to be verified, since the difference is not significant.

This behaviour seems to confirm what Robert et al. demonstrated using different concentration of hyaluronan on glass surface (Robert et al., 2008): by applying the same flow rate, the velocity of the beads changes depending on their height from the surface.

Role of topography on k_{off}. The slopes of the detachment curves showed in Fig. 11.5 highlight that the k_{off} of the bond does not vary in the three examined cases; so it does not present a dependence on the surface topography. Different shear rates were used in the flow chamber, leading to the same results.

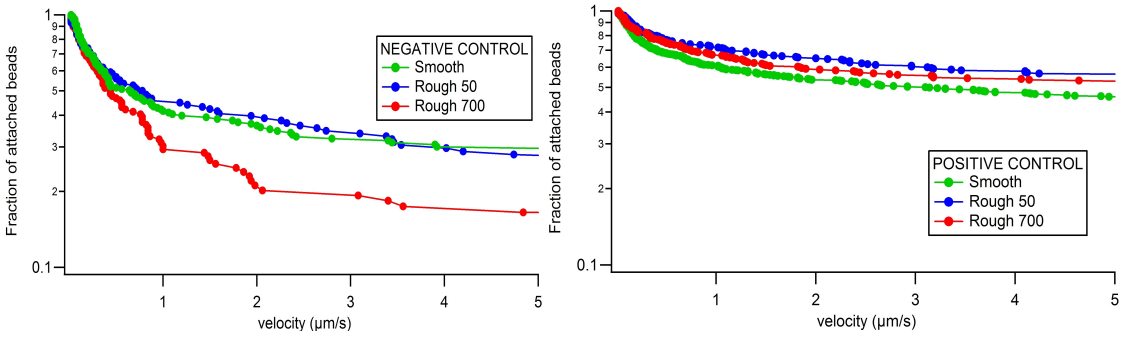

Figure 11.5 Detachment curves for the three surfaces: a representation of the fraction of attached beads as function of time at bead velocity=20 µm/s. The slope of each curve gives the k_{off}. On the left the detachment curves for the negative controls and on the right the ones relative to the positive controls.

The effect of topography on the detachment curves is not so evident, leading to a similar dissociation rate for the different substrates. The detachment curves for tests in Fig. 11.5 are not corrected for the negative ones. However, since the ratios S/NS are very high, particularly in the case of rough slides, one can assume that the curves will not undergo strong modifications when corrected. Moreover, the correction could even make the curves much closer one to the others.

11.4 Discussion

The study of a possible influence of the surface topography on the interaction between adhesive molecules was carried out through laminar flow chamber experiments. The kinetics of the bond was studied for three systems whose difference was the roughness level of the ligand-attached surface. Analysing the adhesion frequencies measured for different bead velocities, no critical difference between the three systems was observed, except at high bead velocity, where the adhesion frequency of molecules grafted on a smooth surface drops faster than in the case of rough substrates. This observation leads to a remark on the localisation of the molecules on the surface, and on the definition of contact area between the two surfaces (bead and slide) supporting the couple of ligand and receptor under study. Ligand density measured by SPT was in the same range for the three systems and it did not show a different

localisation of the molecules on the surface, although influence of the topography on molecule organisation on the surface was observed in other studies (González-García et al., 2010, Hocdè et al., 2009). Although, the density measured with this technique was around 2x lower than what found with intensity measurement, these values are more reliable because these were performed more times.

The analysis of the detachment curves yields the same conclusion as for the adhesion frequency, meaning that there are no evidences of a different dissociative behaviour when the ligands are on smooth or rough surfaces. This trend is confirmed for different applied forces, covering a range from 10 to 70 pN.

In order to understand and explain the similar kinetic behaviour of the ICAM-1 – anti ICAM-1 interaction when molecules lie on surfaces with extremely different topography, a mathematical model should be developed. The geometry of the system, with a particular attention to the real contact area between the surfaces involved in the interaction, has to be taken into account, to better understand the role of asperities and peaks, and why they are not able to introduce any modification on the investigated bonds. Indeed, from a first analysis, it seems that nanostructures on the surface do not increase the effective surface available for ligands, which is confirmed by the similar ligand density found with single-particle counting.

Chapter 12

Study of effect of mobility

The distribution of adhesive ligands and receptors has been widely postulated to be important for efficient cell adhesion. The ability of these molecules to diffuse laterally is predicted to be critical for bond formation in adhesive interactions. In this section, the effect due to diffusion of ligand mobility on the interaction between ligand and receptor will be described, studying two different couples of interacting molecules: pMHC – anti HLA and Fc-ICAM-1 – anti ICAM-1. The ligand is anchored to fluid or immobile SLB whose diffusion is measured. The kinetic parameters describing the interaction are then estimated through laminar flow chamber experiments.

12.1 Results for lipid diffusion

The first step in the investigation of the effect of mobility on ligand-receptor interaction is devoted to ensure the fluidity of the SLB which supports the ligands. As described in §7.4.1, the Langmuir-Blodgett-Schaefer technique was used to create the bilayers, in which a small concentration of fluorescent lipids was included to analyse their diffusion in continuous photobleaching.

The procedure for this type of measurement is explained in §9.5.1. For each sample, five different fields were observed, obtaining five values for the diffusion

coefficient at room temperature. Then, an average of them led to the real value for the diffusion coefficient of the fluorescent lipids. In the case of fluid SLB, namely with DOPC lipids as matrix, the computed diffusion coefficient was often D~2 μm²/s, in accordance with previous studies (Fenz et al., 2009; Thid et al. 2007). However, for some samples this value was much smaller and it was not clear where the difference came from, making the interpretation of these results not straighforward. For SLB at the gel phase (DPPC as matrix or immobile DOPC), the measured diffusion coefficient was D<0.1 μm²/s. To check the integrity of the bilayers even after it has been subjected to flow, the diffusion coefficient of the lipids was measured after flow chamber experiments. In most of the cases, it was not modified.

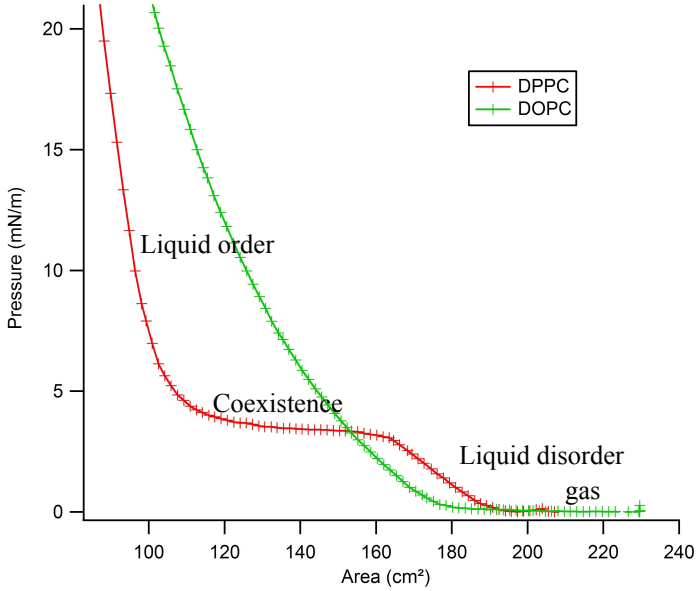

Figure 12.1 Isotherm for the two layers of SLB, showing the transition phases that the lipids can follow by changing the pressure of these molecules. Lipids go from the gas phase at low pressure (initial plateau) to the liquid order phase when the right pressure is reached (20-22 mN/m).

12.2 Results for ligand diffusion coefficient

After having measured the lipid diffusion coefficient, slides were functionalized with the ligands under study, following the procedures described in §7.4.2 (for ICAM-1

– anti ICAM-1 binding) and 7.4.3 (for pMHC – anti HLA interaction). SPT with Qdots and laminar flow chamber experiments were performed respectively in order to analyse the lateral diffusion of ligand, and study the bond formation and dissociation in presence of diffusion.

The program employed to detect and follow the Qdots trajectories was MTT from Sergé (Sergé et al. 2008), with variations of some parameters as described in §9.5.2.

12.2.1 pMHC – anti HLA interaction

Slides were functionalized as described is §7.4.3 and §9.5.2. The diffusion of pMHC on fluid SLB was measured by labelling the interacting anti HLA A2 with Qdots, and then following their trajectories in epi-fluorescence. Next, the mean square displacement (MSD) from these trajectories was computed as an estimation of the ligand diffusion coefficient:

$$MSD = \langle |r(t) - r(0)|^2 \rangle \sim 4Dt \qquad (12.1)$$

An example of histogram of D values for Qdots binding the couple pMHC – anti HLA is shown in fig.12.2, where the median value is D=0.01 µm²/s.

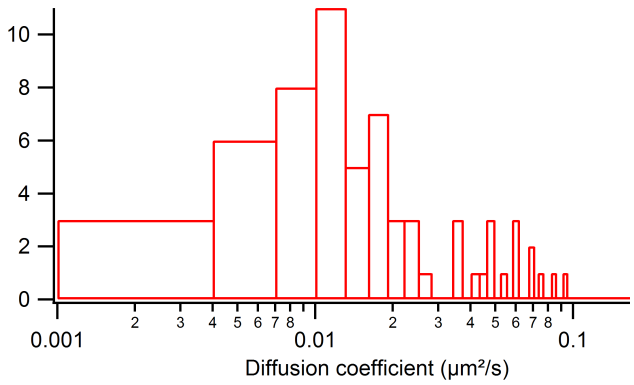

Figure 12.2 Histogram of values of the diffusion coefficient for Qdots labelling the receptor (anti HLA A2) for pMHC. The median value is 0.01 µm²/s, showing a two order of magnitude decrease compare to lipid diffusion (D=2 µm²/s).

This value is two orders of magnitude smaller than the lipid diffusion coefficient, meaning that the ligand diffusion coefficient will be

$$D_{Qdot} \geq D_{pMHC} \geq D_{lipid} \tag{12.3}$$

The slowing down of the Qdots can occur for different reasons:

1. steric constraint due to the relatively big size of this fluorescent nanoparticles (Saxton & Jacobson, 1997);
2. unspecific attachments of Qdots or proteins with the glass substrate, enhanced by possible small holes on the bilayer;
3. formation of aggregates because of the Qdots multivalency (Saxton & Jacobson, 1997).

However, testing the causes of this smaller measured diffusion coefficient is not an easy task. Indeed, although several changes were performed to avoid the above-mentioned problems (cushions between slide and SLB, to avoid denaturation of proteins crossing the bilayer; biotin on Qdot solution to saturate the streptavidin on it; etc.), the value for the diffusion coefficient did not change.

From the analysis of the Qdots trajectories and fluorescence intensities, carried out using IgorPro, the diffusion coefficient values were drawn as function of the dots intensity (Fig. 12.3).

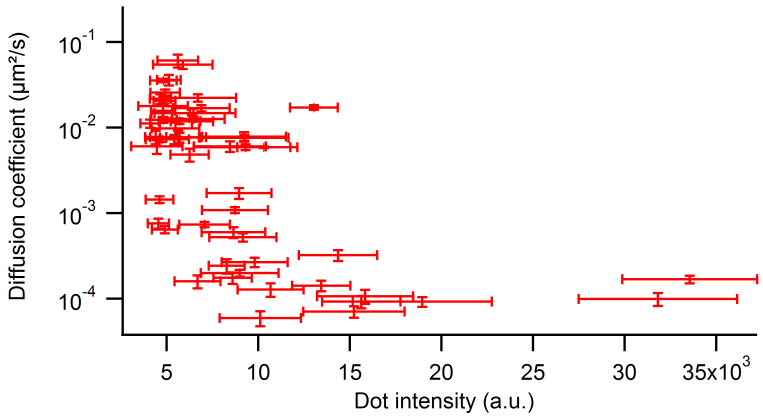

Figure 12.3 Diffusion coefficient measure in µm²/s as function of Qdots intensity given in arbitrary unit.

It is evident that Qdots with higher value of fluorescence intensity are less mobile. This observation allows us to discriminate between mobile Qdots and slower or immobile ones which probably formed aggregates or were binding unspecifically the bilayers, attracted to some possible small imperfections (holes, lipid rafts, etc.). These lasts showed a high value of intensity and a diffusion coefficient going from 10^{-5} μm²/s to 10^{-3} μm²/s, while single dots were faster ($0.01\,\mu m^2/s \leqslant D \leqslant 0.1\,\mu m^2/s$) and less bright.

In addition, single-particle counting experiments were carried out to asses the density of ligand on the surface. Epi-fluorescence was used to detect the Qdots on the surface, yielding the following results for positive and negative controls:

$$\rho_p = (0.27 \pm 0.16) \text{ molecules}/\mu m^2$$

$$\rho_n = 0.014 \text{ molecules}/\mu m^2$$

However, additional trials have to be conducted to obtain more reliable results.

12.2.2 Fc-ICAM-1 – anti ICAM-1 couple

As well as for the ligand-receptor couple formed by pMHc – anti HLA, the interaction between Fc-ICAM-1 and anti ICAM-1 was studied in presence of ligand lateral diffusion. Slides followed the functionalization protocol described in §7.4.2 and §9.5.2. One more time, in order to measure the ligand diffusion, the receptor-coated Qdots binding the ligand-coated substrate were detected and followed using TIRF, and their trajectories were analysed and used for the estimation of the diffusion coefficient. In Fig. 12.4 there is an example of Qdots trajectories detected by MTT in a portion of the sample surface.

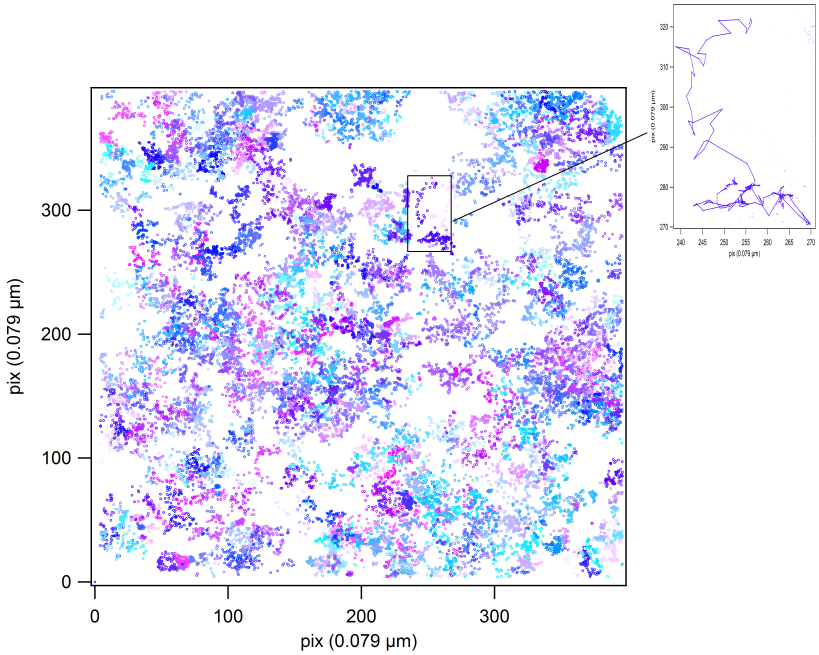

Figure 12.4 Qdots trajectories detected and followed by MTT in a field of the entire sample with dimensions of 998,56 µm². In the square on the right, the zoom of a particular Qdot trajectory, showing the Brownian motion and some confined regions.

The values for the diffusion coefficient were always close to those found in case of pMHC – anti HLA. In some rare cases, the median value for D reached 0.1 µm²/s (Fig. 12.5), one order of magnitude higher than usual, but still lower than lipid diffusion. However, this value is still in the range of membrane protein lateral diffusion that can be found in the literature (10^{-2} to 10^{-1} µm²/s).

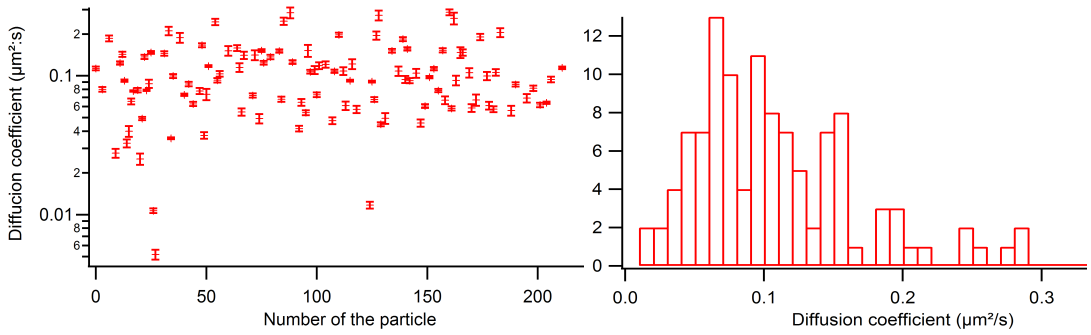

Figure 12.5 Left: diffusion coefficient with standard deviation of the Qdots detected by MTT. Right: Histogram of values of the diffusion coefficient for Qdots labelling the anti ICAM-1 which interact with Fc-ICAM-1 on the slide surface. The median value is 0.1 µm²/s, showing a 20x decrease compare to lipid diffusion (D=2 µm²/s).

The ligand density was also measured for this mobile system through single-Qdot counting in TIRF, leading to the specific density

$$\rho=(1.25\pm0.17)\ \mu m^{-2}$$

$$\rho_p/\rho_n=42.7,$$

the last being the ratio between specific and unspecific densities.

12.3 Flow chamber results

For flow chamber experiments, the couple studied was the one formed by ICAM-1 on SLB and anti ICAM-1, on microspheres coated with either one or two layers of antibody. The pMHC – anti HLA interaction was not exploited any more, since the results for the diffusion coefficient showed low values. In this frame, the kinetics of the bond should not be notably modified. Indeed, to observe differences in the bond association, the time of diffusion should be smaller than the minimal contact time necessary to form the bond. As reported by Robert et al. (Robert et al., 2011), this contact time for the ICAM-1 – anti ICAM-1 couple is t_0=6 ms. In Table 12.1 there are the possible values of the diffusion time considering two different molecular lengths, due to the two different coatings for beads, and two different values of diffusion coefficient, relative to the measured lipid and Qdot diffusion.

$t_{diffusion}=L^2/D$	D~0.1 μm²/s	D~2 μm²/s
L~52 nm	27 ms	1.3 ms
L~36 nm	13 ms	0.6 ms

Table 12.1 In this table is shown the diffusion time for Fc-ICAM-1 whose diffusion coefficient is the one measured for lipids or the one measured for Qdots, and for two different molecular length corresponding to surface-interacting bead with one or two layer of antibody on its surface.

It is clear that when the ligand diffusion is associated to the Qdot diffusion, there are not relevant changes in the k_{on} for all the studied cases. The diffusion time can equal the

minimal contact time for values of diffusion coefficient following:

$$D=L^2/t_{on} \qquad (12.4)$$

Since t_{on} was found being 6 ms, D=0.22 $\mu m^2/s$, in case of 1 layer-coated microspheres (L=36 nm), and D=0.46 $\mu m^2/s$ for the longest molecular chain (L=52 nm). Starting from these two values, an effect on adhesion due to diffusion should occur.

12.3.1 Effect on on-rate

The flow chamber experiments show an agreement in the adhesion frequency trend for molecules anchored to "solid" SLB, or to coverslips coated as described in §7.3.1. The adhesion frequency at several velocities (from 22 to 100 µm/s) and for 1 or 2 layer-beads was measured, showing a decrease when the velocity increased (Fig.12.6). The non specific adhesion frequency as function of bead velocity was measured as well, showing the same behaviour allowing to maintain a reasonable S/NS ratio.

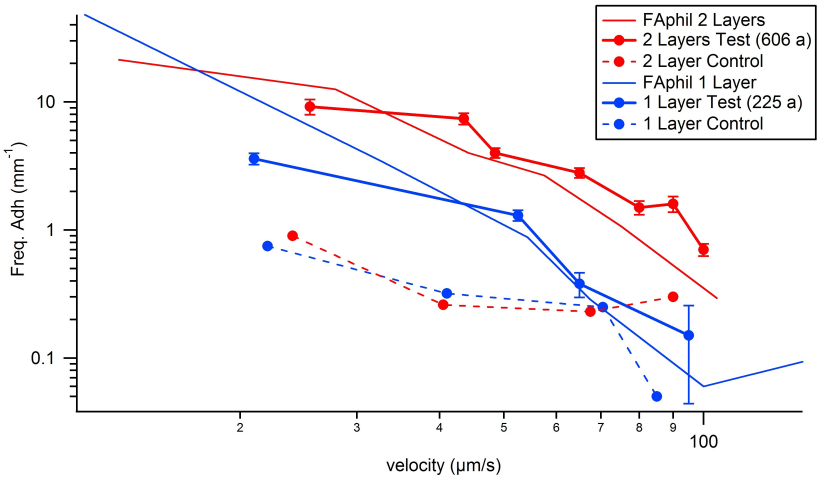

Figure 12.6 Fc-ICAM-1 – anti ICAM-1 molecules on "solid" SLB. In red there are the values for double layer-coated beads: the simple line represent the fixed substrate without SLB, the line+circle is for "solid" SLB, and the dashed line+circle represents the negative control. With the same type of representation, but in blue, there are the values related to 1 layer-beads.

In Fig.12.6, as comparison with the adhesion frequency curves for the SLB

system, there are the curves representing the adhesion frequencies for ICAM-1 – anti ICAM-1 as function of bead velocity for a fixed substrate, without SLB, when either 1 layer- or two layer-beads are employed (Robert thesis, 2009). However, in this case, since the construction of the molecular length is different than the one on the bilayer, only a possible comparison in terms of trend can be done. The adhesion frequency for molecules on SLB decreases as the velocity increases, assuming the same behaviour of the compared curves.

The study of the association rate in flow chamber for mobile interacting molecules led to the results showed in Fig.12.7. One more time, the adhesion frequency showed a decrease when the velocity increased from 22 to 100 μm/s. This behaviour was observed in case of use of beads coated with 2 layers, while it was different in case of shorter molecular length. The S/NS ratio was ~10.

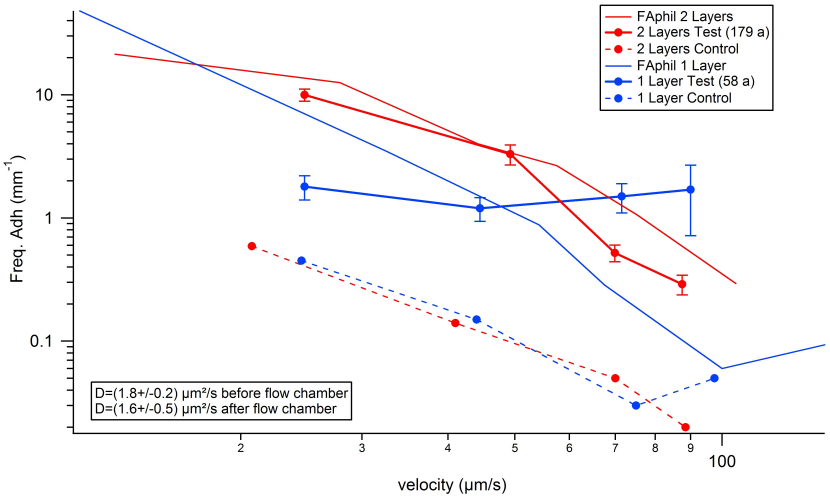

Figure 12.7 Adhesion frequencies for Fc-ICAM-1 – anti ICAM-1. In red there are the values for double layer-coated beads: the simple line represent the fixed substrate without SLB, the line+circle is for molecules on fluid SLB, and the dashed line+circle represents the negative control. With the same type of representation, but in blue, there are the values related to 1 layer-beads.

However, a non negligible variability on the adhesion frequencies was observed during all the flow chamber experiments with both fluid or fixed bilayers. Moreover, at high velocity, the statistics is fairly poor due to the small number of detected arrests. For these reasons, more experiments have to be done to collect a higher amount of data, whose analysis can make the current results more reliable.

The behaviour of the adhesion frequency for attachments subjected to diffusion was also extrapolated through a simulation in which the diffusive elements are the beads and the ligand-coated surface is immobile. Introducing some important physical and structural parameters, such as the minimal contact time (t_{on}), the height of the beads from the surface (z_0) and the length of the molecular chain (L=36 nm or L=52 nm), the graphs of the adhesion frequency as function of the bead velocity were drawn (Fig.12.8).

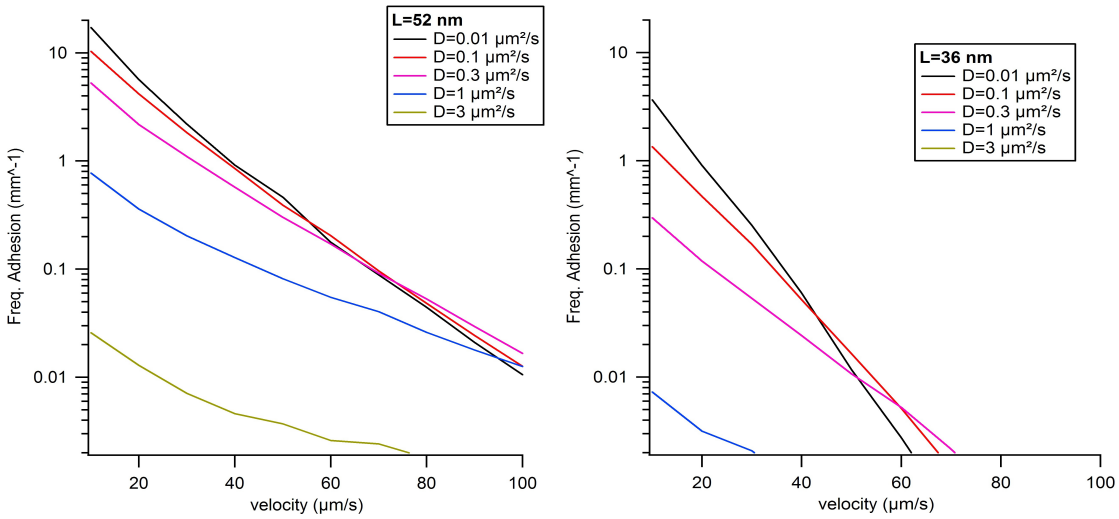

Figure 12.8 Adhesion frequency as function of bead velocity resulting from the numerical simulation. The curves were built for the two molecular length and for different values of the diffusion coefficient.

Considering as fixed the system where the diffusion coefficient is equal to 0.1 $\mu m^2/s$ (value for bead diffusion simply due to thermal fluctuations), it is clear that an effect of the molecules mobility becomes evident already for 3x higher diffusion. This is more striking in case of smaller molecular length. By further increasing the value of D, a strong fall of the adhesion frequency is recorded. An interesting aspect of these curves is their behaviour at high velocities. In this range, it can be observed an inversion of tendency where the adhesion frequency shows a faster decrease at lower values of diffusion. This phenomenon can be explained by considering that at high velocities, if the diffusion is high the probability of a ligand to move and get in contact with different receptors can be higher, increasing the adhesion frequency compared to low diffusive molecules. The inversion of tendency was already observed in some experiments, but

not yet reported because of a strong variability in the data.

12.3.2 Effect on off-rate

The results obtained for the detachment curves of the couple ICAM-1 – anti ICAM-1 on fluid or fixed SLB show an influence of the mobility on the dissociation rate due to a huge number of definitive arrests recorded in the case of fluid SLB. A possible explanation for this phenomenon can be found in the formation of multiple bonds enhanced by the ligand lateral diffusion. To confirm this hypothesis, additional data are necessary.

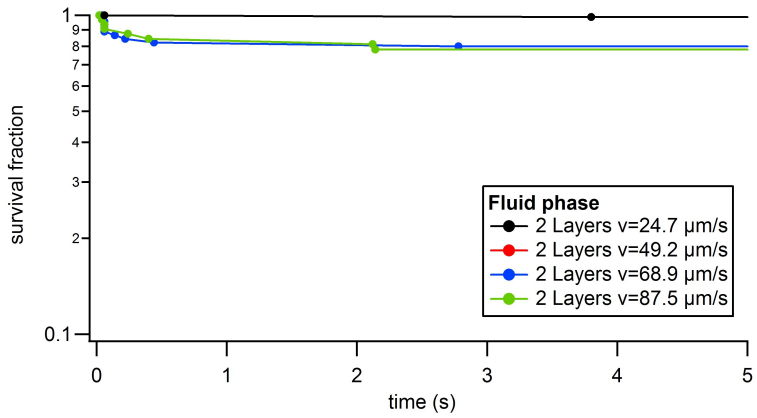

Figure 12.10 Detachment curves of Fc-ICAM-1 – anti ICAM-1 bond when ligands are anchored to fluid SLB (D~2 µm^2/s) and receptors to M450 beads coated with two layers of antibody. The curves are built shear rates.

The detachment curves for molecules on fixed SLB showed a partial agreement with the ones for molecules coating a fixed substrate without SLB. Indeed, the dissociation rate for ICAM-1 – anti ICAM-1 anchored to immobile bilayers, and in case of monolayer-beads, equals the one measured without bilayers, but using beads with two layers of antibody. While the dissociation rate for the highest molecular length, in the case of fixed SLB looks much smaller.

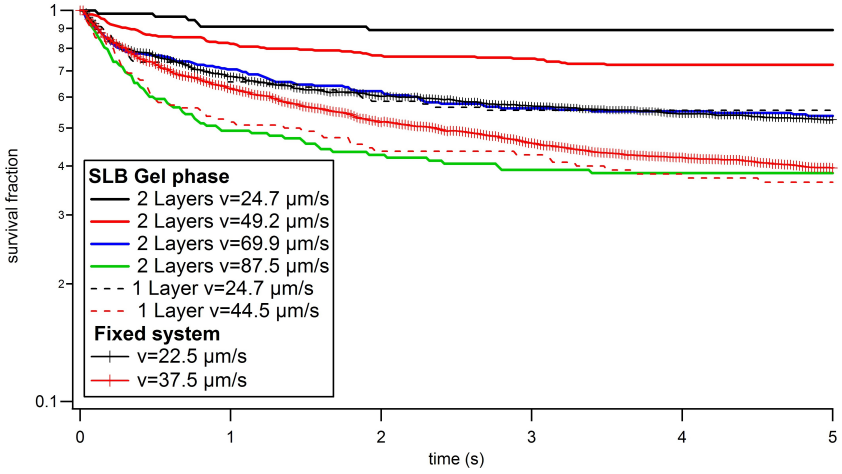

Figure 12.11 Fraction of arrested beads as function of time for ligands anchored to "solid" SLB ($D<0.1$ $\mu m^2/s$) interacting with M450 beads coated with one (dashed lines) or two (lines) layers of antibody. Comparison with fixed system, without SLB, represented by the black and red lines+markers. The curves are built for different shear rates.

12.4 Discussion

The diffusion coefficient for lipids was measured to ensure their mobility. These measurements, performed on two different systems (ICAM-1 – anti ICAM-1 and pMHC- anti HLA), led to different values probably because of the two different protocols used for the measurements. Indeed, the protocol for ICAM-1 – anti ICAM-1 has been developed more recently, yielding more interesting results. The ligand is directly attached to the NTA lipids on the bilayer through the his-tag. Differently from the pMHC-anti HLA protocol, the slide is mounted on the same chamber for both the CP experiment and the flow chamber experiment. This drastically reduces the risk of the sample being damaged during the mounting and dismounting procedures. Finally, because of the low number of experiments with the pMHC – anti HLA system, the corresponding results are less reliable.

The effect of ligand lateral diffusion on the frequency of adhesion of the investigated pair was not so sharp. The study was conducted by using microspheres coated in two different ways, in order to reach two diverse molecular lengths: with 1 or 2 layers of antibody (L=36 nm or L=52 nm). The adhesion frequencies relative to these

two systems showed a similar behaviour for fixed and fluid bilayers. Their trend well matches the adhesion frequency behaviour for molecules on a fixed substrate without bilayer. This result is in contrast with what many authors concluded (Kucik et al., 1996; Chan et al., 1991; Thid et al., 2007). Indeed, they found an improved bond formation in presence of diffusive ligands.

Additionally, a numerical simulation for the adhesion frequency in presence of ligand diffusion predicted an effect of the mobility already for D~0.3 $\mu m^2/s$ and, more interestingly an inversion of tendency at high velocity. Indeed, higher values for the adhesion frequency were computed for higher values of diffusion coefficient. This can find an interpretation if considering the formula (10.1), in which the adhesion frequency is formed by two terms: a first term proportional to the number of encounter and a second one related to the contact time. The diffusion can give rise to two main effects on the system:

1. can lead to an accumulation of ligands on the contact area. A ligand can move and more likely enter in contact with different receptors, leading to an increase in the adhesion frequency compared to low diffusive molecules;
2. can reduce the contact time between ligand and receptor. If the diffusion of ligand is sufficiently high, the time in which the molecule is in contact with its receptor is too small to give rise to the bond. This leads to a decrease in the adhesion frequency.

At high velocity, the first effect might exceed the second one, showing that inversion of tendency observed in the simulation.

The mobility of ligand seems to play a role in bond dissociation. Indeed, for fluid bilayer the value of the k_{off} was strongly reduced. This effect can be explained by the possible presence of multiple bonds due to the mobility effect of ligand accumulation on the contact area. A confirmation of these possible aggregates comes from the difficulty in collecting data of transient arrests on fluid bilayers. The experiments showed a strong adhesion which did not decrease its strength, even when higher forces were applied onto the bond, by changing the shear rate of the flow. On the other hand, there was a good agreement between the k_{off}, measured on fixed SLB and on fixed substrate without SLB, and a noticeable difference on fixed SLB when the

molecular length changed. A higher value for the detachment rate was estimated when 1 layer-beads were used in the flow chamber, showing higher stability of the longer molecular length. This trend was not modified by the different values of the shear rate reached in flow.

Conclusions and perspectives

Cell adhesion has been shown to be important for many biological processes, such as cell migration, proliferation, differentiation, activation, immune system functions and wound healing. It has also been shown that it is implicated in the origin of a large number of common human disorders, such as rheumatoid arthritis and tumour cell metastasis in cancer (Mould et al., 1995). Single-molecule techniques, such as laminar flow chamber and single-particle tracking allow us to investigate this process at single-molecule level. These techniques were used for this thesis work in order to better understand the mechanisms of adhesion and the behaviour of interacting molecules. Two couples of ligand and receptor have been studied here: ICAM-1 – anti ICAM-1 and pMHC – anti HLA. The aim of this work was to study the changes in the interaction of these molecules due to modifications in molecular environment. For this purpose, the ligand-receptor interaction was explored:

1. in presence of different valence of the interacting ligands. A comparison in the ICAM-1 – anti ICAM-1 bonds was performed using monomeric and dimeric ICAM-1.
2. In case of different ligand-coated surface topography. Ligands were grafted on three differently rough substrates and the kinetics of the ICAM-1 – anti ICAM-1 interaction was studied.
3. In presence of ligand lateral diffusion. Supported lipid bilayers were deposited on glass slide and ligands (ICAM-1 and pMHC) were anchored to them.

The comparison between the association and dissociation kinetics of monovalent and divalent attachments in the ICAM-1 – anti ICAM-1 was performed in presence of a pulling force and at zero force. In the last case, TIRF experiments were carried out, showing a much higher stability of divalent attachments for timescale ranging from minutes to hours. With laminar flow chamber differences in the k_{on} of monvalent and divalent bonds were measured and explained accounting for the different length of the mICAM-1 and dICAM-1. A comparison of the association rate of other monovalent and divalent molecules should be done, in order to see if the higher bond formation in case of dimeric molecules can be explained by only considering different structural parameters.

The stability of the bonds was also investigated, leading to the observation that

monomeric and dimeric attachments initially depend on the applied force, according to the Bell law (Bell, 1978). Then, they show a force- and time-dependent strengthening. The study of this dependence shows that divalent attachments exhibit an intermediate behaviour between shared and not shared mechanical applied force between the two formed bonds. This leads to high stability of divalent bonds, explaining the high binding efficiency of many ligand-receptor interactions. This study could be important for molecules, like integrins, selectins, or cadherins, since most of the adhesion receptors show a dimeric structure *in vivo*.

The study of the influence of surface topography on adhesion interactions did not show any difference in the k_{on} and k_{off} of bonds on rough and smooth substrates. These results seem to be in contrast with other previous works involving cells. To interpret them, the contact area between the surfaces involved in the interaction should be studied, to understand why asperities and peaks do not introduce any modification on the studied bonds. Then, a comparison with already studied interactions taking place on rough surfaces could be carried out, sheding new light on the ICAM-1 – anti ICAM-1 bonds.

Unexpectedly, the mobility of ligand seemed to play a role more in the dissociation than in the association of bond. Indeed, for diffusive interacting molecules the value of k_{off} was strongly reduced, probably because of the possible presence of multiple bonds due to ligand accumulation on the contact area. A confirmation came from the high number of definitive arrests recorded during the flow chamber experiments. Nevertheless, a theoretical study of the bond formation in presence of ligand diffusion showed a decrease of the adhesion frequency already at low diffusion. In addition, a smoother fall of this quantity was calculated for a higher diffusion, denoting increased probability of mobile ligands to encounter and bind receptors. Further experiments are going to be performed, in order to confirm this tendency. This study can be adapted to other adhesion receptors on cell membranes and then subjected to diffusion.

During this thesis work, the capability of laminar flow chamber in measuring the kinetic parameters of the studied bonds at single-molecule level has been demonstrated. The laminar flow chamber allowed us to carry out measurements on molecules in

different environmental conditions.

Future prospects can involve replacing beads by cells in flow chamber in order to study the effects of these three investigated environmental parameters (divalency, roughness and diffusion) in a more realistic system.

The coupling of SPT and flow chamber can also be a relevant tool fo localising precisely the ligands which give rise to bonds with receptors. This can lead to a much deeper knowledge of the adhesion mechanisms in various environmental conditions. Further work on the mobility of ligand studied through SPT can shed light on the phenomenon of multimerization. Indeed, simply looking at the Qdots intensity and diffusion it was possible to discriminate between single dots and possible aggregates.

Finally, kinetic studies can be performed for other pairs of ligands and receptors. During this thesis work, experiments on pMHC-anti HLA were performed, showing results which have to be confirmed with further experiences. These studies can represent a basis for the TCR-pMHC interaction which is extremely important in immune response.

Bibliography

Adamson, A. W. & Gast, A. P. (1997). Physical chemistry of surfaces. *Wiley-Interscience (6th edition)*.

Agarwal, A., Katira, P., & Hess, H. (2009). Millisecond curing time of a molecular adhesive causes velocity-dependent cargo-loading of molecular shuttles. *Nano Letters*, *9*, 1170-1175.

Alon, R., Hammer, D. A. & Springer, T. A. (1995). Lifetime of the P-selectin: carbohydrate bond and its response to tensile force in hydrodynamic flow. *Nature, 374*, 539-542.

Arciola, C. R., Alvi, F. I., An, Y. H., Campoccia, D., & Montanaro, L. (2005). Implant infection and infection resistant materials: a mini review. *The International Journal of Artificial Organs*, *28*, 1119-1125.

Atkins, P., & de Paula, J. (2002). Physical chemistry. *OUP Oxford (7th edition)*.

Axelrod, D. (2008). Total internal reflection fluorescence microscopy (chapter 7). *Methods in Cell Biology*, *89*, 169-221.

Baumgartner, W., Hinterdorfer, P., Ness, W., Raab, A., Vestweber, D., Schindler, H., & Drenckhahn, D. (2000). Cadherin interaction probed by atomic force microscopy. *Proceedings of the National Academy of Sciences*, *97*, 4005 -4010.

Baumgartner, W., Schütz, G. J., Wiegand, J., Golenhofen, N., & Drenckhahn, D. (2003). Cadherin function probed by laser tweezer and single molecule fluorescence in vascular endothelial cells. *Journal of Cell Science*, *116*, 1001-1011.

Bayas, M. V., Leung, A., Evans, E., & Leckband, D. (2006). Lifetime measurements reveal kinetic differences between homophilic cadherin bonds. *Biophysical Journal*, *90*, 1385-1395.

Bell, G. I. (1978). Models for the specific adhesion of cells to cells. *Science*, *200*(4342),

618-627.

Benoit, M., Gabriel, D., Gerisch, G., & Gaub, H E. (2000). Discrete interactions in cell adhesion measured by single-molecule force spectroscopy. *Nature Cell Biology*, *2*, 313-317.

Billadeau, D. D., Nolz, J. C., & Gomez, T. S. (2007). Regulation of T-cell activation by the cytoskeleton. *Nature Reviews. Immunology*, *7*, 131-143.

Bongrand, P. (1999). Ligand-receptor interactions. *Reports on Progress in Physics*, *62*, 921-968.

Brunetti, V., Maiorano, G., Rizzello, L., Sorce, B., Sabella, S., Cingolani, R., & Pompa, P. P. (2010). Neurons sense nanoscale roughness with nanometer sensitivity. *Proceedings of the National Academy of Sciences of the United States of America*, *107*, 6264-6269.

Calderwood, D. A., Shattil, S. J., & Ginsberg, M. H. (2000). Integrins and Actin Filaments: Reciprocal Regulation of Cell Adhesion and Signaling. *Journal of Biological Chemistry*, *275*, 22607 -22610.

Carson, M. (1997). Ribbons. *Methods in Enzymology*, *277*, 493-505.

Chan, P. Y., Lawrence, M. B, Dustin, M. L., Ferguson, L. M., Golan, D. E., & Springer, T. A. (1991a). Influence of receptor lateral mobility on adhesion strengthening between membranes containing LFA-3 and CD2. *The Journal of Cell Biology*, *115*, 245-255.

Chen, S., & Springer, T. A. (2001). Selectin receptor-ligand bonds: Formation limited by shear rate and dissociation governed by the Bell model. *Proceedings of the National Academy of Sciences of the United States of America*, *98*, 950-955.

Chen, X., Kim, T. D., Carman, C. V., Mi, L.-Z., Song, G., & Springer, T. A. (2007). Structural plasticity in Ig superfamily domain 4 of ICAM-1 mediates cell surface dimerization. *Proceedings of the National Academy of Sciences*, *104*, 15358

-15363.

Cooper, K., Gupta, A., & Beaudoin, S.. (2001). Simulation of the Adhesion of Particles to Surfaces. *Journal of Colloid and Interface Science*, *234*, 284-292.

Cotman, C. W., Hailer, N. P., Pfister, K. K., Soltesz, I., & Schachner, M. (1998). Cell adhesion molecules in neural plasticity and pathology: similar mechanisms, distinct organizations? *Progress in Neurobiology*, *55*, 659-669.

Dahan, M., Lévi, S., Luccardini, C., Rostaing, P., Riveau, B., & Triller, A. (2003). Diffusion dynamics of glycine receptors revealed by single-quantum dot tracking. *Science*, *302*, 442-445.

Decuzzi, P., & Ferrari, M. (2010). Modulating cellular adhesion through nanotopography. *Biomaterials*, *31*, 173-179.

Deligianni, D. D., Katsala, N. D., Koutsoukos, P. G., & Missirlis, Y. F. (2001). Effect of surface roughness of hydroxyapatite on human bone marrow cell adhesion, proliferation, differentiation and detachment strength. *Biomaterials*, *22*, 87-96.

Dudko, O. K., Hummer, G., & Szabo, A. (2008). Theory, analysis, and interpretation of single-molecule force spectroscopy experiments. *Proceedings of the National Academy of Sciences of the United States of America*, *105*, 15755-15760.

Dustin, M. L., Ferguson, L. M., Chan, P. Y., Springer, T. A, & Golan, D. E. (1996). Visualization of CD2 interaction with LFA-3 and determination of the two-dimensional dissociation constant for adhesion receptors in a contact area. *The Journal of Cell Biology*, *132*, 465-474.

Dustin, M. L., Rothlein, R., Bhan, A. K., Dinarello, C. A., & Springer, T. A. (1986). Induction by IL 1 and interferon-gamma: tissue distribution, biochemistry, and function of a natural adherence molecule (ICAM-1). *Journal of Immunology*, *137*, 245-254.

Dwir, O., Kansas, G. S., & Alon, R. (2000). An activated L-selectin mutant with

conserved equilibrium binding properties but enhanced ligand recognition under shear flow. *The Journal of Biological Chemistry*, *275*, 18682-18691.

Eichenlaub, S., Gelb, A., & Beaudoin, S. (2004). Roughness models for particle adhesion. *Journal of Colloid and Interface Science*, *280*, 289-298.

English, T. J., & Hammer, D. A. (2005). The effect of cellular receptor diffusion on receptor-mediated viral binding using Brownian adhesive dynamics (BRAD) simulations. *Biophysical Journal*, *88*, 1666-1675.

Eske, L. D., & Galipeau, D. W. (1999). Characterization of SiO2 surface treatments using AFM, contact angles and a novel dewpoint technique. *Colloids and Surfaces A: Physicochemical and Engineering Aspects*, *154*, 33-51.

Evans, E., Berk, D., & Leung, A. (1991). Detachment of agglutinin-bonded red blood cells. I. Forces to rupture molecular-point attachments. *Biophysical Journal*, *59*, 838-848.

Evans, E., Leung, A., Hammer, D., & Simon, S. (2001). Chemically distinct transition states govern rapid dissociation of single L-selectin bonds under force. *Proceedings of the National Academy of Sciences of the United States of America*, *98*, 3784-3789.

Evans, E., Ritchie, K., & Merkel, R. (1995). Sensitive force technique to probe molecular adhesion and structural linkages at biological interfaces. *Biophysical Journal*, *68*, 2580-2587.

Evans, E., Kinoshita, K., Simon, S., & Leung, A. (2010). Long-lived, high-strength states of ICAM-1 bonds to beta2 integrin, I: lifetimes of bonds to recombinant alphaLbeta2 under force. *Biophysical Journal*, *98*, 1458-1466.

Evans, E., Leung, A., Heinrich, V., & Zhu, C. (2004). Mechanical switching and coupling between two dissociation pathways in a P-selectin adhesion bond. *Proceedings of the National Academy of Sciences of the United States of*

America, *101*, 11281-11286.

Fenz, S. F., Merkel, R., & Sengupta, K. (2009). Diffusion and intermembrane distance: case study of avidin and E-cadherin mediated adhesion. *Langmuir: The ACS Journal of Surfaces and Colloids*, *25*, 1074-1085.

Florin, E. L., Moy, V. T. & Gaub H. E. (1994). Adhesion forces between individual ligand-receptor pairs. *Science, 264*, 415-417.

Foote, J., & Milstein, C. (1991). Kinetic maturation of an immune response. *Nature*, *352*, 530-532.

Gengler, R. Y. N., thesis (2010). A modified Langmuir Schaefer method for the creation of functional thin films. *University of Groningen*.

Gentile, F., Tirinato, L., Battista, E., Causa, F., Liberale, C., di Fabrizio, E. M., & Decuzzi, P. (2010). Cells preferentially grow on rough substrates. *Biomaterials*, *31*, 7205-7212.

González-García, C., Sousa, S. R., Moratal, D., Rico, P., & Salmerón-Sánchez, M. (2010). Effect of nanoscale topography on fibronectin adsorption, focal adhesion size and matrix organisation. *Colloids and Surfaces. B, Biointerfaces*, *77*, 181-190.

Ha, T., & Selvin, P. R. (2008). The new era of biology in singulo. *Single-molecule techniques* (Chapter 1). CSHL Press.

Hammer, D. A. (2005). Leukocyte adhesion: what's the catch? *Current Biology: CB*, *15*, R96-99.

Harington, K. J., & Syrigos, K. N. (2000). The Role of E-Cadherin-Catenin Complex: More Than an Intercellular Glue? *Annals of Surgical Oncology*, *7*, 783-788.

Haun, J. B., & Hammer, D. A. (2008). Quantifying nanoparticle adhesion mediated by specific molecular interactions. *Langmuir: The ACS Journal of Surfaces and Colloids*, *24*, 8821-8832.

Hillis, G. S., & Flapan, A. D. (1998). Cell adhesion molecules in cardiovascular disease: a clinical perspective. *Heart (British Cardiac Society)*, *79*, 429-431.

Hinterdorfer, P;, Baumgartner, W., Gruber, H. J., Schilcher, K., & Schindler, H. (1996). Detection and localization of individual antibody-antigen recognition events by atomic force microscopy. *Proceedings of the National Academy of Sciences of the United States of America*, *93*, 3477-3481.

Hinterdorfer, P, Schütz, G., Kienberger, F., & Schindler, H. (2001). Detection and characterization of single biomolecules at surfaces. *Journal of Biotechnology*, *82*, 25-35.

Hinterdorfer, P., & Dufrêne, Y. F. (2006). Detection and localization of single molecular recognition events using atomic force microscopy. *Nature Methods*, *3*, 347-355.

Hocdé, S. A., Hyrien, O., & Waugh, R. E. (2009). Cell adhesion molecule distribution relative to neutrophil surface topography assessed by TIRFM. *Biophysical Journal*, *97*, 379-387.

Huang, J., Chen, J., Chesla, S. E., Yago, T., Mehta, P., McEver, R. P., Zhu, C., & Long, M. (2004). Quantifying the effects of molecular orientation and length on two-dimensional receptor-ligand binding kinetics. *The Journal of Biological Chemistry*, *279*, 44915-44923.

Huppa, J. B., Axmann, M., Mörtelmaier, M. A., Lillemeier, B. F., Newell, E. W., Brameshuber, M., Klein, L. O., et al. (2010). TCR-peptide-MHC interactions in situ show accelerated kinetics and increased affinity. *Nature*, *463*, 963-967.

Hynes, R. O. (2002). Integrins: bidirectional, allosteric signaling machines. *Cell*, *110*, 673-687.

Jang, Y., Lincoff, A. M., Plow, E. F., & Topol, E. J. (1994). Cell adhesion molecules in coronary artery disease. *Journal of the American College of Cardiology*, *24*, 1591-1601.

Jaqaman, K., Loerke, D., Mettlen, M., Kuwata, H., Grinstein, S., Schmid, S. L., & Danuser, G. (2008). Robust single-particle tracking in live-cell time-lapse sequences. *Nature Methods*, *5*, 695-702.

Jun, C. D., Carman, C. V., Redick, S. D., Shimaoka, M., Erickson, H. P., & Springer, T. A. (2001a). Ultrastructure and function of dimeric, soluble intercellular adhesion molecule-1 (ICAM-1). *The Journal of Biological Chemistry*, *276*, 29019-29027.

Jun, C. D., Shimaoka, M., Carman, C. V., Takagi, J., & Springer, T. A. (2001b). Dimerization and the effectiveness of ICAM-1 in mediating LFA-1-dependent adhesion. *Proceedings of the National Academy of Sciences of the United States of America*, *98*, 6830-6835.

Kaplanski, G., Farnarier, C., Tissot, O., Pierres, A, Benoliel, A. M., Alessi, M. C., Kaplanski, S., & Bongrand P. (1993). Granulocyte-endothelium initial adhesion. Analysis of transient binding events mediated by E-selectin in a laminar shear flow. *Biophysical Journal*, *64*, 1922-1933.

Kim, D. T., Rothbard, J. B., Bloom, D. D., & Fathman, C. G. (1996). Quantitative analysis of T cell activation: role of TCR/ligand density and TCR affinity. *Journal of Immunology*, *156*, 2737-2742.

Kinoshita, K., Leung, A., Simon, S., & Evans, E.. (2010). Long-lived, high-strength states of ICAM-1 bonds to beta2 integrin, II: lifetimes of LFA-1 bonds under force in leukocyte signaling. *Biophysical Journal*, *98*, 1467-1475.

Kramers, H. (1940). Brownian motion in a field of force and the diffusion model of chemical reactions. *Physica*, *7*, 284-304.

Kucik, D F, Dustin, M. L., Miller, J. M., & Brown, E. J. (1996). Adhesion-activating phorbol ester increases the mobility of leukocyte integrin LFA-1 in cultured lymphocytes. *The Journal of Clinical Investigation*, *97*, 2139-2144.

Kunzler, T. P., Huwiler, C., Drobek, T., Vörös, J., & Spencer, N. D. (2007). Systematic

study of osteoblast response to nanotopography by means of nanoparticle-density gradients. *Biomaterials*, *28*, 5000-5006.

Lawrence, M. B., & Springer, T. A. (1991). Leukocytes roll on a selectin at physiologic flow rates: distinction from and prerequisite for adhesion through integrins. *Cell*, *65*, 859-873.

Lee, G.U., Kidwell, D.A. & Colton, R.J. (1994a). Sensing discrete streptavidin biotin interactions with atomic-force microscopy. *Langmuir, 10*, 354-357.

Lieto, A. M., Cush, R. C., & Thompson, N. L. (2003). Ligand-receptor kinetics measured by total internal reflection with fluorescence correlation spectroscopy. *Biophysical Journal*, *85*, 3294-3302.

Ling, X., Ye, J. F., & Zheng, X. X. (2003). Dynamic investigation of leukocyte-endothelial cell adhesion interaction under fluid shear stress in vitro. *Acta Biochimica Et Biophysica Sinica*, *35*, 567-572.

Lipman, N. S., Jackson, L. R., Trudel, L. J., Weis-Garcia, F. (2005). Monoclonal versus polyclonal antibodies: distinguishing characteristics, applications, and information resources. *ILAR journal*, *46*, 258-68.

Llères, D., Swift, S., & Lamond, A. I. (2007). Detecting Protein-Protein Interactions In Vivo with FRET using Multiphoton Fluorescence Lifetime Imaging Microscopy (FLIM). *Current Protocols in Cytometry.*

Marshall, B. T., Long, M., Piper, J. W., Yago, T., McEver, R. P., & Zhu, C. (2003). Direct observation of catch bonds involving cell-adhesion molecules. *Nature*, *423*, 190-193.

Meilhac, N., Le Guyader, L., Salomé, L., & Destainville, N. (2006). Detection of confinement and jumps in single-molecule membrane trajectories. *Physical Review. E, Statistical, Nonlinear, and Soft Matter Physics*, *73*, 011915.

Merkel, R., Nassoy, P., Leung, A., Ritchie, K., & Evans, E. (1999). Energy landscapes

of receptor-ligand bonds explored with dynamic force spectroscopy. *Nature*, *397*, 50-53.

Merkel, R. (2001). Force spectroscopy on single passive biomolecules and single biomolecular bonds. *Physics Reports*, *346*, 343-385.

Mould, A. P., Akiyama, S. K., & Humphries, M. J. (1995). Regulation of integrin α5β1-fibronectin interactions by divalent cations. *The Journal of Biological Chemistry*, *270*, 26270–26277.

Moy, V. T., Florin, E. L., & Gaub, Hermann E. (1994). Adhesive forces between ligand and receptor measured by AFM. *Colloids and Surfaces A: Physicochemical and Engineering Aspects*, *93*, 343-348.

Neuman, K. C., & Nagy, A. (2008). Single-molecule force spectroscopy: optical tweezers, magnetic tweezers and atomic force microscopy. *Nature Methods*, *5* 491-505.

Okegawa, T., Li, Y., Pong, R. C., & Hsieh, J. T. (2002). Cell adhesion proteins as tumor suppressors. *The Journal of Urology*, *167*, 1836-1843.

Orsello, C. E., Lauffenburger, D. A., & Hammer, D. A. (2001). Molecular properties in cell adhesion: a physical and engineering perspective. *Trends in Biotechnology*, *19*, 310-316.

Peressadko, A. G., Hosoda, N., & Persson, B. N. J. (2005). Influence of surface roughness on adhesion between elastic bodies. *Physical Review Letters*, *95*, 124301.

Perret, E., Leung, A., Feracci, H., & Evans, E. (2004). Trans-bonded pairs of E-cadherin exhibit a remarkable hierarchy of mechanical strengths. *Proceedings of the National Academy of Sciences of the United States of America*, *101*, 16472-16477.

Pierres, A, Benoliel, A. M., & Bongrand, P. (1995). Measuring the lifetime of bonds

made between surface-linked molecules. *The Journal of Biological Chemistry*, *270*, 26586-26592.

Pierres, A., Touchard, D., Benoliel, A. M., & Bongrand, P. (2002). Dissecting streptavidin-biotin interaction with a laminar flow chamber. *Biophysical Journal*, *82*, 3214-3223.

Pierres, A., Benoliel, A. M., & Bongrand, P. (2008). Studying Molecular Interactions at the Single Bond Level with a Laminar Flow Chamber. *Cellular and Molecular Bioengineering, 1*, 247-262.

Pincet, F., & Husson, J. (2005). The solution to the streptavidin-biotin paradox: the influence of history on the strength of single molecular bonds. *Biophysical Journal*, *89*, 4374-4381.

Richardsson, T., Petty, M. C., Bryce, M. R., & Bloor, D. (1995). *Introduction to molecular electronics* (Chapter 10). Oxford University Press, New York.

Rinker, K. D., Prabhakar, V., & Truskey, G. A. (2001). Effect of contact time and force on monocyte adhesion to vascular endothelium. *Biophysical Journal*, *80*, 1722-1732.

Ritort, F. (2006). Single-molecule experiments in biological physics: methods and applications. *Journal of Physics. Condensed Matter: An Institute of Physics Journal*, *18*, R531-583.

Robert, P., Limozin, L., Benoliel, A. M., Pierres, A. & Bongrand, P. (2006). Glycocalyx regulation of cell adhesion (Chapter 7). *In Principles of Cellular Engineering*. Elsevier.

Robert, P., thesis (2009). Étude dynamique de l'adhésion leucocytaire avec une chambre à flux laminaire: de la physique à la médecine. Université de la Méditerranée Aix-Marseille II.

Robert, P., Limozin, L., Pierres, A., & Bongrand, P. (2009). Biomolecule association

rates do not provide a complete description of bond formation. *Biophysical Journal*, *96*, 4642-4650.

Robert, P., Nicolas, A., Aranda-Espinoza, S., Bongrand, P, & Limozin, L. (2011). Minimal encounter time and separation determine ligand-receptor binding in cell adhesion. *Biophysical Journal*, *100*, 2642-2651.

Robert, P., Sengupta, K., Puech, P. H., Bongrand, P, & Limozin, L. (2008). Tuning the formation and rupture of single ligand-receptor bonds by hyaluronan-induced repulsion. *Biophysical Journal*, *95*, 3999-4012.

Saint-Michel, E., Giannone, G., Choquet, D., & Thoumine, O. (2009). Neurexin/neuroligin interaction kinetics characterized by counting single cell-surface attached quantum dots. *Biophysical Journal*, *97*, 480-489.

Sarangapani, K. K., Yago, T., Klopocki, A. G., Lawrence, M. B, Fieger, C. B., Rosen, S. D., McEver, R. P., & Zhu C. (2004). Low force decelerates L-selectin dissociation from P-selectin glycoprotein ligand-1 and endoglycan. *The Journal of Biological Chemistry*, *279*, 2291-2298.

Sarantos, M. R., Raychaudhuri, S., Lum, A. F. H., Staunton, D. E., & Simon, S. I. (2005). Leukocyte function-associated antigen 1-mediated adhesion stability is dynamically regulated through affinity and valency during bond formation with intercellular adhesion molecule-1. *The Journal of Biological Chemistry*, *280*, 28290-28298.

Saxton, M. J., & Jacobson, K. (1997). Single-particle tracking: application to membrane dynamics. *Annual Reviews for Biophisical and Biomolecular Structure*, 26, 373-399.

Saxton, M. J. (2008). Single-particle tracking: connecting the dots. *Nature Methods*, *5*, 671-672.

Seifert, U. (2000). Rupture of multiple parallel molecular bonds under dynamic loading.

Physical Review Letters, *84*, 2750-2753.

Sergé, A., Bertaux, N., Rigneault, H., & Marguet, D. (2008). Dynamic multiple-target tracing to probe spatiotemporal cartography of cell membranes. *Nature Methods*, *5*, 687-694.

Simson, R., Sheets, E. D., & Jacobson, K. (1995). Detection of temporary lateral confinement of membrane proteins using single-particle tracking analysis. *Biophysical Journal*, *69*, 989-993.

Smith, A. S., Sengupta, K., Goennenwein, S., Seifert, U., Sackmann, E., (2008). Force-induced growth of adhesion domains is controlled by receptor mobility. *PNAS*, 105, 6906-6911.

Springer, T. A. (1994). Traffic signals for lymphocyte recirculation and leukocyte emigration: the multistep paradigm. *Cell*, *76*, 301-314.

Stockton, B. M., Cheng, G., Manjunath, N., Ardman, B., & von Andrian, U. H. (1998). Negative regulation of T cell homing by CD43. *Immunity*, *8*, 373-381.

Sulchek, T., Friddle, R. W., & Noy, A. (2006). Strength of multiple parallel biological bonds. *Biophysical Journal*, *90*, 4686-4691.

Swift, S. R., & Trinkle-Mulcahy, L. (2004). Basic principles of FRAP, FLIM and FRET. *Proceedings of the Royal Microscopical Society, 39*, 3–11.

Taite, L. J., Rowland, M. L., Ruffino, K. A., Smith, B. R. E., Lawrence, M. B, & West, J. L. (2006). Bioactive hydrogel substrates: probing leukocyte receptor-ligand interactions in parallel plate flow chamber studies. *Annals of Biomedical Engineering*, *34*, 1705-1711.

Thid, D., Bally, M., Holm, K., Chessari, S., Tosatti, S., Textor, M., & Gold, J. (2007). Issues of ligand accessibility and mobility in initial cell attachment. *Langmuir: The ACS Journal of Surfaces and Colloids*, *23*, 11693-11704.

Thomas, W. E., Trintchina, E., Forero, M., Vogel, V., & Sokurenko, E. V. (2002).

Bacterial adhesion to target cells enhanced by shear force. *Cell*, *109*, 913-923.

Thoumine, O., Ewers, H., Heine, M., Groc, L., Frischknecht, R., Giannone, G., Poujol, C., Lgros, P., Lounis, B., Cognet, L., & Choquet, D. (2008). Probing the dynamics of protein-protein interactions at neuronal contacts by optical imaging. *Chemical Reviews*, *108*, 1565-1587.

Tissot, O., Pierres, A., Foa, C., Delaage, M., Bongrand, P. (1992). Motion of cells sedimenting on a solid surface in a laminar shear flow. *Biophysical Journal, 61*, 204-215.

Uyemura, K., Takeda, Y., Asou, H., & Hayasaka, K. (1994). Neural cell adhesion proteins and neurological diseases. *Journal of Biochemistry*, *116*, 1187-1192.

Vitte, J., Pierres, A., Benoliel, A. M., & Bongrand, P. (2004). Direct quantification of the modulation of interaction between cell- or surface-bound LFA-1 and ICAM-1. *Journal of Leukocyte Biology*, *76*, 594-602.

Walter, N. G., Huang, C.-Y., Manzo, A. J., & Sobhy, M. A. (2008). Do-it-yourself guide: how to use the modern single-molecule toolkit. *Nature Methods*, *5*, 475-489.

Waugh, R. E., & Lomakina, E. B. (2009). Active site formation, not bond kinetics, limits adhesion rate between human neutrophils and immobilized vascular cell adhesion molecule 1. *Biophysical Journal*, *96*, 268-275.

Wayman, A. M., Chen, W., McEver, R. P., & Zhu, C. (2010). Triphasic Force Dependence of E-Selectin/Ligand Dissociation Governs Cell Rolling under Flow, *Biophysical Journal, 99*, 1166-1174.

Wayment, J. R., & Harris, J. M. (2009). Biotin-avidin binding kinetics measured by single-molecule imaging. *Analytical Chemistry*, *81*, 336-342.

Webster, T. J., & Ejiofor, J. U. (2004). Increased osteoblast adhesion on nanophase metals: Ti, Ti6Al4V, and CoCrMo. *Biomaterials*, *25*, 4731-4739.

Weisel, J. W., Shuman, H., & Litvinov, R. I. (2003). Protein-protein unbinding induced

by force: single-molecule studies. *Current Opinion in Structural Biology*, *13*, 227-235.

Wesseling, J., van der Valk, S. W., & Hilkens, J. (1996). A mechanism for inhibition of E-cadherin-mediated cell-cell adhesion by the membrane-associated mucin episialin/MUC1. *Molecular Biology of the Cell*, *7*, 565-577.

Wiese, G., Barthel, S. R., & Dimitroff, C. J. (2009). Analysis of physiologic E-selectin-mediated leukocyte rolling on microvascular endothelium. *Journal of Visualized Experiments: JoVE*.

Williams, T. E., Nagarajan, S., Selvaraj, P., & Zhu, C. (2001). Quantifying the impact of membrane microtopology on effective two-dimensional affinity. *The Journal of Biological Chemistry*, *276*, 13283-13288.

Wu, L., Xiao, B., Jia, X., Zhang, Y., Lü, S., Chen, J., & Long, M. (2007). Impact of carrier stiffness and microtopology on two-dimensional kinetics of P-selectin and P-selectin glycoprotein ligand-1 (PSGL-1) interactions. *The Journal of Biological Chemistry*, *282*, 9846-9854.

Yamada, K. M. (2003) Cell Adhesion (Chapter 9). *Current Protocols in Cell Biology.*

Yang, Y., Jun, C. D., Liu, J. H., Zhang, R., Joachimiak, A., Springer, T. A, & Wang, J. H. (2004). Structural basis for dimerization of ICAM-1 on the cell surface. *Molecular Cell*, *14*, 269-276.

Sako, T. Y. (2003). Single-molecule visualization in cell biology. *Nature reviews. Molecular cell biology.*

Yildiz, A., Forkey, J. N., McKinney, S. A., Ha, T., Goldman, Y. E., & Selvin, P. R. (2003). Myosin V walks hand-over-hand: single fluorophore imaging with 1.5-nm localization. *Science*, *300*, 2061-2065.

Yu, T., Wu, X., Gupta, K. B., & Kucik, D. F. (2010). Affinity, lateral mobility, and clustering contribute independently to β2-integrin-mediated adhesion. *American*

Journal of Physiology - Cell Physiology, *299*, C399 -C410.

Zhang, X., Wojcikiewicz, E., & Moy, V. T. (2002). Force spectroscopy of the leukocyte function-associated antigen-1/intercellular adhesion molecule-1 interaction. *Biophysical Journal*, *83*, 2270-2279.

Zhu, C., Yago, T., Lou, J., Zarnitsyna, V. I., & McEver, R. P. (2008). Mechanisms for Flow-Enhanced Cell Adhesion. *Annals of biomedical engineering*, *36*, 604-621.

Article

Quantitative modeling assesses the contribution of bond strengthening, rebinding and force sharing to the avidity of biomolecule interactions

Valentina Lo Schiavo[1,2,3], Philippe Robert[1,2,3,4], Laurent Limozin[1,2,3] Pierre Bongrand[1,2,3,4,*]

[1] - Aix-Marseille Université, LAI, 13288 Marseille, France
[2] - Inserm UMR 1067, LAI, Marseille France
[3] - CNRS UMR 7333, LAI, Marseille, France
[4] - Assistance Publique - Hôpitaux de Marseille (APHM), Hôpital de la Conception, France
* author for correspondence, pierre.bongrand@inserm.fr

ABSTRACT

Cell adhesion is mediated by numerous membrane receptors. It is desirable to derive the outcome of a cell-surface encounter from the molecular properties of interacting receptors and ligands. However, conventional parameters such as affinity or kinetic constants are often insufficient to account for receptor efficiency. Avidity is a qualitative concept frequently used to describe biomolecule interactions: this includes incompletely defined properties such as the capacity to form multivalent attachments. The aim of this study is to produce a working description of monovalent attachments formed by a model system, then to measure and interpret the behavior of divalent attachments under force. We investigated attachments between antibody-coated microspheres and surfaces coated with sparse monomeric or dimeric ligands. When bonds were subjected to a pulling force, they exhibited both a force-dependent dissociation consistent with Bell's empirical formula and a force- and time-dependent strengthening well described by a single parameter. Divalent attachments were stronger and less dependent on forces than monovalent ones. The proportion of divalent attachments resisting a force of 30 piconewtons for at least 5 s was 3.7 fold higher than that of monovalent attachments. Quantitative modeling showed that this required rebinding, i.e. additional bond formation between surfaces linked by divalent receptors forming only one bond. Further, experimental data were compatible with but did not require stress sharing between bonds within divalent attachments. Thus many ligand-receptor interactions do not behave as single-step reactions in the millisecond to second timescale. Rather, they exhibit progressive stabilization. This explains the high efficiency of multimerized or clustered receptors even when bonds are only subjected to moderate forces. Our approach provides a quantitative way of relating binding avidity to measurable parameters including bond maturation, rebinding and force sharing, provided these parameters have been determined. Also, this provides a quantitative description of the phenomenon of bond strengthening.

INTRODUCTION

Cell-cell or cell-surface interactions are mediated by highly diverse membrane adhesion receptors. Collectively, these receptors impart attachment a high mechanical strength of typically hundreds of nanonewtons (1,2) due to multivalent binding (3,4). However, the

critical step of cell adhesion is probably the formation of the first few bonds. These bonds will generate weak contacts resisting only several tens of piconewtons before subsequent strengthening. A remarkable example is the tethering of leukocytes to endothelial cells in flowing blood through transient interactions between selectins and their ligands (5). Adhesion efficiency is critically dependent on the kinetics of bond formation and rupture between interacting surfaces in presence of forces.

During the last two decades, remarkable progress was achieved in measuring interactions between surface-attached biomolecules in presence of forces at the single bond level. Investigators used laminar flow chambers, atomic force microscopes or micropipette-based methods (reviewed in 6). The following conclusions were obtained: i) in the simplest cases (7,8), the dissociation rate of a ligand-receptor bond exhibited exponential increase in presence of a disruptive force, as suggested by Bell (9). Bond rupture might be modeled as the passage of a single potential energy barrier in a unidimensional reaction path, following Kramers theory (10-13). ii) In many cases including antigen-antibody (14) streptavidin-biotin (15) or integrin-ligand (16) interaction, bond rupture involved the passage of several sequential energy barriers. These barriers generated multiple bound states for a given ligand-receptor couple. This might provide an explanation for the time-dependent strengthening of antigen-antibody (14), selectin-ligand (17) or streptavidin-biotin (18-19) bonds. iii) More recently, two different teams (20-21) provided experimental evidence that a disruptive force might paradoxically increase the lifetime of lectin-sugar (20) or P-selectin-PSGL-1 (21) bonds. These force-increasing bonds were dubbed catch-bonds following an early theoretical paper (22). While the mechanistic basis of the catch-bond phenomenon remains incompletely understood, an important possibility is that bond rupture may not follow an unidimensional path (23) and force might facilitate an alternative rupture path by deforming a multidimensional energy landscape (24-26).

A noticeable point is that single bond rupture was studied either by subjecting molecules to a constant force, usually with a flow chamber, or with a steadily increasing force ramp, usually with an atomic force microscope or a biomembrane force probe. In the former case, results were reported as survival curves of bonds subjected to a constant force. In the latter case, authors reported the dependence of rupture force on the rate of force increase, a method called dynamic force spectroscopy (15). Recently, different authors developed new ways of analyzing data, and they were able to extract the dependence of dissociation rates on instantaneous force from both sets of data (17, 26-27). In some (17, 19) but not all (27) cases, the dissociation rate was found to depend on bond history as well as instantaneous force.

However, while most efforts were focused on single bond studies, much experimental evidence suggests that initial binding is strongly facilitated when at least two bonds can form simultaneously. It has long been reported that the "functional" affinity of divalent IgG or even (Fab')2 fragments could be 100-1,000 fold higher than that of monovalent Fab fragments (28-29). Further, typical adhesion receptors such as ICAM-1 (30) or PSGL-1 (31) appear as dimers and these dimers are more efficient than monomers in mediating adhesive interactions (30, 31). This cannot be due to a modification of binding sites, since it was formally shown on ICAM-1 that dimerization was not required to assemble a full binding site (32). The functional importance of integrin micro- or nano-scale clustering is supported by many experiments (33-35) even if conformation is also important (36). Similar conclusions were found on cadherins (37). Therefore, it is warranted to explore quantitatively the effects of multivalency on adhesion efficiency.

According to several theoretical studies (38-42), the kinetics and mechanics of multivalent attachment rupture should depend on poorly known parameters such as receptor

and surface topography, lateral mobility, length and flexibility of membrane anchors, and rebinding rate. Therefore, there is an obvious need for accurate experimental studies of the effect of multivalency on receptor binding properties.

Sulchek et al. (43) used atomic force microscopy to measure the effect of multivalency on attachment mediated by antibodies and MUC-1 antigens connected to surfaces through long polymers : they concluded that forces were shared by parallel bonds. Also, the unstressed dissociation rate was about 40 fold lower with double bonds than with single bonds. Kinoshita et al. (45) used a biomembrane force probe to compare single and double bonds formed by ICAM-1 and LFA-1 receptors borne by polymorphonuclear cells. They concluded that forces were equally shared by divalent bonds. Loritz et al. (46) compared the rupture of single and double antigen-antibody bonds with dynamic force spectroscopy: the yield force of double bonds slightly exceeded that of single bonds.

Here, we used a laminar flow chamber to compare monovalent and divalent attachments between surfaces coated with **low densities** of ICAM-1 monomers or dimers and flowing microspheres coated with a **high density** of anti-ICAM-1 antibodies. The rationale of our approach was as follows: (i) Use monomers to measure the kinetics of single bond rupture in presence of a constant pulling force F of varying intensity. (ii) Use dimers to measure the dissociation rate of attachments mediated by one or two bonds. (iii) Build two algorithms allowing us to determine rupture kinetics of dimer-mediated attachment with two limiting cases : A – When a microsphere is attached by two bonds, then force applies only on one bond. B – When a microsphere is attached by two bonds, force is equally shared between bonds. Each algorithm made use of the experimental rupture kinetics of single bonds (determined with step i) and an adjustable parameter that was the frequency k_r of formation of an additional bond between a microsphere attached through one bond and a dimer. This parameter was called rebinding frequency. (iv) Determine with both algorithms A and B the value of parameter k_r allowing the best fit between calculated and experimental rupture of dimer-mediated attachments.

As compared with atomic force microscope or biomembrane force probe, the differences are as follows : i) the lag between bond formation and force application was less than 10 milliseconds as compared with typical contact durations of 100 milliseconds with aforementioned techniques. ii) The force applied on a bond remained constant in contrast with the force ramp usually applied with atomic force microscopes. iii) The range of applied forces was narrower with the flow chamber. iv) Since flowing particles sampled a high amount of ligand-coated surfaces, it was possible to use a very low coating density, thus making highly improbable the simultaneous interaction of microspheres with more than one ICAM-1 monomer or dimer. This is a key point for comparing single and double bonds. In another set of experiments, the binding and detachment of nanospheres in absence of flow was quantified. This allowed direct monitoring of force-free bond rupture, instead of merely using extrapolation procedures as usually done with atomic force microscope or biomembrane force probe.

We conclude that bond formation is not an all-or-none process but rather involves progressive strengthening on the subsecond timescale. Strengthening followed a simple empirical law involving a single adjustable parameter. Further, quantitative modeling showed that rebinding of particles maintained by a single bond, i.e. formation of an additional bond by a ligand dimer, was required to account for the force-resistance of attachments mediated by multivalent molecules. Thus, our results provide a quantitative assessment of the importance of multivalent binding in initial attachment. Also, this may provide a quantitative way of accounting for receptor efficiency or avidity.

MATERIALS AND METHODS

Surface and bead functionalization

Glass coverslides were washed three times with pure ethanol, then rinsed with deionized water and cleaned in piranha solution (H_2SO_4/H_2O_2 4:3, Sigma-Aldrich, St Quentin-Fallavier, France) before being coated as previously described (47) with poly-L-lysine (300 kDa, Sigma-Aldrich), then glutaraldehyde and anti-poly-histidine tag IgG1 mAb (AbD Serotec, Oxford, UK). Unreacted aldehyde groups were then blocked with 0.2 M glycine before incubation with 200 µl of 0.04 µg/ml solution of poly-histidine tagged ICAM-1 or Fc(ICAM-1)$_2$ chimera (Sinobiological, Beijing, China). The surface density of ICAM-1 groups was estimated at about 1/µm^2 as obtained after labeling with fluorescent anti-ICAM-1 antibodies and fluorescence determination (47). The probability that a same anti-histag antibody might bind two poly-histidine-tagged molecules was therefore very low. These estimates were also checked when surfaces were coated with fluorescent nanoparticles and observed with total internal reflection fluorescence (TIRF) microscopy as described below. In this case, glass coverslides were incubated in 200 µl of PBS containing 10 nM of fluorescent streptavidin-coated nanoparticles (605 streptavidin Qdot, Invitrogen, Cergy-Pontoise, France), 10 nM biotinylated anti-ICAM-1 (clone HA58, eBiosciences, San Diego, CA, USA) and 6 % BSA.

Microspheres were tosyl-activated M450 dynabeads of 4.5 µm diameter and 1,500 kg/m^3 density (Invitrogen) that were coated as previously described (47) first with rat anti-mouse Fc (AbD Serotec, Colmar, France), then with either mouse anti-human ICAM-1 (clone HA58, eBioscience) or mouse IgG1 K isotype control (eBioscience). They were stored at 4°C in a solution of 0.1% BSA and 0.1% sodium azide. For the reader's convenience, molecular assemblies are depicted on Fig. 1A.

Microscopy and data acquisition for Qdot binding (force-free detachment)

We used TIRF microscopy to measure the surface density of ligands and force-free dissociation kinetics of ICAM-1/anti-ICAM-1 bond. Since the excitation field decreases exponentially from the interface, it penetrates to a depth of only approximately 100-200 nm into the sample. We used an inverted Axiovert 200M microscope (Zeiss, Jena, Germany) equipped with a polarized laser (series 77, LASOS lasertechnik, Jena, Germany), a 100X objective with 1.45 numerical aperture, and a filter cube with 458/10 excitation, 470 dichroic and 605/40 emission filters. Image sequences were recorded with an iXon camera running on iQ software (Andor, Belfast, UK), using an exposure time of 100 ms and a frame rate of 9.6 Hz (48).

Slides were observed immediately after adding streptavidin-coated Qdots and biotinylated anti-ICAM-1, and images were recorded during 20 minutes. Samples were then rinsed five times before resuming observation for about 100 minutes. The Qdot surface density was determined with a multiple-target tracing algorithm (49). Nonspecific binding was determined on control surfaces that had been treated as described excepted that ICAM-1 addition was omitted. Specific binding was determined by subtracting nonspecific values. Nonspecific binding was always lower than 20% of specific binding. Results were expressed as survival curves by plotting the fraction of Qdots remaining bound versus time after the fivefold wash.

Data acquisition in flow chamber experiments.

Experiments were performed as previously described (47,50). Briefly, microspheres were suspended in PBS supplemented with 1 mg/ml BSA and driven into a parallel-plate flow chamber with an automatic syringe pump (NE500, ProSense BV, Munich, Germany), on the stage of an inverted microscope using a 20X objective and a standard video camera (Sony N50, Clichy, France). The video signal was subjected to real-time digitization (Win TV digitizer, Hauppauge, Paris, France) and compression (DivX codec), then recorded for delayed analysis. Pixel size was 0.5 μm. Particle velocity ranged between about 11 μm/s and 37.5 μm/s. Microsphere tracking was performed with a custom-made software determining the centroid of microsphere images with 40 nm resolution. Full-frame images were disinterlaced allowing 20 ms temporal resolution. The analysis presented in this report is based on the determination of about 27.8×10^6 microsphere positions, corresponding to a total displacement of 16.5 m and yielding 11,636 binding events.

Data analysis.
Basic features of motion are depicted on Fig. 1B. It was extensively checked (47,50) that microsphere motion was consistent with numerical prediction based on low Reynold's number hydrodynamics (51). As a result of gravity and short-range colloidal forces, sphere-to-surface distance h fluctuates with a most probable value measured at about 25 nm (52, 53). As a consequence, the sphere translational velocity parallel to the flow is expected to fluctuate with a peak value $u_p \approx 0.54$ aG, where a is the microsphere radius and G is the wall shear rate (52). A sphere was defined as arrested when its displacement δx was lower than 0.5 μm during the following period of time δt=200 ms. The true arrest duration d_{true} was derived from the apparent arrest duration d_{app} with the correction $d_{true} = d_{app} + \delta t - 2\delta x/u_p$ (50). The true number of arrests was estimated by extrapolating at time zero the initial part of experimental survival curve ($t \leq 0.5$s) (50). This segment was nearly linear with a correlation coefficient between time and survival greater than 0.99 (not shown).
Each set of experiments thus yielded the following information: i) the set of arrest durations. Data were used to build survival curves by plotting the fraction s of bonds surviving at time t after formation versus time t. This experimental setup allows direct visualization of the rupture statistics of bonds subjected to a constant force within a range of tens of milliseconds, corresponding to molecule and microsphere repositioning after attachment, to seconds. The statistical uncertainty SD(s) was calculated with binomial law :

$$SD(s) = [s\,(1-s)\,/N_t]^{1/2} \qquad (1)$$

where N_t is the total number of arrest and s the fraction of remaining bonds at time t.
ii) The **binding frequency f** (per millimeter) was defined as the number of recorded binding events divided by the total trajectory length L of monitored particles. The statistical uncertainty SD(f) was calculated with Poisson's law as (18):

$$SD(f) = (f/L)^{1/2} \qquad (2)$$

A key advantage of the flow chamber is to yield substantial statistics with surfaces bearing very low densities of receptor molecules. In our experiments, the surface density of ICAM-1 was about $1/\mu m^2$, yielding a binding probability lower than 10^{-3} per μm bead displacement. This gave a high probability that binding events were generated by single molecular interactions on the basis of Poisson's law (54). Another check that was repeatedly performed with this molecular system (55) was that sequential ligand dilutions resulted in proportional

decrease of binding frequency without any alteration of survival curves. Thus, we may assume with high confidence that binding events were due to single molecule interactions, which is a key requirement of the present work.

A common difficulty met in studies of rare binding events is the importance of incompletely defined nonspecific binding events. We accounted for this possibility by carefully determining the lifetime distribution and frequency of nonspecific events that were obtained by replacing specific anti-ICAM-1 antibodies by nonspecific immunoglobulins of similar isotype. This information was used to subtract the expected nonspecific contribution from survival curves as was previously done in other studies performed with biomembrane force probe (27).

As shown on Fig. 1B, when a microsphere was maintained at rest by a single bond, the force on the bond could be derived from the standard equations of mechanics, based on the known force F and torque Γ exerted on the sphere by the flow and assuming absence of friction at the sphere-to-surface contact. The tension T on the bond is only weakly dependent on the bond length and is equal to $(F+\Gamma/a)\,(a/2L)^{1/2}$ (Fig. 1B and (14)), yielding T = 0.904 G and T = 0.855 G respectively when surfaces were coated with ICAM-1 or $Fc(ICAM\text{-}1)_2$ receptors, assuming respectively L=68nm and L=76nm. Here, T is expressed in piconewton and G in s^{-1}.

Empirical representation of survival curves

It was important to represent experimental data accurately with curves involving a minimal number of parameters. However, a common finding obtained with the flow chamber (14, 18, 47) and atomic force microscopy (17, 19) as well as with soluble phase studies (56-57) is that the stability of ligand-receptor bonds is related to their history. An at least partial explanation stems in the multiplicity of binding states and time-dependent passage of ligand-receptor complexes towards the deepest and innermost energy wells. Unfortunately, quantitative account of multiphasic reactions, i.e. reactions involving a number of intermediate states and steps, requires a high number of parameters. Thus, Foote and Milstein (56) needed 8 parameters to describe an antigen-antibody reaction involving only two intermediate states. Here, we looked for a simple way of describing experimental survival curves with only two global parameters. Experimental and fitted curves were compared by calculating the mean squared difference (MSD) between the logarithm of predicted and experimental survival over 19 points spread on the [0,6s] time interval (namely 0 and $1.25^i/10$ - 1, for $1 \leq i \leq 18$). As shown below, an excellent fit was obtained for all tested curves by assuming for the dissociation rate the simple function:

$$k(F,t) = k(F,0)/(1 + a(F)\,t) \qquad (3)$$

Where F is the force applied on the bond which is assumed to be constant in a given experiment, k(F,t) is the dissociation rate in presence of a disrupting force F and at time t after bond formation, and a(F) is an empirical parameter that is defined as the bond-strengthening rate and is only dependent on F. Writing parameters k(F,0) and a(F) as k and a for short, this yields for the survival curve :

$$S(t) = (1 + a\,t)^{-(k/a)} \qquad (4)$$

In addition to its simplicity, this formula allows a natural interpretation of k(F,0) as the **initial dissociation rate** and a(F) as the **bond strengthening rate.** It must be emphasized that Eq. 3

should be used for time values on the order of 1/k, i.e. within the second range: It would be meaningless to use it do derive information on the events occurring during the initial ligand-receptor encounter and before force application on the bond, which is on the order of milliseconds.

Simulation of the dissociation of dimer-mediated attachments.
Predicted survival curves were built for divalent ligands by computer simulation. The starting point was an initial attachment with 1 or 2 bonds. The instantaneous dissociation rate k(F,t) was calculated with Eq.3 and parameters k(F,0) and a(F) derived from monomer binding studies. Parameter k(F,t) was used to generate random dissociation events. In some cases a random bond formation with frequency k_r was allowed to occur when a single bond existed. Parameter k_r may be defined as the rebinding rate since it represents the rate of formation of an additional bond between surfaces already attached with a single bond formed by a divalent receptor. Note that the same parameter was relevant to predict the formation of a bond between a free ICAM-1 and the antibody coated-surface, whether this had already be bound and released, or not. Parameter k_r is entirely different from the rate of bond formation between a freely moving sphere and a surface. k_r was the only **freely fitted** parameter since k and a were derived from studies made on monomer binding. In addition, two cases were considered, assuming either equal force sharing between two bonds or lack of force sharing. Typically, the time step for a simulation was set at 0.001 second and a theoretical survival curve was built by averaging 5,000 independent time series.

RESULTS
Microspheres displayed non specific binding events whose dissociation rate decreased as a function of both time after arrest and shear force.
Microspheres coated with anti-ICAM-1 or irrelevant antibodies were driven along surfaces coated with very low densities of monovalent ICAM-1 ligand, on the order of 1 molecule per μm^2. Microspheres displayed periods of translation with a constant velocity interspersed by arrests. The consequence of using low coating densities was that a significant proportion of binding events were not due to specific ICAM-1/anti-ICAM-1 interactions but rather consisted of so-called nonspecific interactions. This is a common finding in this type of experiments.
The duration of nonspecific binding events was determined by using microspheres coated with isotype-matched immunoglobulin controls instead of anti-ICAM-1 antibodies. As shown on Fig. 2, survival plots of nonspecific arrests displayed a typical time-dependent decrease of dissociation rate. Also, the dissociation rate decreased when the wall shear rate was increased. The average dissociation rate determined during the first 500 ms following bond formation was respectively 2.53 s^{-1}, 1.74 s^{-1} and 1.75 s^{-1} when the wall shear rate was 9.3 s^{-1}, 19.5 s^{-1} and 30.9 s^{-1}. This revealed a clearcut increase of arrest lifetime when the shear rate was increased, as described in other systems (20-22).
The frequency of nonspecific binding events was respectively 1.19±0.12 mm^{-1} (9 experiments, 399 arrests), 0.62±0.10 mm^{-1} (32 experiments, 1,362 arrests) and 0.19±0.03 mm^{-1} (21 experiments, 544 arrests) when the wall shear rate was 9.3 s^{-1}, 19.5 s^{-1} and 30.9 s^{-1}.

Specific ligand-receptor bonds displayed lower dissociation rate than nonspecific bonds, but this dissociation rate increased as a function of shear force.
When microspheres were coated with anti-ICAM-1 antibodies instead of nonspecific immunoglobulins, arrest frequency displayed 3.45 fold increase in a total of 67 experiments.

Thus, about 71% (i.e. 2.45/3.45) of binding events observed on anti-ICAM-1-coated particles were mediated by specific bonds. It was thus warranted to improve the description of specific events by subtracting the contribution of nonspecific interactions as previously done by other authors (27). Thus we investigated the variations of the frequency of specific and nonspecific arrests. We tested each ICAM-1-coated slide to determine first the frequency of nonspecific arrests with control microspheres, then the frequency of specific arrests. A strong correlation was found between the frequencies of specific and nonspecific arrests measured on a same slide: indeed, the correlation coefficient r derived from 67 different experiments was 0.8264 ($P=7.3\ 10^{-18}$). Secondly, specific binding was fairly low in some experiments, suggesting that coating might alter the conformation of ICAM-1 molecules. Experiments where the ratio between specific and nonspecific bindings was lower than 3 were thus discarded. In remaining experiments, the correlation between specific and nonspecific binding measured on the same slide remained significant. Thirdly, the correlation coefficient between the wall shear rate and the ratio between arrest frequencies measured on control and anti-ICAM-1-coated microspheres was only 0.180 (38 experiments, P=0.27).
Based on these findings, the fraction P_{NS} of nonspecific binding events was derived from the pooled number of arrests. We obtained P_{NS} = 0.226 (±0.020 SD) on surfaces coated with monomeric ICAM-1 interacting with anti-ICAM-1-coated microspheres and 0.199 (±0.020 SD) on surfaces coated with Fc(ICAM-1)$_2$ ligands.
The survival plots of attachments formed between specific antibodies and surfaces coated with monomeric ICAM-1 are shown before (Fig. 3A) and after (Fig.3B) correcting for non specific arrests. The difference between these plots demonstrated the importance of this correction. Indeed, the average dissociation rate measured during the first 500 ms under the lowest shear rate was respectively estimated at 0.577 s^{-1} and 0.254 s^{-1} before and after correction. In contrast with nonspecific arrests, the lifetime of specific bonds was decreased when the shear rate was increased. Average dissociation rates measured during the first 500 ms were respectively 0.254 s^{-1}, 0.532 s^{-1} and 1.059 s^{-1} when the pulling force exerted on bonds was estimated at 8.4, 16.7 and 26.6 pN.

Divalent attachment results in markedly increased resistance to shearing forces as compared to monovalent attachment.
Microspheres were made to bind surfaces coated with low densities of divalent Fc(ICAM-1)$_2$ ligand, and survival curves are shown on Fig. 4A. Interactions measured under the lowest wall shear rate were fairly comparable to those observed with monomeric ICAM-1, with a survival slightly higher than 50 % at time 5 second. However, the sensitivity to shear was much lower since the highest force reduced potentially divalent binding by only 40 %, i.e. **1.7 fold decrease**, 5 s after bond formation, whereas the survival of monovalent binding exhibited **6 fold** decrease under the same conditions.

Even in absence of shearing forces, divalent attachment results in much higher lifetime than monovalent attachment.
We monitored the release of Qdots bound to surfaces coated with monomeric or dimeric ICAM-1 ligand through anti-ICAM-1, in absence of flow. Since binding was allowed to occur during a period of 20 minutes, ICAM-1/anti-ICAM-1 bonds were expected to have matured sufficiently to generate more durable attachment than obtained after less than a few seconds of contact. As shown on Fig.5, attachment was much more durable than observed in the flow chamber, as expected. Further, the difference between monovalent and divalent attachment was still more impressive than found with the flow chamber, since no substantial Qdot release

was observed during 120 minutes when binding was potentially divalent, while 90 % detachment was observed within 100 minutes when attachment was monovalent.

Single bond rupture under forces is well described by two parameters: the initial dissociation rate and the strengthening rate.

As shown on Figure 3, single-bond attachments displayed time-dependent decrease of dissociation rate. Thus, we used Eq. 3 as a simple way of achieving an empirical description of bond rupture during the timescale of experiments. The basic assumption was that the initial dissociation rate k_0 was divided by (1+at) at time t, thus introducing a single strengthening parameter a. As shown on Fig. 3B and Table 1, this simple formula allowed a close fit with experimental values, since the mean square of relative difference (MSD) between fitted curves and experimental points was less than 0.0015. Interestingly, this formula also allowed a satisfactory fit of force-free detachment data (Fig.5 and Table 1**).**

Experimental data were used to estimate the dependence of the initial dissociation rate k(F,0) and bond strengthening parameter a(F) on the force F applied to a bond under tension. As shown on Fig.6, results suggested a linear dependence of k and a on exp(F), similarly to Bell's law. The regression lines shown on Fig. 6 were used to estimate the dependence of k and a on F in a force interval of about [0, 35 pN]. It must be emphasized that the range of data points was insufficient to yield detailed information on the force dependence of parameters a and k. The numerical values obtained under force-free conditions were not deemed comparable to those estimated under flow extrapolated at zero forces since the time scales of periods between bond formation and rupture measurement were respectively on the order of minutes (Qdots) and seconds (flow chamber).

The two-parameter description of single bond rupture allows derivation of rebinding rates between surfaces exposing divalent receptors and linked by a single bond.

We used the numerical data summarized on Table 1 to build simulated survival curves in order to test different independent assumptions: i) a force applied on a divalent attachment is applied on a single bond, or it is equally shared between both bonds (**no force sharing or force sharing**). ii) There is a zero or non-zero bond forming rate k_r between a microsphere and a surface linked by a single bond involving a divalent receptor (**no rebinding or rebinding**). iii) During the first milliseconds of attachment between anti-ICAM-1 coated microspheres and Fc(ICAM-1)$_2$-coated surfaces, a single or two bonds are formed (**monovalent or divalent initial attachment**). A number of simulated curves are displayed on Figures 4B-D and compared to experimental data. The following conclusions could thus be drawn sequentially:

First, we found that the **initial attachment was monovalent**. This was seen most clearly with the lowest velocity (Fig. 4.B): The MSD between experimental and theoretical curves (that were obtained by assuming that two bonds were formed at time zero) was higher than 0.7. Further, since calculated survival was higher than experimental values, the fit would have been still worse if the rebinding parameter k_r was nonzero. Also, similar findings were found with and without force sharing. Thus, whatever the other parameters, it could be safely concluded that initial attachment was monovalent.

Secondly, we found that a satisfactory fit between experimental and calculated survival curves required the occurrence of additional bond formation (ie nonzero k_r parameter). Our reasoning is illustrated on Fig. 4:

- For the lowest shear velocity, in absence of rebinding, the simulated curve was visibly different from experimental one, with a MSD of 0.0135. However, a satisfactory fit could be

obtained with k_r= 0.3 s^{-1}, yielding a MSD of 0.0022 and 0.0017 respectively with force sharing or not sharing (Fig. 4B).
- For the intermediate shear velocity, a good fit was obtained with both assumptions of force sharing and not sharing and k_r = 1.1 s^{-1}. The MSDs were respectively 0.0019 and 0.0008. In absence of rebinding, MSDs were higher than 0.04 with 1 or 2 bonds, whatever the assumption concerning force sharing (Fig. 4.C)
- For the highest velocity, a fairly poor fit could be obtained with both force sharing and no force sharing assumptions, MDSs were respectively 0.023 (k_r = 6 s^{-1}) and 0.009 (kr = 12 s^{-1}) in two representative simulations, which is fairly reasonable, but the shape of experimental and predicted curves were clearly different (Fig. 4D).

In conclusion, simulated curves could only be fitted to experimental data by assuming that i) initial attachment was monovalent, ii) rebinding could occur, and iii) force sharing between bonds had a small influence on survival curves which made it difficult to draw definitive conclusions concerning this point.

Both bond strengthening and rebinding play a key role in contributing the divalent bond capacity to resist moderate forces.
The conclusion of our study is that rebinding, bond strengthening and to a lesser extent force sharing all have the capacity to contribute the divalent attachment resistance to forces. Our model allows some estimate of the relative contribution of these effects, although this is not fully significant since they are not additive: We built survival curves for the highest force (Figure 4D) with the following assumptions: i) force sharing, rebinding and bond strengthening, ii) rebinding and bond strengthening, iii) force sharing and bond strengthening, and iv) force sharing and rebinding. While attachment survival in presence of the highest force is about 44% after 5 seconds with all three mechanisms simultaneously allowed, it would be about 1.9 fold lower in absence of force sharing, which was felt to represent a modest change, 5.9 fold lower in absence of bond formation, and 24.3 fold lower in absence of bond strengthening. These figures provide a quantitative insight into the hierarchical importance of these mechanisms.

DISCUSSION

During the last fifteen years, much work was done to describe the formation and rupture of bonds between surface-attached biological receptors and ligands at the single molecule level. All these studies revealed a growing complexity of ligand-receptor interaction. It was first considered that the kinetic rates of bond formation and rupture could give a reasonable account of ligand-receptors interactions (58). It was then recognized that an independent parameter must be added to account for the bond mechanical strength. In many cases this was done with Bell's empirical formula (9, 59). Other factors of complexity were that bond formation and rupture behaved as multi-step phenomena with an impressive hierarchy of binding states (14, 15, 27) and other bonds displayed so-called catch-bond behavior, i.e. the bond lifetime was increased by moderate pulling forces (20-22). In comparison, fewer studies were devoted to the theoretical (38-42) or experimental (43-46) behavior of multivalent attachments.
The strategy followed in this study was to use a model system in order to produce a working description of monovalent attachments, then to measure and interpret the behavior of dimer-mediated attachments under force. The main conclusion are that i) A new empirical parameter called the **bond strengthening** rate is required to account for the maturation of newly formed bonds. While the structural basis of our results remains to be investigated, it must be

emphasized that the conclusion that ligand-receptor bonds are expected to display extensive maturation with a timescale ranging from subsecond to hundreds of seconds or more is consistent with the expected complexity of energy landscapes and experimental reports on kinetic rates ranging between tenths of s^{-1} (56) or less (60) and more than 100 s^{-1} (50). ii) Both bond formation (as accounted for by the rebinding parameter) and bond strengthening play a major role in increasing the survival of divalent attachments as compared to monovalent attachments. The dramatic difference between monomer-mediated and dimer-mediated attachments made with a given receptor-ligand couple may provide an explanation for the common finding that many cell membrane receptors act as dimers.

The present study provides both a detailed example of this general concept and a simple experimental and theoretical framework for data analysis. In order to fully assess the significance of our results, several points need to be discussed.

Firstly, the flow chamber operated under low shear rate is well suited to study the behavior of single bonds subjected to moderate forces (61). Indeed, when the microspheres we used were subjected to a wall shear rate of 10 s^{-1}, they experienced a pulling force of only 1.62 pN, and their velocity was about 12 μm/s. Thus, during a 20 millisecond interval corresponding to the standard acquisition rate, their displacement of 240 nm was easily measurable with our tracking software, allowing optimal sensitivity for detecting the weakest binding events. Also, since microspheres scanned extensive areas, it was possible to use very low coating densities of ligands, thus providing optimal elimination of binding events involving more than one ligand, which was a key requirement in our study.

Secondly, we assumed that the rupture of specific sphere-to-surface attachments resulted from the rupture of transient ICAM-1/anti-ICAM-1 interactions rather than his-tag/anti-hist-tag or Fc/anti-Fc interactions. This assumption was supported by the following two points : first, a general finding with most ligand-receptor couples was that the off-rate exhibited steady decrease during the first tens of seconds or minutes following bond formation. This makes more likely that rupture events were due to the disruption of the newest bond even if it was as strong as the streptavidin-biotin interaction (18). Secondly, if most ruptures involved his-tag/anti-his-tag or Fc/anti-Fc interaction, no difference would be found between the monovalent and divalent ICAM-1/anti-ICAM-1 attachments, in contrast with our experimental data.

Thirdly, our results illustrate the importance of so-called nonspecific binding events, and the importance of taking care of them as was indeed recognized by other investigators (27). We provided some quantitative information on these events, and we found that their lifetime was of the same order of magnitude as those generated by single bonds. The difficulty of ruling out artifacts potentially generated by this occurrence is certainly the most demanding part of data collection. This raises at least two specific points. i) It is important to rule out the possibility that the progressive development of nonspecific interactions between surfaces held together by a specific bond might artefactually decrease experimental dissociation rates. This possibility is made unlikely by our recent finding that dissociation rates measured between surface-attached molecules with the flow chamber were consistent with results obtained on soluble ligands with surface plasmon resonance (62). We suggest this is understandable because the hydrodynamic force on the bead is too low to prevent thermal fluctuations (14), thus decreasing contact between surfaces. In addition, the specific engagement of ICAM-1 and anti-ICAM-1 should restrict the range of available molecular orientations, thus decreasing the probability of nonspecific interactions. ii) Our finding that nonspecific interactions were less sensitive to forces that specific ones might seem surprising. It must be argued that this is consistent with previous experimental studies made on protein-

RNA interaction (63). Note that wide differences were reported between nonspecific interactions detected between different surfaces (63-65), and certainly more work would be required to determine whether nonspecific interactions detected in our experiments displayed *bona fide* catch bond behavior.

Fourthly, it is important to exclude the possibility that reported bond strengthening might be an artefact due to progressive lengthening of the microsphere tether, thus decreasing the force on the bond. This hypothesis may be excluded as follows: the tether between the microsphere and the surface may be modeled as a freely jointed chain (66) consisting of approximately 4 links separated by flexible hinges. Since the rotation timescale of an immunoglobulin domain falls within the submicrosecond rate (67) and a force of more than 100 pN is required to unfold an immunoglobulin domain (68), no tether lengthening is expected in the timescale of bond strengthening we reported. Note also that this tether model may be used to support the hypothesis that the stress applied on bonds by the microsphere brownian motion is negligible as compared to the flow-generated forces. Indeed, it may be shown from standard statistical mechanics that the average force <F> exerted by a particle bound to a spring of stiffness s is (for one degree of freedom): $<F>=(2sk_BT/\pi)^{1/2}$, where k_B is Boltzmann's constant and T is the absolute temperature. If we approximate the molecular link between a bead and a surface as a freely jointed chain with 4 segments of length a=15 nm, the stiffness s is $3kT/4a^2$ (66), yielding an average force <F> of 0.19 pN, which is markedly lower than the hydrodynamic force that ranged between 1.6 and 4.8 pN in our experiments.

A fifth point is the accurate determination of single bond strengthening with a single measurable parameter. Indeed, while a number of results illustrated the multiplicity of binding states formed by ligand-receptor couples (14, 15, 27, 56, 57), there was a need for a simple way to deal with this complexity and provide a workable description of bond rupture. We think that the combination of parameters k(F,0) and a(F) meets with this requirement. It must be emphasized that a(F) should be considered as an empirical parameter and more work is required to relate it to the precise structure of interacting molecules.

A sixth point is that results obtained with ICAM-1 monomers were sufficiently accurate to allow us to predict the behavior of divalent ligands with a single fitted parameter (i.e. the rebinding rate k_r). A fully quantitative fit was obtained for the lowest two forces, and a semi-quantitative fit for the highest force. It must be emphasized that these results might be deemed satisfactory, since we had to neglect the influence of the nanometer-scale topography of receptors and ligands on force sharing and rate of formation of a second bond when a particle was maintained at rest by a first bond.

A fairly unexpected finding was that the fitted value of the rebinding rate increased as a function of the applied force. While this might be due to a forced alignment of binding molecules and exclusion of a range of conformations incompatible with bond formation, a better definition of interacting surfaces would be required to discuss this point. Indeed, there is very little available information on the effect of forces on binding rates between surfaces coated with binding molecules (see also remarks in the methods section of (27)).

In conclusion, we provided a simple experimental and theoretical framework for comparing the behavior of monovalent and divalent attachments. In view of the known importance and wide occurrence of mutivalency, it would be instructive to apply this approach to a number of situations by varying the structure of surfaces, nature of ligand-receptor couples, and properties of connection between molecules and surfaces. This might provide a basis for a better understanding of the incompletely defined concept of avidity. Indeed, avidity is often used as a qualitative way of accounting for the efficiency of cell membrane receptors to bind to multivalent ligands, and it is felt to represent the capacity to

form multivalent bonds. Avidity is thus different from affinity (69), which is a rigorously defined parameter accounting for the thermodynamics of a well-defined ligand-receptor couple. Avidity is closely related to the premium of multivalent over monovalent binding. Our results suggest that the bond strengthening rate parameter we defined accounts for part of avidity.

Acknowledgments. The authors thank Dr. Zohar Mishal for the excellent advice for manuscript presentation and writing.

REFERENCES

1. Bongrand P, Bell GI (1984) Cell-cell adhesion : parameters and possible mechanisms. In: Perelson AS, DeLisi C, Wiegel FW editors. Cell surface dynamics: concepts and models. New York: Marcel Dekker. pp. 459-493.

2. Palecek SP, Loftus JC, Ginsberg MH, Lauffenburger DA, Horwitz AF (1997) Integrin-ligand binding properties govern cell migration speed through cell-substratum adhesiveness. Nature 385: 537-539.

3. McCloskey MA, Poo MM (1986). Contact-induced redistribution of specific membrane components: local accumulation and development of adhesion. J. Cell Biol. 102: 2185-2196.

4. André P, Benoliel AM, Capo C, Foa C, Buferne M, Boyer C, Schmitt-Verhulst AM, Bongrand P (1990) Use of conjugates made between a cytolytic T cell clone and target cells to study the redistribution of membrane molecules in contact areas. J. Cell Sci. 97: 335-347.

5. Lawrence MB, Springer TA (1991) Leukocytes roll on a selectin at physiologic flow rates : distinction from and prerequisite for adhesion through integrins. Cell, 65: 859-873.

6. Bongrand P (1999) Ligand-receptor Interactions. Rep. Prog. Phys. 62: 921-968

7. Chen S, Springer TA (2001) Selectin receptor-ligand bonds : formation limited by shear rate and dissociation governed by the Bell model. Proc. Natl. Acad. Sci. USA. 98: 950-955.

8. Hummer G, Szabo A (2003) Kinetics of nonequilibrium single-molecule pulling experiments. Biophys. J. 85: 5-15.

9. Bell GI (1978) Models for the specific adhesion of cells to cells. Science 200: 618-627.

10. Kramers HA (1940) Brownian motion in a field of force and the diffusion model of chemical reactions. Physica VII: 284-304.

11. Hänggi P, Talkner P, Borkovec M (1990) Reaction-rate theory : fifty years after Kramers. Rev. Mod. Phys. 62: 251-341.

12. Evans E, Ritchie K (1997) Dynamic strength of molecular adhesion bonds. Biophys. J. 72 : 1541-1555.

13. Dudko OK, Hummer G, Szabo A (2006) Intrinsic rates and activation free energies from single-molecule pulling experiments. Phys. Rev. Letters 96: 108101.

14. Pierres A, Benoliel AM, Bongrand P (1995) Measuring the lifetime of bonds made between surface-linked molecules. J. Biol. Chem. 270: 26586-26592.

15. Merkel R, Nassoy P, Leung A, Ritchie K, Evans E (1999) Energy landscapes of receptor-ligand bonds explored with dynamic force spectroscopy. Nature 397: 50-53.

16. Zhang X, Vojcikiewicz E, Moy VT (2002) Force spectroscopy of the leukocyte function associated 1/Intercellular adhesion molecule 1 interaction. Biophys. J. 83: 2270-2279.

17. Marshall BT, Sarangapani KK, Lou J, McEver RP and Zhu C (2005) Force history dependence of receptor-ligand dissociation. Biophys. J. 88: 1458-1466.

18. Pierres A, Touchard D, Benoliel AM, Bongrand P (2002) Dissecting streptavidin-biotin interaction with a laminar flow chamber. Biophys. J. 82: 3214-3223.

19. Pincet F, Husson J (2005) The solution to the streptavidin-biotin paradox : the influence of history on the strength of single molecular bonds. Biophys. J. 89: 4374-4381.

20. Thomas WE, Trintchina E, Forero M, Vogel V, Sokurenko E (2002) Bacterial adhesion to target cells enhanced by shear forces. Cell 109: 913-923.

21. Marshall B, Long M, Piper JW, Yago T, McEver RP, Zhu C (2003) Direct observation of catch bonds involving cell-adhesion molecules. Nature 423: 190-193.

22. Dembo M, Torney DC, Saxman K, Hammer D (1988) the reaction-limited kinetics of membrane-to-surface adhesion and detachment. Proc. Roy. Soc. Lond. B 234: 55-83.

23. Eyring H (1935) The activated complex in chemical reactions. J. Chem. Phys. 3 : 107-115.

24. Evans E, Leung A, Heinrich V and Zhu C (2004) Mechanical switching and coupling between two dissociation pathways in a P-selectin adhesion bond. Proc. Natl. Acad. Sci. USA 101: 11281-11286.

25. Pereverzev V, Perzhdo OV, Thomas WE, Sokurenko EV (2005) Distinctive features of the biological catch bond in the jump-ramp force regime predicted by the two-pathway model. Phys. Rev. E 72: 010903.

26. Dudko OK, Hummer G, Szabo A (2008) Theory, analysis and interpretation of single-molecule force spectroscopy experiments. Proc. Natl. Acad. Sci. USA 105:15755-15760.

27. Evans E, Kinoshita K, Simon S, Leung A (2010) Long-lived, high-strength states of ICAM-1 bonds to beta 2 integrin. I: lifetimes of bonds to recombinant $alpha_L$ $beta_2$ under force. Biophys. J. 98: 1458-1466.

28. Hornick CL, Karush F (1972) Antibody affinity. III. The role of multivalence. Immunochemistry 9:325-340.

29. Bystryn JC, Siskind GW, Uhr JW (1973) Binding of antigen by immunocytes. I. Effect of ligand valence on binding affinity of MOPC 315 cells for DNP conjugates. J. Exp. Med. 137:301-316.

30. Miller J, Knorr R, Ferrone M, Houdei R, Carron CP, Dustin ML (1995) Intercellular adhesion molecule-1 dimerization and its consequences for adhesion mediated by lymphocyte function associated-1. J. Exp. Med. 182: 1231-1241.

31. Yang J, Furie BC, Furie B (1999) The biology of P-selectin glycoprotein ligand-1: its role as a selectin counterreceptor in leukocyte-endothelial and leukocyte-platelet interaction. Thromb. Haemost. 81: 1-7.

32. Jun CD, Carman CV, Redick SD, Shimaoka M, Erickson HP, Springer TA (2001) Ultrastructure and function of dimeric soluble intercellular adhesion molecule-1 (ICAM-1) J. Biol. Chem. 276: 29019-29027.

33. Detmers PA, Wright SD, Olsen E, Kimball B, Cohn ZA (1987) Aggregation of complement receptors of human neutrophils in the absence of ligand. J. Cell Biol., 105 : 1137-1145.

34. van Kooyk Y, Weder P, Heije K, Figdor CJ (1994) Extracellular Ca2+ modulates leukocyte function-associated antigen-1 cell surface distribution on T lymphocytes and consequently affects cell adhesion. J. Cell Biol. 124: 1061-1070.

35. Cambi A, Joosten B, Koopman M, de Lange F, Beeren I, Torensma R, Fransen JA, Garcia-Parajo M, van Leeuwen FN, Figdor CG (2006) Organization of the integrin LFA-1 in nanoclusters regulates its activity. Mol. Biol. Cell 17: 4270-4281.

36. Kim M, Carman CV, Yang W, Salas A, Springer TA (2004) The primacy of affinity over clustering in regulation of adhesiveness of the integrin alphaLbeta2. J. Cell Biol. 20: 1241-1253.

37. Yap AS, Brieher WM, Pruschy M, Gumbiner BM (1997) Lateral clustering of the adhesive ectodomain : a fundamental determinant of cadherin function. Current Biol. 7: 308-315.

38. Seifert U (2000) Rupture of multiple parallel molecular bonds under dynamic loading. Physical Review Letters 84: 2750-2753.

39. Seifert U (2001) Dynamic strength of adhesion molecules: role of rebinding and self-consistent rates. Europhys. Lett 58: 792-798.

40. Irvine DJ, Hue KA, Mayes AM, Griffith L (2002) Simulations of cell-surface integrin binding to nanoscale-clustered adhesion ligands. Biophys. J. 82: 120-132.

41. Erdmann T, Schwarz US (2004) Stability of adhesion clusters under constant force. Phys. Rev. Letters 92: 108102.

42. Sulchek T, Friddle RW, Noy A (2006) Strength of multiple parallel biological bonds. Biophys. J. 90: 4686-4691.

43. Sulchek, T. A., R. W. Friddle, K. Langry, E. Y. Lau, H. Albrecht, T. V. Ratto, S. J. DeNardo, M. E. Colvin, and A. Noy. 2005. Dynamic force spectroscopy of parallel individual Mucin1-antibody bonds. Proc. Natl. Acad. Sci. USA 102:16638-16643.

44. Guo S, Ray C, Kirkpatrick A, Lad N, Akhremitchev BB (2008) Effects of multiple-bond ruptures on kinetic parameters extracted from force spectroscopy measurements: revisiting biotin-streptavidin interaction. Biophys. J. 95: 3964-3976.

45. Kinoshita K, Leung A, Simon S, Evans E (2010) Long-lived, high-strength states of ICAM-1 bonds to beta2 integrin, II:lifetimes of LFA-1 bonds under force in leukocyte signaling. Biophys. J. 98: 1467-1475.

46. Loritz HM, Kirchgessner N, Born S, Hoffmann B, Merkel R (2011) Mechanical strength of specific bonds acting isolated or in pairs: a case study on engineered proteins. J. Phys. Chem. B 115:2582-2592.

47. Robert P, Sengupta K, Puech PH, Bongrand P, Limozin L (2008) Tuning the formation and rupture of single ligand-receptor bonds by hyaluronan-induced repulsion Biophys. J. 95: 3999-4012.

48. Sengupta K, Moyen E, Macé M, Benoliel AM, Pierres A, , Thibaudau F, Masson L, Limozin L, Bongrand P, Hanbücken M (2009) Large-scale ordered plastic nanopillars for quantitative live-cell imaging. Small 5:449-453.

49. Sergé A, Bertaux N, Rigneault H, Marguet D (2008) Dynamic multiple-target tracing to probe spatiotemporal cartography of cell membranes. Nature Methods 5: 687-694.

50. Pierres A, Prakasam A, Touchard D, Benoliel AM, Bongrand P, Leckband D (2007) dissecting subsecond cadherin bound states reveals an efficient way for cells to achieve ultrafast probing of their environment. FEBS Lett. 581: 1841-1846.

51. Pierres A, Benoliel AM, Zhu C, Bongrand P (2001) Diffusion of microspheres in shear flow near a wall : use to measure binding rates between attached molecules. Biophys. J. 81: 25-42.

52. Goldman AJ, Cox RG, Brenner H (1967) Slow viscous motion of a sphere parallel to a plane wall. II - Couette flow. *Chem Engn. Sci*. 22 :653-660.

53. Robert P, Nicolas A, Aranda-Espinoza S, Bongrand P, Laurent L (2011) Minimal encounter time and separation determine ligand-receptor binding in cell adhesion. Biophys. J. 100: 2642-2651.

54. Zhu C, Long M, Chesla SE, Bongrand P (2002) Measuring receptor/ligand interaction at the single-bond level : experimental and interpretative issues. Ann. Biomed. Engineering 30: 305-314.

55. Robert P, Limozin L, Pierres A, Bongrand P (2009) Biomolecule rates do not provide a complete description of bond formation. Biophys. J. 96:4642-4650.

56. Foote J, Milstein C (1994) Conformational isomerism and the diversity of antibodies. Proc. Natl. Acad. Sci. USA 91: 10370-10374.

57. Beeson C, McConnell HM (1994) Kinetic intermediates in the reactions between peptides and proteins of major histocompatibility complex class II. Proc. Natl. Acad. Sci. USA 91: 8842-8845.

58. Williams AF (1991) Out of Equilibrium. Nature 352: 473-474.

59. Chen S, Springer TA (2001) Selectin receptor-ligand bonds : formation limited by shear rate and dissociation governed by the Bell model. Proc. Natl. Acad. Sci. USA. 98: 950-955.

60. Wierenga PA, Egmond MR, Voragen AGJ, de Jongh HHJ (2006) The adsorption and unfolding kinetics determines the folding state of proteins at the air-water interface and thereby the equation of state. J. colloid Interface Sci. 299: 850-875.

61. Pierres A, Benoliel AM, Bongrand P (2008) Studying molecular interactions at the single bond level with a laminar flow chamber. Cell. Mol. Bioengineering 1: 247-262.

62. Robert P, Aleksic M, Dushek O, Cerundolo V, Bongrand P, van der Merwe PA (2012) Kinetics and mechanics of two-dimensional interactions between T cell receptors and different activating ligands. Biophys. J. 102: 248-257.

63. Fuhrmann A, Schoening JC, Anselmetti D, Staiger D, Ros R (2009) Quantitative analysis of single-molecule RNA-Protein interaction. Biophys. J 96: 5030-5039.

64. Ray C, Guo S, Brown J, Li N, Akhremitchev BB (2010) Kinetic parameters from detection probability in single molecule force spectroscopy. Langmuir 26: 11951-11957.

65. Bartsch T, Fisinger S, Kochanczyk MD, Huang R, Jonas A, Florin EL (2009) Detecting sequential bond formation using three-dimensional thermal fluctuation analysis. Chem Phys Chem 10:1541-1547.

66. Doi M, Edwards SF (1988) The theory of polymer dynamics. Oxford Scientific Publications. Oxford.

67. Holowka DA, Cathou RE (1976) Conformation of immunoglobulin M. 2. Nanosecond fluorescence depolarization analysis of segmental flexibility in anti-epsilon-I-dimethylamino-5-naphtalenesulfonyl-L-lysine anti-immunoglobulin form horse, pig and shark. Biochemistry 15: 3379-3390.

68. Rief M, Gautel M, Oesterhelt F., Fernandez JM, Gaub HE (1997) Reversible unfolding of individual titin immunoglobulin domains by AFM. Science 276: 1109-1112.

69. Glynn E, Steward MV (1977). Immunochemistry: an advanced textbook. 2nd edition, New York, Wiley. p240.

FIGURE LEGENDS

Figure 1 : Experimental model.

Fig.1A : Microspheres (1) were coated with two immunoglobulin layers made of an anti-immunoglobulin (red) and an anti-ICAM-1 (blue) forming a sequence of four segments of 8 nm length connected by flexible hinges. The surface of flow chambers was coated with polylysine, then an anti-poly-histidine IgG (green) and either a single ICAM-1 moiety terminated with a short poly-histidine (yellow :2) or a Fc(ICAM-1)$_2$ fragment (green+yellow: 3). Since the density of tagged ICAM-1 moieties was much lower than that of antibodies, there was a very low probability that an antibody might bind simultaneously two ICAM-1-bearing molecules.

Fig.1B : sedimented microspheres of radius a = 2,250 nm were measured to flow with an average distance of about 25 nm to the surface, as a result of brownian motion and short range interactions (45, 50), resulting in a translational velocity (in μm/s) of about 1.215 times the wall shear rate G (in s^{-1}). When a molecular bond was formed between the sphere and the surface (right) the force exerted by the flow was dependent on the bond length and was estimated (in piconewton) at about $0.85 \times G$ (14).

Figure 2 : Lifetime of nonspecific arrests.

The figure shows the survival curves of binding events recorded between ICAM-1-coated surfaces and microspheres coated with irrelevant antibodies. Squares: wall shear rate 9.3 s^{-1}, microsphere velocity 11.25 μm/s, 213 binding events recorded. Crosses: wall shear rate 18.5

s^{-1}, microsphere velocity: 22.5 μm/s, 717 binding events recorded. Circles: wall shear rate 29.4 s^{-1}, microsphere velocity: 35.7 μm/s, 526 binding events recorded. Vertical bar length is twice the standard error.

Figure 3 : Lifetime of binding events recorded on surfaces coated with monovalent ICAM-1.
The figure shows the survival curves of binding events recorded between surfaces coated with low densities of monovalent ICAM-1 and microspheres coated with anti-ICAM-1 antibodies. Red, squares: wall shear rate 9.3 s^{-1}, microsphere velocity 11.25 μm/s, 47 binding events recorded. Green, triangles: wall shear rate 18.5 s^{-1}, microsphere velocity 22.5 μm/s, 1,725 binding events recorded. Blue, circles: wall shear rate 29.4 s^{-1}, microsphere velocity 35.7 μm/s, 936 binding events recorded. **Fig3A**: the raw values were used. **Fig 3B**: values were corrected to account for nonspecific events as explained. The curves represented the best fits of experimental curves with Eq. 2. Squares: Force on bond is 8.37 pN, $k(F,0)=0.441\ s^{-1}$, $a(F)=1.099\ s^{-1}$, red line: calculated fit, MSD=3.7 10^{-3}. Crosses: Force on bond is 16.75 pN, $k(F,0)=1.735\ s^{-1}$, green line: calculated fit, MSD = 0.99 10^{-3}. Circles: Force on bond is 26.61 pN, $k(F,0)=4.603\ s^{-1}$, $a(F) = 6.149\ s^{-1}$, MSD = 12.4 10^{-3}. Vertical bar length is twice standard error.

Figure 4 : Lifetime of binding events recorded on surfaces coated with divalent ICAM-1.
The figure shows the survival curves of binding events recorded between surfaces coated with low densities of $Fc(ICAM\text{-}1)_2$ molecules and microspheres coated with anti-ICAM-1 antibodies. **Fig. 4A**: all survival curves corrected for non specific arrests. Squares: wall shear rate 10.3 s^{-1}, microsphere velocity 12.5 μm/s, 122 binding events recorded. Force on bond is 8.80 pN. Triangles: wall shear rate 18.5 s^{-1}, microsphere velocity 22.5 μm/s, 1009 binding events recorded. Force on bond is 15.84 pN. Circles: wall shear rate 30.9 s^{-1}, microsphere velocity 37.5 μm/s, 1939 binding events recorded. Force on bonds is 26.40 pN. **Fig.4B.** Squares: experimental data, lowest wall shear rate: 10.3 s^{-1}. Theoretical curves are shown for the following conditions: two bonds at time zero, $k_r = 0$, force not shared (red) or shared (green) between bonds. One bond at time zero, $k_r = 0$, (blue), one bond at time zero, $k_r = 0.3\ s^{-1}$, force not shared (cyan) or shared (purple) between bonds. **Fig.4.C**. Triangles: experimental data, intermediate wall shear rate 18.5 s^{-1}. Theoretical curves are shown for the following conditons : Two bonds at time zero, $k_r = 0$, force not shared (red) or shared (green) between bonds. One bond at time zero, $k_r = 0$ (blue), one bond at time zero, $k_r = 1.1\ s^{-1}$, force not shared (cyan) or shared (purple) between bonds. **Fig.4D**. Circles: experimental data, highest shear rate 30.9 s^{-1}. Theoretical curves are shown for the following conditions: Two bonds at time zero, $k_r = 0$, force not shared (red) or shared (green) between bonds. One bond at time zero, $k_r = 0$ (blue), one bond at time zero, $k_r = 12\ s^{-1}$, force not shared, (cyan) or $k_r=6s^{-1}$, force shared (purple) between bonds. Vertical bar length is twice the standard error.

Figure 5 : Force free survival of attachments between microspheres and ICAM-1-coated surfaces. Anti-ICAM-1-coated Qdots were incubated with surfaces coated with monovalent (diamonds) or divalent (triangles) ICAM-1 and spontaneous detachment was determined by counting bound Qdots on a microscope area of 1 μm^2. Each point represents about 800-1000 particles. Green line : fit of monovalent binding with constants $k(0,0) = 0.167\ mn^{-1}$ and $a(0) = 0.252\ mn^{-1}$ (Eq. 2). Red line: calculated survival curve for dimers, two bonds at time zero, $k_{on} = 0$, MSD=0.0105. Blue line: calculated survival for dimers, one bond at time zero, $k_{on} = 0$,

MSD = 0.025. Yellow line: calculated survival curve for dimers, one bond at time zero, k_{on} = 1.4 mn^{-1}, MSD = 0.0052.

Figure 6 : Force dependence of off-rate and bond strengthening parameter.
The dependence of bond initial dissociation rate (Fig. 6A) and strengthening rate (Fig. 6B) on applied forces are shown. Open triangles represent data obtained with the flow chamber and filled triangles represent data obtained with Qdots in absence of flow. Since time scales were markedly different, only results obtained with the flow chamber were used to estimate the rupture behavior of bonds formed with $Fc(ICAM\text{-}1)_2$ in the flow chamber, with either force sharing or non sharing assumption. Estimated values are shown on Table 1.

TABLE 1
Estimated parameters for rupture of ICAM-1/anti-ICAM-1 bonds subjected to force

Wall shear rate (s^{-1})	Force (pN)	k(F,0) (s^{-1})	a(F) (s^{-1})	k(F/2,0) (s^{-1})	a(F/2) (s^{-1})
0	0	0.168	0.512	0.168	0.512
10.3	8.80	0.519	1.171	0.295	0.775
18.5	15.84	1.277	2.270	0.463	1.078
30.9	26.4	4.934	6.126	0.911	1.772

The numerical values of parameters used to build simulated survival curves of attachments formed by microspheres and $Fc(ICAM\text{-}1)_2$ - coated surfaces are shown as derived by extrapolating results displayed on Fig. 6

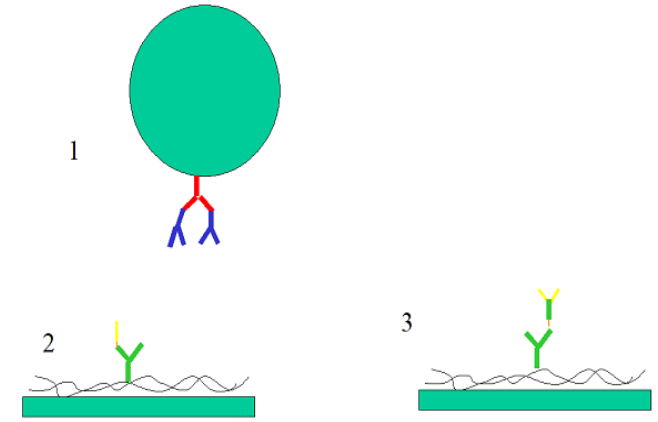

A

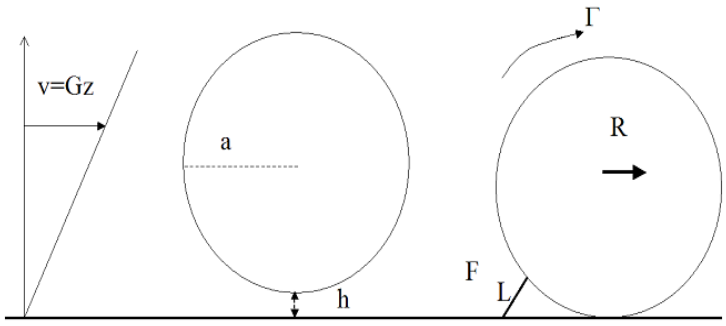

B

Fig.1

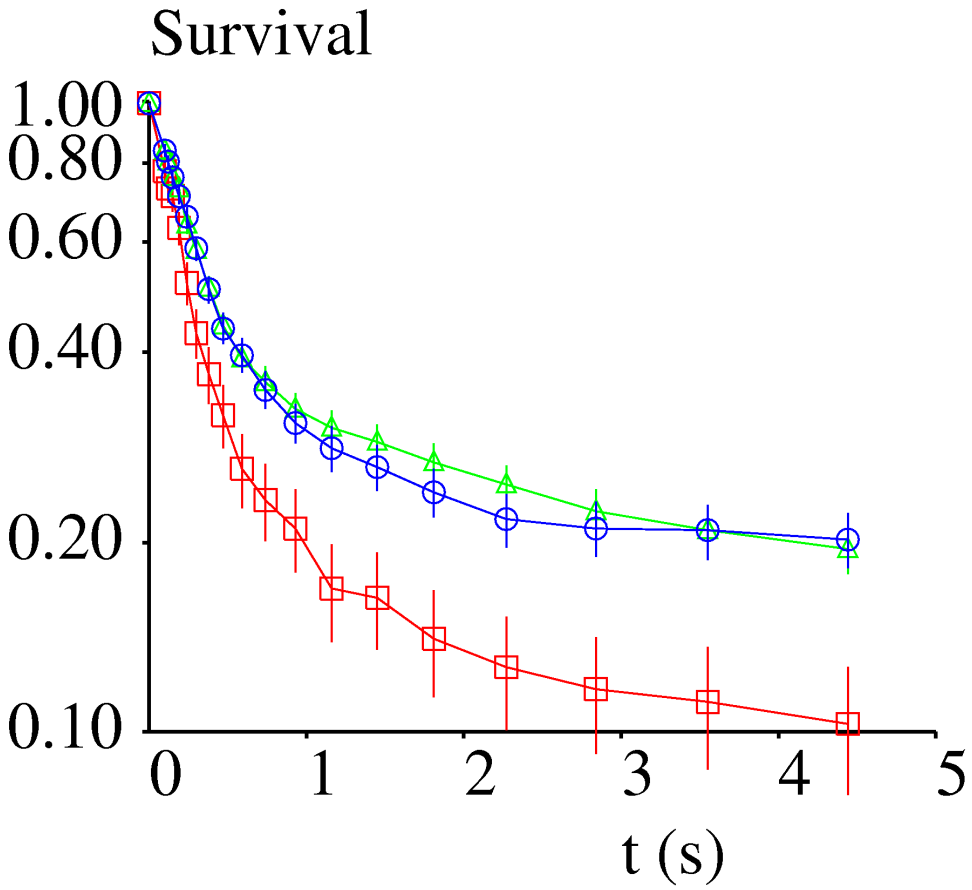

Fig 2

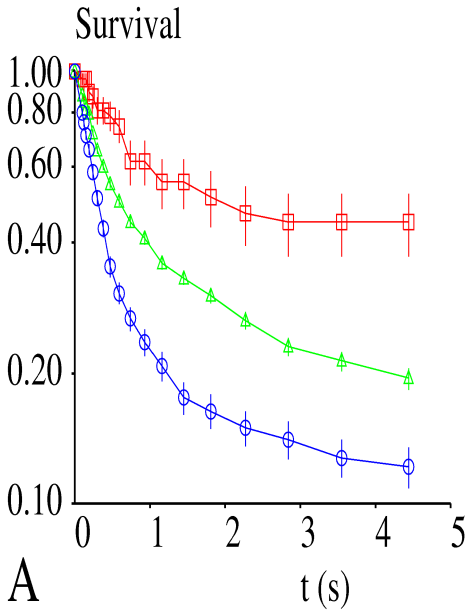
Survival
1.00
0.80
0.60
0.40
0.20
0.10
0
1
2
3
4
5
A
t (s)

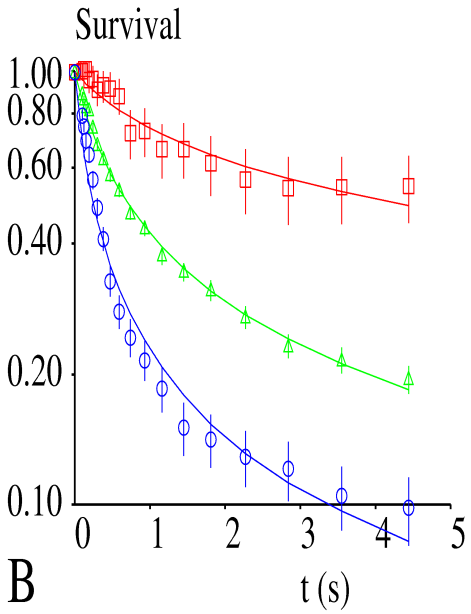
Survival
1.00
0.80
0.60
0.40
0.20
0.10
0
1
2
3
4
5
B
t (s)

Fig. 3

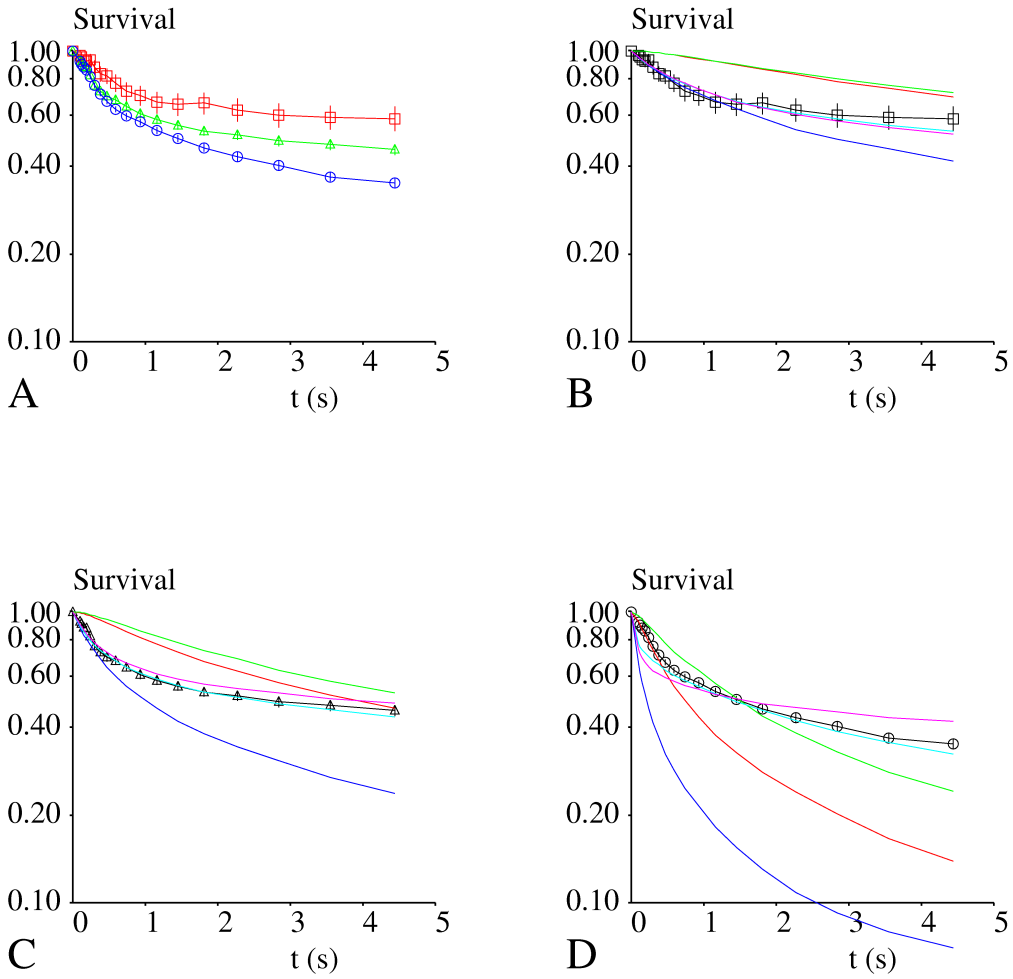

Fig. 4

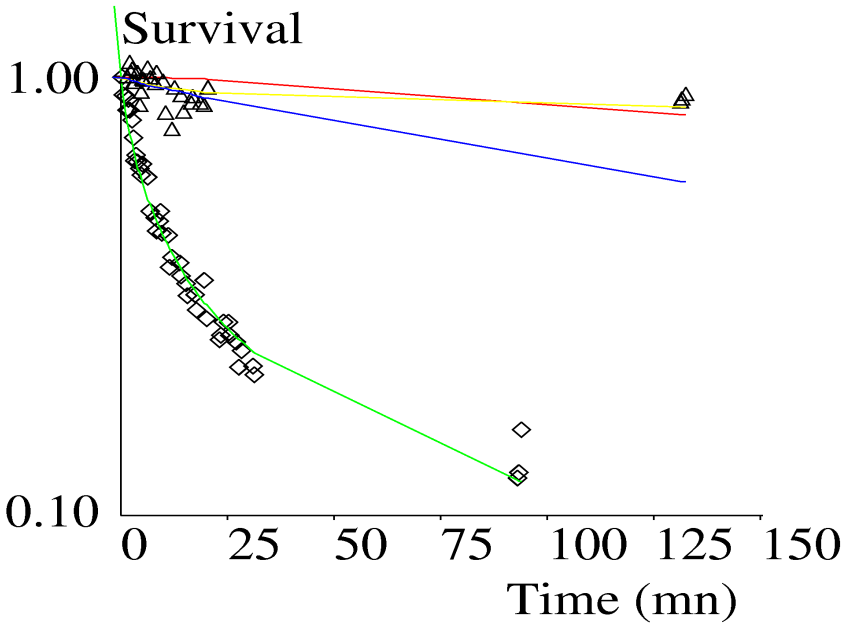

Fig 5

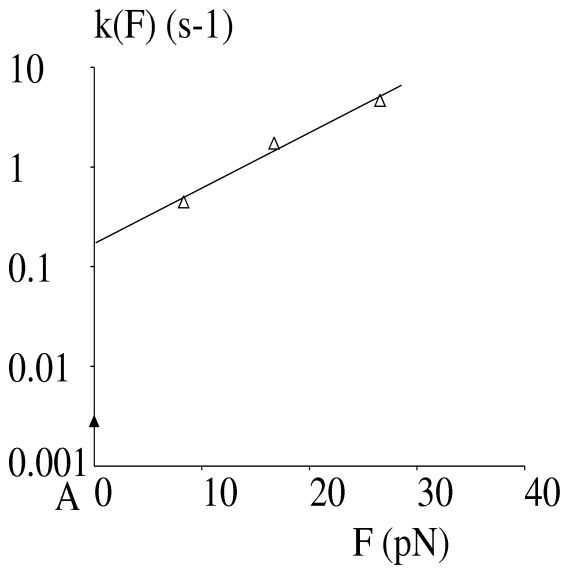
k(F) (s-1)
10
1
0.1
0.01
0.001
A
0
10
20
30
40
F (pN)

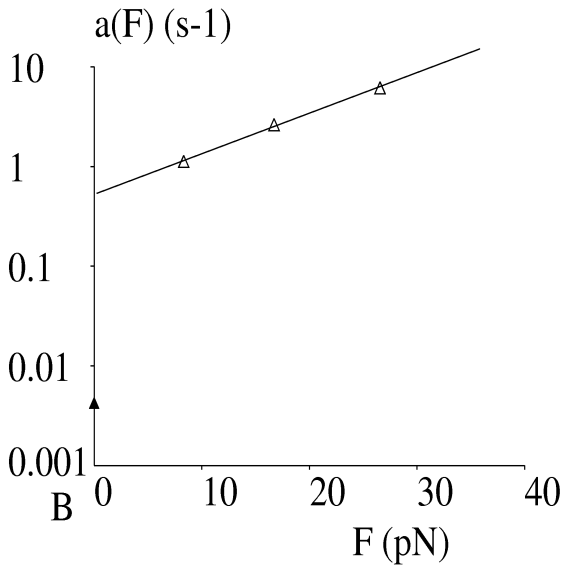
a(F) (s-1)
10
1
0.1
0.01
0.001
B
0
10
20
30
40
F (pN)

Fig 6